Functionalized Polymer Nanofibrous Substrates as Capturing Platforms for Mycobacteria

by

Anja du Plessis

Dissertation presented for the degree of MSc in Chemistry and Polymer Science

Stellenbosch University
Faculty of Science
Department of Chemistry and Polymer Science

Promotor: Dr. L. Cronje

March 2016

I dedicate this work to my family and friends whose words of encouragement still ring in my ears: my loving parents, Paul and Anne-Marie, and my two best friends, Daniël and Marlé. Your attributes are invaluable.

Declaration

By submitting this thesis electronically, I declare that the entirety of the work contained therein is my own, original work, that I am the sole author thereof (save to the extent explicitly otherwise stated), that reproduction and publication thereof by Stellenbosch University will not infringe any third party rights and that I have not previously in its entirety or in part submitted it for obtaining any qualification.

Anja du Plessis March 2016

Abstract

Tuberculosis (TB) remains one of the world's deadliest communicable diseases. In 2013, an estimated 9.0 million people developed TB and 1.5 million died from the disease. The treatment of children with TB is often not considered a priority by tuberculosis control programmes. Paediatric TB is frequently more difficult to diagnose due to non-specific clinical and radiological features as opposed to adult TB cases that are often easily recognizable and accompanied by a positive sputum smear test. Most cases of childhood TB are paucibacillary, and therefore mycobacterial culture of specimens is required to optimise diagnostic yield, which can take weeks. If the TB bacilli can be concentrated in specimens, this problem could be circumvented and rapid diagnosis could be possible using existing microscopy methods.

In this thesis, styrene maleimide copolymer (SMI) derivatives were synthesized and electrospun to develop nanofibrous substrates with an affinity for the mycobacterial cell wall of *Mycobacterium tuberculosis* (*Mtb*) to potentially act as capturing platforms for these bacilli. SMA was modified with a variety of low molecular weight modification agents that were chosen based on their known or possible affinity for the mycobacterial cell wall before being electrospun into nanofibrous membranes. Prefabricated SMA nanofibers were also surface-functionalized with a lectin-binding protein, namely Concanavalin A (Con A).

Affinity studies were carried out between the modified polymer nanofibers and an attenuated strain of *Mtb*, namely *Mycobacterium bovis* bacillus Calmette-Guérin (BCG) to evaluate the ability of each polymer nanofibrous substrate to capture BCG at decreasing concentrations. The successful capture of BCG onto the substrates was confirmed using fluorescence microscopy (FM). Analysis of the FM images revealed that SMA functionalized with Con A captured BCG the most effectively due to the saccharide binding properties of the protein. This interaction is specific between BCG and the Con A protein due to the mannose binding ability of Con A and the mannose molecules present on the outer cell surface of BCG. SMA modified with aliphatic quaternary ammonium moieties of chain lengths C_8-C_{12} also showed exceptional capturing abilities through a combination of ionic and hydrophobic interactions. This interaction is non-specific as it is only dependent on the electrostatic and hydrophobic-hydrophobic interaction between BCG and the polymer nanofibrous surfaces. These interactions were visible even at the lowest tested BCG concentration.

Opsomming

Tuberkulose (TB) bly een van die wêreld se dodelikste oordraagbare siektes. In 2013 het ‘n geskatte 9.0 miljoen mense TB ontwikkel en 1.5 miljoen het gesterf as gevolg van die siekte. Die behandeling van kinders met TB word dikwels nie as ‘n prioriteit beskou deur tuberkulose programme nie. Pediatriese TB is dikwels moeilik om te diagnoseer as gevolg van nie-spesifieke kliniese en radiologiese kenmerke in teenstelling met volwasse TB-gevalle wat dikwels maklik herkenbaar is en vergesel word deur ‘n positiewe sputum smeer toets. Die meeste gevalle van kinder TB word geken aan die teenwoordigheid van min basille, daarom word mikobakteriële kultuur van monsters benodig om diagnostiese opbrengs te optimaliseer. Hierdie prosedure kan weke neem. Indien die TB-basille gekonsentreer kan word vanuit die monsters kan hierdie probleem omseil word en sodoende ‘n vinnige diagnose bewerkstellig deur gebruik te maak van bestaande mikroskopiese metodes.

In hierdie tesis is stireen maleimied kopolimeer (SMI) afgeleides gesintetiseer en elektrogespin om nanoveselagtige substrate te ontwikkel met ‘n affiniteit vir die mikobakteriële selwand van *Mycobacterium tuberkulose* (*Mtb*) wat potensieël as vaslegging platforms vir hierdie basille kan optree. SMA is gemodifieer met ‘n verskeidenheid van lae molekulêre massa verbindings wat gekies is op grond van hul bekende of moontlike affiniteit vir die mikobakteriële selwand, waarna die polimere elektrogespin is in nanoveselagtige membrane. Voorafvervaardigde SMA nanovesels was ook gemodifiseer met ‘n koolhidraat-bindende proteïen, naamlik Concanavalin A (Con A) deur oppervlak-funksionalisering.

Affiniteitstudies is uitgevoer tussen die gemodifiseerde polimeer nanovesels en ‘n verswakte stam van *Mtb*, naamlik *Mycobacterium bovis* bacillus Calmette-Guérin (BCG) om die vermoë van elke polimeriese nanoveselagtige substraat om BCG vas te vang, te evalueer met vermindering van BCG konsentrasie. Die suksesvolle vasvang van BCG op die substrate is bevestig met behulp van fluoressensie mikroskopie (FM). Ontledig van die FM beelde het aangedui dat SMA gemodifiseer met Con A as die doeltreffendste substraat opgetree het deurdat hierdie vesels die meeste BCG vasgevang het as gevolg van die sakkaried-bindende eienskappe van die proteïen. Hierdie interaksie is spesifiek tussen BCG en die Con A proteïen as gevolg van die mannose-bindingsvermoë van Con A en die mannose molekules teenwoordig op die buitenste seloppervlak van BCG. SMA wat gemodifiseer is met alifatiese kwaternêre ammonium groepe met kettinglengtes van C_8-C_{12} het ook uitsonderlike vasvang vermoëns getoon deur middel van ‘n kombinasie van ioniese en hidrofobiese interaksies. Hierdie interaksie is nie-spesifiek omdat dit slegs afhanklik is van die elektrostatiese en hidrofobiese-hidrofobiese interaksie tussen BCG en die polimeriese nanoveselagtige oppervlaktes. Hierdie interaksies was selfs by die laagste konsentrasie BCG sigbaar.

Table of contents

INDEX

LIST OF FIGURES

LIST OF SCHEMES

LIST OF TABLES

LIST OF SYMBOLS

C*	Critical chain overlap concentration
C_e	Entanglement concentration
Đ	Polydispersity index
K_d	Binding affinity
kV	Kilovolt
M_w	Weight average molecular weight

LIST OF ACRONYMS

^{13}C-NMR	Carbon nuclear magnetic resonance spectroscopy
^{1}H-NMR	Proton nuclear magnetic resonance spectroscopy
Abs	Absolute peak height
ABTS	2,2'-Azino-bis(3-ethylbenzthiazoline-6-sulfonic acid)
Acetone-d6	Deuterated acetone
AFB	Acid-fast bacilli
AIBN	2,2'-Azobis(2-methylpropionitrile)
AP	4-Aminophenol
ATR-FTIR	Attenuated total reflectance Fourier transform infrared spectroscopy
BCG	*Mycobacterium bovis* bacillus Calmette-Guérin
BET	Brunauer-Emmett-Teller
$CaCl_2$	Calcium chloride
$CDCl_3$	Deuterated chloroform
CFP-10	Culture filtrate protein 10
CLPAs	Cross-linked protein aggregates
Con A	Concanavalin A
CT	Computerized tomography
DC	Degree of conversion
d-DMSO	Deuterated dimethyl sulfoxide
DMAPA	3-(*N,N*-dimethylamino)-1-propylamine
DMF	Dimethylformamide
DMSO	Dimethyl sulfoxide
DQ	Degree of quaternization
DR-TB	Drug resistant tuberculosis
ELISA	Enzyme-linked immunosorbent assay
ELISpot	Enzyme-linked immunospot assay
ESAT-6	Early secretory antigen target-6

EtOH	Ethanol
FM	Fluorescence microscopy
GA	Gastric aspirate
GL	Gastric lavage
GLA	Glutaraldehyde
H_2O_2	Hydrogen peroxide
HIV	Human immunodeficiency virus
HRP	Horseradish peroxidase
IFN- γ	Interferon-gamma
IGRA	Interferon-gamma release assay
IS	Induced sputum
KCl	Potassium chloride
KCN	Potassium cyanide
KH_2PO_4	Potassium phosphate monobasic
LM	Lipomannan
LTBI	Latent tuberculosis infection
M. bovis	*Mycobacterium bovis*
Manh	Maleic anhydride
Man-LAM	Mannose-capped lipoarabinomannan
MDR-TB	Multi-drug-resistant tuberculosis
MEK	Methyl ethyl ketone
MeOH	Methanol
$MnCl_2$	Manganese(II) chloride
MPI	Mannosyl-phosphatidyl-*myo*-inositol
Mtb	*Mycobacterium tuberculosis*
MW	Molecular weight
MWD	Molecular weight distribution
Na_2HPO_4	Sodium phosphate dibasic
NaCl	Sodium chloride
Ninhydrin	2,2-Dihydroxyindane-1,3-dione

NPA	Nasopharyngeal aspiration
OD	Optical density
PBS	Phosphate buffer solution
PCR	Polymerase chain reaction
PEO	Polyethylene oxide
PIMs	Phosphatidyl-*myo*-inositol mannosides
PPD	Purified protein derivative
ppm	Parts per million
Pr	Propylamine
PS	Polystyrene
RH	Relative humidity
RP	Ruhemann's purple
SEC	Size exclusion chromatography
SEM	Scanning electron microscopy
SMA	Poly(styrene-*alt*-maleic anhydride)
SMI	Poly(styrene-*alt*- maleimide)
SMI-Con A	Poly(styrene-*N*-Concanavalin A maleimide)
SMI-CLPA	Poly(styrene-*N*-Concanavalin A maleimide) cross-linked protein aggregates
SMI-AP	Poly(styrene-*N*-[4-hydroxyphenyl] maleimide)
SMI-Pr	Poly(styrene-*N*-propylmaleimide)
SMI-qC_{10}	Poly(styrene-[*N*-3-(*N'*-decyl-*N',N'*-dimethylammonium)propyl maleimide])
SMI-qC_{12}	Poly(styrene-[*N*-3-(*N'*-dodecyl-*N',N'*-dimethylammonium)propyl maleimide])
SMI-qC_{14}	Poly(styrene-[*N*-3-(*N'*-tetradecyl-*N',N'*-dimethylammonium)propyl maleimide])
SMI-qC_8	Poly(styrene-[*N*-3-(*N'*-octyl-*N',N'*-dimethylammonium)propyl maleimide])
SMI-qC_x	Styrene maleimide quaternary ammonium alkyl conjugates
SMI-tC	Poly(styrene-[*N*-3-(*N',N'*-dimethylamino)propyl maleimide])
TB	Tuberculosis
THF	Tetrahydrofuran
TMS	Tetramethylsilane

TST	Tuberculin skin test
XDR-TB	Extensively drug resistant tuberculosis
ZN	Ziehl-Neelsen stain

Chapter 1: Introduction and objectives

1.1 Introduction

Tuberculosis (TB) is one of the world's deadliest communicable diseases and is caused by *Mycobacterium tuberculosis*.[1] In 2013, an estimated 9.0 million people developed TB and 1.5 million died from the disease, 360 000 of whom were HIV positive.[2] Exposure to *Mycobacterium tuberculosis* (*Mtb*) often results in the development of latent tuberculosis infection (LTBI) with a 5-10% lifetime risk of progressing to active tuberculosis (TB), with the majority of TB cases occurring within the first two years after infection.[3,4]

Childhood TB is frequently more difficult to diagnose due to non-specific clinical and radiological features as opposed to adult TB cases that are often easily recognizable and accompanied by a positive sputum smear test.[5] Children with TB usually have paucibacillary disease which is sputum smear-negative due to the size of the bacillary population being less than 10^4 colony-forming units (CFU) and consequently contribute little to disease transmission within the community. However, children account for a major proportion of the global TB disease burden, especially in endemic areas.[6,7]

Conventional TB diagnosis continues to rely on sputum smear microscopy, culture, the tuberculin skin test, and chest radiography. Although these tests have been used for nearly a century, they have several limitations and perform poorly in populations affected by the HIV epidemic.[8]

The accurate diagnosis of childhood TB proves to be more difficult than TB in adults. The diagnosis of TB in children is traditionally based on chest radiography, the tuberculin skin test, and mycobacterial staining/culture, although these methods are not always reliable. The gold standard for the diagnosis of active pulmonary disease is a positive *Mtb* culture from a clinical specimen. However, such specimens are difficult to obtain from children since they mostly develop extrapulmonary TB that requires invasive specimen collection procedures. Furthermore, children younger than 5 years with pulmonary TB rarely produce sputum.[9] Newer methods, such as polymerase chain reaction (PCR) and immune-based methods are increasingly being used but are not widely available and have a limited role in routine clinical practice.[10]

The aim of this study was therefore to develop nanofibrous substrates that could act as concentrators for *Mtb* leading to improved specimen collection methods for sputum samples and ultimately faster diagnosis of TB. For this study an *Mtb*-mimic was used, namely *Mycobacterium bovis* bacillus Calmette-Guérin (BCG)[11,12] BCG is a live-attenuated strain derived from *M. bovis* that is genetically similar to *Mtb*[13-15] with the advantage of being non-pathogenic.[16] The goal was thus to "capture" BCG from cultured samples using various functionalized nanofibrous substrates by means of chemical interactions between the mycobacterial cell wall and the functionalized nanofibrous surfaces. The modification compounds chosen for the functionalization of the polymer substrates were selected based on their known[17] or possible chemical interaction[18] with the *Mycobacterium tuberculosis* (*Mtb*) cell wall. Fluorescence microscopy could be used to evaluate this interaction and thus determine which chemical entity had the greatest affinity for the BCG cell wall.

Poly(styrene-*alt*-maleic anhydride) (SMA) was chosen as parent polymer for this study due to its ease of synthesis,[19] solubility in a variety of solvents and reactive anhydride functional groups that

can easily undergo imidization,[20] esterification[21] and hydrolysis. The functionalized polymers were electrospun into nanofibrous substrates.

Electrospinning is a straightforward, convenient and inexpensive method that allows for the production of continuous fibers with submicron diameters.[22] Nanofibers possess an inherently large specific surface area, rendering them useful in a variety of applications such as tissue engineering scaffolds[23], filtration devices,[24] protective clothing, controlled drug delivery platforms and affinity membranes.[25]

These functionalized polymer nanofibers were therefore considered good candidates to act as capturing substrates for BCG.

1.2 Objectives

The basic motivation for this work was to synthesize functionalized polymer nanofibers to act as capturing platforms for BCG in aqueous media. For this purpose, SMA was chosen as parent polymer to undergo chemical modification with a variety of low molecular weight compounds before being electrospun into nanofibrous membranes. Electrospinning was chosen as technique for the production of continuous, submicron diameter fibers with a high surface to volume ratio. SMA nanofibers were also surface-functionalized with a protein with an affinity for BCG. Modification took place at the reactive maleic anhydride moiety via imidization to yield styrene maleimide derivatives.

The functionalized polymer nanofibers were subsequently subjected to affinity studies with BCG to evaluate its ability to capture mycobacteria in samples containing various concentrations of BCG in decreasing quantities.

The objectives for this study can therefore be summarized as follows:

1. To synthesize a medium molecular weight alternating styrene-maleic anhydride (SMA) copolymer using conventional free radical copolymerization that can be electrospun into nanofibers.
2. To synthesize various functionalized styrene maleimide copolymers (SMI) by modifying SMA at the maleic anhydride moiety via imidization before electrospinning these compounds into nanofibers.
3. To synthesize SMA and electrospin this polymer into nanofibers followed by surface-functionalization with a protein via imidization.
4. To evaluate the interaction between BCG as *Mtb*-mimic and all the functionalized polymer nanofibers using BCG to determine whether these substrates can act as capturing platforms for the mycobacteria.

1.3 Layout of the thesis

Chapter 1: A brief introduction to the scope of this study is offered and the objectives set out to achieve are summarized.

Chapter 2: A literature review related to tuberculosis (TB) and the diagnostic limitations are presented, with specific focus on the difficulties in diagnosing paediatric tuberculosis. Limitations of current diagnostic approaches are briefly discussed. The synthesis, modification and electrospinning proposals to develop polymer substrates to act as capturing devices for BCG are discussed.

Chapter 3: This chapter describes the synthesis of poly(styrene-*alt*-maleic anhydride) (SMA) and subsequent modification with low molecular weight compounds to produce maleimide derivatives. The electrospinning and characterization thereof are included.

Chapter 4: This chapter entails the surface functionalization of SMA nanofibers with a protein using two approaches. The characterization of the functionalized SMI nanofibers is included.

Chapter 5: In this chapter, affinity studies between the functionalized polymer nanofibers and BCG are presented. These affinity studies were done at different concentrations of BCG to obtain the lowest limit of detection for each of the functionalized nanofibers. The evaluation of interaction was done using fluorescence microscopy (FM).

Chapter 6: Conclusions and recommendations for future research are highlighted in this chapter.

1.4 References

1. Jacobs, W.R. *HS Talks: Biomedical & Life Sciences Collection* **2009**, 2-4.

2. Baddeley, A; *et al*. *WHO Report: Global tuberculosis report* **2014**, 17-23

3. Hartman-Adams, H.; Clark, K.; Juckett, G. *Am. Fam. Phys*. **2014**, *89*, 889-896.

4. Mack, U.; Migliori, G.B.; Sester, M.; *et al*. *Eur. Respir. J*. **2009**, *33*, 956-973.

5. Nicol, M.P.; Zar, H.J. *Paediatr. Resp. Rev*. **2011**, *12*, 16-21.

6. Nelson, L.J.; Wells, C.D. *Sem. Pediatr. Infect. Dis*. **2004**, *15*, 150-154.

7. Nelson, L.J.; Wells, C.D. *Int. J. Tuber. Lung. Dis*. **2004**, *8*, 636-647.

8. Pai, M.; O'Brien, R. *Semin. Respir. Crit. Care. Med*. **2008**, *29*, 560.

9. Lalvani, A.; Millington, K.A. *Curr Opin Infect Dis*. **2007**, *20*, 264-271.

10. Shingadia, D.; Novelli, V. *Lancet* **2003**, *3*, 624-632.

11. Menzies, D.; Pai, M.; Comstock, G. *Ann. Intern. Med*. **2007**, *146*, 340-388.

12. Corrigan, D.; Paton, J. *Breathe* **2007**, *3*, 351-363.

13. Marais, B.J.; Pai, M. *Arch. Dis. Child*. **2007**, *92*, 446-452.

14. Kolattukudy, P.; Fernandes, N.D.; Azad, A.; Fitzmaurice, A.M.; Sirakova, T.D. *Mol. Microbiol*. **1997**, *24*, 263-270.

15. Maeda, N.; Nigou, J.; Herrmann, J.L.; *et al*. *J. Biol. Chem*. **2003**, *278*, 5513-5516.

16. Sasano, K.T.; Medlar, E.M. *Tubercle* **1931**, *12*, 214-219.

17. Jeong, J.; Byoun, Y.; Ko, S.; Lee, T.Y. *J. Ind. Eng. Chem*. **2001**, *7*, 310-315.

18. Vermeesch, I.; Groeninckx, G. *J. Appl. Polym. Sci*. **1994**, *53*, 1365-1373.

19. Hou, S.; Kuo, P. *Polymer* **2001**, *42*, 2387-2394.

20. Cronje, L.; Warren, R.; Klumperman, B. *J. Mat. Chem. B.* **2012**, *48*, 6608-6618.

21. Bshena, O.; Heunis, T.D.J.; Dicks, L.M.T.; Klumperman, B. *Fut. Med. Chem.* **2011**, *3*, 1821-1847.

22. Reneker, D.H.; Chun, I. *Nanotechnology* **1996**, *7*, 216-223.

23. Matthews, J.A.; Wnek, G.E.; Simpson, D.G.; Bowlin, G.L. *Biomacromolecules* **2002**, *3*, 232-238.

24. Qin, X.; Wang, S. *J. Appl. Polym. Sci*. **2006**, *102*, 1285-1290.

25. Kenawy, E.; Bowlin, G.L.; Mansfield, K.; *et al*. *J. Controlled. Release* **2002**, *81*, 57-64.

Chapter 2: Literature review

2.1 Introduction

Tuberculosis (TB) is one of the world's deadliest communicable diseases and is caused by *Mycobacterium tuberculosis* (*Mtb*).[1] In 2013, an estimated 9.0 million people developed TB and 1.5 million died from the disease, 360 000 of whom were HIV positive. TB is slowly declining each year and it is estimated that 37 million lives were saved between 2000 and 2013 through effective diagnosis and treatment. However, since TB is a preventable disease, the death toll from the disease is still unacceptably high.[2] Several factors contribute to the global resurgence of tuberculosis, including poverty, co-infection with HIV, overcrowding, increased travel and immigration, breakdown of tuberculosis control programmes, multi-drug-resistant tuberculosis (MDR-TB) and incomplete treatment.[3]

Exposure to *Mtb* often results in the development of latent tuberculosis infection (LTBI) with a 5-10% lifetime risk of progressing to active tuberculosis (TB), with the majority of TB cases occurring within the first two years after infection.[4,5] Estimations claim that one third of the world's population is latently infected with TB, which emphasizes the importance to accurately and efficiently identify those with LTBI at greatest risk of progression and to provide targeted preventative therapy in order to achieve TB eradication globally.[6]

2.2 Infection

TB is primarily a pulmonary disease. Infection occurs with deposition of a single aerosol droplet containing 1–3 tubercle bacilli in the terminal bronchioles or alveoli. According to experimental data, 10–50 infectious units must be inhaled to reliably establish infection.[7] In humans, the pathological finding of primary infection is a single small tubercle, suggesting that infection is initiated by a single infective droplet.[8] After initial exposure, there is a three day lag before initiation of bacilli replication which occurs for 19 – 20 days, and then is controlled by the emerging adaptive immune response.[9] Insufficient number of bacilli will only result in latent tuberculosis infection, unless some changes in immunological response allow these bacilli to metabolise and multiply at a higher rate, reaching such numbers that result in tuberculosis disease.[5]

The tubercle bacillus is a facultative intracellular parasite that grows well in non-activated macrophages. Activated macrophages can be defined as cells that secrete inflammatory mediators that kill intracellular pathogens.[10] When large numbers of these bacilli have grown intracellularly within such macrophages, a cytotoxic immune response, called tissue-damaging (or necrotizing) delayed-type hypersensitivity (DTH), kills the macrophages and consequently some of the surrounding tissue as well, forming the caseous centre of the developing tubercle. In solid caseum, tubercle bacilli may survive, but do not multiply.[7]

In some cases the caseous centre may liquefy in resistant hosts. The bacilli can now grow extracellularly in the liquefied menstruum, reaching tremendous numbers and resulting in tissue necrosis, including erosion of the walls of small bronchi, leading to cavity formation. From these cavities, the bacilli can spread to other parts of the lung and to the environment. The main reason

why tuberculosis perpetuates itself in mankind is because of extracellular multiplication of tubercle bacilli in the liquefied caseum. It is also the reason why antimicrobial drug-resistant bacillary strains develop.[7]

2.3 Drug resistant tuberculosis

It is important to distinguish between "infection" and "disease", where infection refers to the initial exposure to a case of transmissible tuberculosis, and disease is characterized by the development of signs and symptoms and/or radiographical changes. The former can be treated with a single drug, whereas the latter needs a combination of three or more anti-tuberculosis drugs. Without the use of these anti-TB drugs, 40-50% of infants and 15% of older children with infection will develop the disease within 1-2 years.[11]

Many patients, lacking careful supervision, would stop taking medication midway through a one- to two-year-course of treatment. This could result in the naturally drug-resistant strains of *Mtb* to thrive, resulting in the development of drug-resistant TB (DR-TB), and increasing the probability of spreading these resistant pathogens to other humans.

Globally, 3.5% of new and 20.5% of previously treated TB cases in 2013 were estimated to have had MDR-TB of which an estimated 9.0% of these patients had extensively drug resistant TB (XDR-TB).[2] The imaging presentations of MDR-TB are the same as those of non-MDR TB. MDR-TB is also no more infectious than normal TB.[12] It is, however, a more serious infection that requires prolonged administration of more toxic second-line drugs associated with higher morbidity and mortality rates. Furthermore, patients with MDR-TB remain infectious for a longer period once treatment has started, posing a higher risk of infecting others.[12] High quality treatment of drug-susceptible TB, fast and accurate testing and detection of MDR-TB and access to quality care are but a few actions that must take priority to address the TB epidemic. This includes improved specimen collection and testing as an area of focus.

2.4 Childhood tuberculosis

Children with TB usually have paucibacillary disease which is sputum smear-negative due to the size of the bacillary population being less than 10^4 colony-forming units (CFU)/mL and consequently contribute little to disease transmission within the community. The treatment of children with TB is therefore often not considered a priority by tuberculosis control programmes. Childhood TB is frequently more difficult to diagnose due to non-specific clinical and radiological features as opposed to adult TB cases that are often easily recognizable and accompanied by a positive sputum smear test.[13] However, children account for a major proportion of the global TB disease burden, especially in endemic areas.[14,15] An estimated 8.3 million new cases of TB was reported globally in 2000, of which 884 019 (11%) were children.[15] A common misconception is that children develop mild forms of TB and that severe disease manifestations are the exception. TB reportedly accounts

for 15% of all paediatric deaths in some Indian hospitals,[16] and a survey from Malawi reported a mortality of 17% in children diagnosed with TB.[17]

The diagnosis of childhood TB is complicated by the absence of a practical gold standard.[18,19] Sputum microscopy, often the only diagnostic test available in endemic areas, is positive in <10-15 % of children with suspected tuberculosis, and culture yields are also low in children (<30-40%)[19,20] resulting in smear-negative results. Most cases of childhood TB are paucibacillary, and therefore mycobacterial culture of specimens is required to optimise diagnostic yield, which can take weeks.[21] This has important implications for a disease that progresses rapidly in young children, with associated morbidity and mortality.[13,20]

The major advantages of obtaining microbiological confirmation are the ability to make a definitive diagnosis and to perform drug susceptibility testing to exclude DR-TB. Increasing occurrence of MDR-TB and XDR-TB highlights the importance of this information in order to guide appropriate therapy.[13]

2.5 Diagnosis of tuberculosis

Despite the enormous global burden of tuberculosis, case detection continues to be a problem.[2] Conventional TB diagnosis continues to rely on sputum smear microscopy, culture, the tuberculin skin test, and chest radiography. Although these tests have been used for nearly a century, they have several limitations and perform poorly in populations affected by the HIV epidemic.[22] Major advances have been made with the introduction of several new diagnostic techniques for TB to diagnose latent tuberculosis infection (LTBI), active pulmonary disease and extrapulmonary tuberculosis. Rapid and accurate diagnosis of symptomatic patients remains a cornerstone of global tuberculosis control strategies.[23]

2.5.1 Latent tuberculosis infection

Although much remains unknown about its pathophysiology, latent tuberculosis infection (LTBI) is a continuum between self-cure and asymptomatic, yet active tuberculosis disease (TB).[6] LTBI is classically defined as a measurable immune sensitization to *Mtb* in the absence of active disease manifestations, such as fever, chills, night sweats, weight loss, cough, haemoptysis, or a new opacity on the patient's chest radiograph. However, direct identification of LTBI is not possible. The diagnostic tests used to identify individuals latently infected with *Mtb*, namely the *in vivo* tuberculin skin test (TST) and the *ex vivo* interferon-γ release assays (IGRAs), are designed to identify an adaptive immune response against, but not necessarily a latent infection with *Mtb*. In other words, a person may show a positive TST or IGRA result due to an adaptive immune response to *Mtb* antigens that persist in the absence of live mycobacteria.[5]

(a) Tuberculin skin test

The *in vivo* tuberculin skin test (TST) uses a mixture of antigens obtained from *Mtb* and *Mycobacterium bovis* bacillus Calmette-Guérin (BCG) as a protein precipitate from the supernatant of liquid cultures of *Mtb*.[24] The two major techniques used are the Mantoux test and the multi-puncture technique. The Mantoux test, which uses 5-10 tuberculin units of purified protein derivative (PPD), involves the intradermal injection of the PPD solution into the most superficial layer of the skin on the patient's forearm. The reaction is measured as millimetres of induration,[25] in other words: if a hard, raised red bump appears within 48 to 72 hours, it means the patient is likely to be infected with *Mtb*.

However, false-positive reactions can occur if the patient has recently been vaccinated with BCG, an attenuated strain of *M. bovis*, which leaves an immunological imprint for a prolonged period of time.[26] The sensitivity of the TST is also compromised in individuals with immunosuppression due to disease or treatment.[5] False-negative tests often occur in children, the elderly, HIV infected people or people with active tuberculosis.[25-27] Other reasons could include people who have recently been infected with TB, but whose immune systems haven't yet reacted to the bacteria.[27]

(b) Interferon-γ release assay

The interferon-γ release assays (IGRAs) have been developed as an alternative immunodiagnostic approach to the TST for detecting *Mtb* infection.[28,29] These tests are designed to identify a memory of an adaptive immune response against mycobacterial antigens.[24] IGRAs are based on the *ex vivo* detection of interferon-gamma (IFN-γ) released from pre-sensitized *Mtb*-specific T-cells in response to two immunodominant secreted proteins: early secretory antigen target-6 (ESAT-6) and culture filtrate protein 10 (CFP-10).[5,24] T-cell responses to these antigens are absent from BCG[30] and most environmental mycobacteria,[31] making IGRAs a more specific immune marker of *Mtb* infection than the TST.[26]

Until recently, the tuberculin skin test was the only test available for detecting LTBI, but three new T-cell-based tests for diagnosing latent TB infection have been developed. These IGRAs are now commercially licenced, namely the T-SPOT.TB test (Oxford Immunotec Ltd, Abingdon, UK), based on the *ex vivo* 16-20h enzyme-linked immunospot (ELISpot) assay developed by Lalvani; the QuantiFERON (QFT)-TB Gold (Cellestis, Carnegie, Australie) and QuantiFERON-TB Gold in-tube (Cellestis), which are both based on the 16-24 h whole blood enzyme-linked immunosorbent assays (ELISA), which measures the antigen-specific production of IFN-γ by circulating T-cells in whole blood. Although only one patient visit is required for these testing methods, disadvantages include the high material cost, the need for an equipped laboratory, and a requirement to draw blood with subsequent careful handling to maintain the viability of the lymphocytes.[26] The accurate diagnosis of LTBI is hampered by the absence of a gold standard for LTBI due to the use of small samples with a widely varying likelihood of true positive and false-positive test results. Furthermore, IGRAs performed on children, immune-compromised persons, and the elderly show insufficient specificity.[26]

2.5.2 Active pulmonary disease

Traditionally, the diagnosis of active pulmonary disease has been based on radiological findings on chest X-rays, smear microscopy and culture.[23]

(a) Radiology

A positive skin test is often followed by a chest X-ray or a CT scan, which may show white spots on the patient's lungs where the immune system has walled off TB bacteria. High-resolution CT is more sensitive than conventional radiography for detecting TB because it provides more detailed images than X-rays.[32] Normal chest radiographic findings are not always that reliable and may only be seen in up to 15% of patients with proven TB.[33]

Although pulmonary tuberculosis almost always shows abnormalities on the chest X-ray,[34] radiological diagnosis alone can only be presumptive since the diagnostic criteria are non-specific.[35] Furthermore, almost one-fourth of all TB cases are extrapulmonary and in such cases X-rays are of limited use.[36]

(b) Sputum microscopy and sputum culture

Sputum smear microscopy and sputum culture have been advocated as two useful tools for the diagnosis of active pulmonary TB. The culture for acid-fast bacilli (AFB) takes 6-8 weeks to be interpretable as positive or negative results, which limits the usefulness of culture as a first-line diagnostic test. Under these circumstances, sputum smear microscopy examination for the detection of AFB is the most useful test. However, the AFB smear microscopy examination has a sensitivity of only 50-60%,[37] since a positive smear requires 5 000 – 10 000 AFB per µL sputum sample.[38] Sputum culture, on the other hand, requires only 10 – 100 AFB per µL[39,40] and can detect pulmonary TB in 80% of true cases.[41]

For the diagnosis of TB to be effective, clinical samples are examined for acid-fast bacilli using the Ziehl-Neelsen (ZN) stain. Up to 70% of culture positive samples with a lower limit of detection of 5 x 10^3 organisms/mL can be detected by microscopy. Auromine and rhodamine are but two of the newer fluorochrome stains available that are superior to the ZN stain due to their ease of use and rapid results.[42] However, young children with pulmonary TB rarely produce sputum due to insufficient lung capacity, which leads to the use of gastric lavage to produce gastric samples. Gastric lavage is an uncomfortable and invasive procedure, and yields a positive ZN stain result in less than 20% of children with proven TB, compared to 75% in adults.[43]

2.6 Diagnosis of paediatric tuberculosis

The accurate diagnosis of childhood tuberculosis proves to be more difficult than the diagnosis of tuberculosis in adults. Furthermore, inadequate health information systems in developing countries and the lack of importance attributed to childhood tuberculosis by control authorities contribute to this burden.[25] Childhood tuberculosis is commonly extrapulmonary, disseminated and severe, especially in children younger than 3 years and is associated with high morbidity and mortality.[44] The diagnosis of TB in children is traditionally based on chest radiography, the tuberculin skin test, and mycobacterial staining/culture, although these methods are not always reliable. Newer methods, such as PCR and immune-based methods are increasingly being used but are not widely available and have a limited role in routine clinical practice. Short-course, multi-drug treatment has been adopted as standard therapy for adults and children with tuberculosis, with or without directly observed therapy. MDR-TB, although uncommon in children, is also increasing and involves longer treatment courses of therapy with second-line anti-tuberculosis drugs.[25]

Difficulty in early diagnosis of paediatric tuberculosis and the progression from infection to disease, which occurs more rapidly in children,[25] proves to be a hurdle yet to be bridged. Children who develop active TB often do so within several months after initial infection and, since infection is usually recent, prompt diagnosis and treatment of asymptomatic infection is essential.

The gold standard for the diagnosis of active pulmonary disease is a positive *Mtb* culture from a clinical specimen. Such specimens are however difficult to obtain from children since they mostly develop extrapulmonary TB that requires invasive specimen collection procedures. Furthermore, children younger than 5 years with pulmonary TB rarely produce sputum.[24] Even when specimens are obtained from children, fewer than 20% are smear positive for AFB[43] and culture results are frequently negative and usually too late to effect initial management. Without accurate diagnostic tools for children, both underdiagnosis and overdiagnosis are common.[45] The advantage of obtaining microbiological confirmation is the ability to make a definite diagnosis. Optimum methods for specimen collection are discussed below.

2.6.1 Specimen collection methods

Since young children are frequently unable to expectorate, additional procedures are often required to obtain samples from the lower respiratory tracts. For many years the collection of three consecutive early morning gastric lavage (GL) or gastric aspirate (GA) samples has been the accepted method for attempting microbiological confirmation. However GL is unpleasant and relatively invasive with low yields for *Mtb*.[46] A number of less invasive alternative methods have been proposed, including induced sputum (IS), nasopharyngeal aspiration (NPA) and the string test.

(a) Induced sputum

This technique involves the administration of an inhaled bronchodilator followed by nebulised hypertonic (3-5%) saline and then nasopharyngeal aspiration or expectoration of mucus from the lower respiratory tract. This method is safe to use and satisfactory yields are obtainable in most cases, with one IS sample providing the same yield as three sequential GL samples.[47] This has shifted clinical practice to include induced sputum as a specimen collection procedure in young children and infants with suspected pulmonary TB.

(b) Nasopharyngeal aspiration

Nasopharyngeal aspiration (NSA) entails suctioning of the nasopharynx to sample upper respiratory tract secretions. Since passing a nasal cannula elicits a cough reflex in many children, NPA may be regarded as a form of sputum induction.[48] Stimulation of the cough reflex may include lower respiratory secretions. This procedure is relatively non-invasive and yields are similar to that of IS.[49]

(c) String test

The string test was first evaluated as a sampling method for TB in HIV-infected adults with suspected TB. Patients are asked to swallow a gelatine capsule containing a coiled nylon string which unravels as the capsule descends into the stomach. After 4 hours the string is removed and used for mycobacterial culture with yields similar to IS. Although the test proved successful in adults, it is unlikely to be feasible in young children (<2 years) who account for a high proportion of TB cases in some settings.[50]

The samples collected in any of the before mentioned methods can be used for TB diagnosis using sputum smear microscopy or culture as detection methods. Due to the low culture yields of these methods (10-24%)[13], the search is still on for improved specimen collection methods as well as better diagnostic techniques. The development of a substrate that could concentrate bacilli, more specifically *Mtb*, in low yield samples could drastically improve the timely diagnosis of TB in young children with paucibacillary disease. In order to achieve this, chemical groups must be identified that will facilitate the binding and concentration of these bacilli onto the substrate. These chemical groups should enable interaction with surface structures on the outer cell surface of *Mtb* for mycobacterial binding onto the polymer substrate.

2.7 *Mycobacterium tuberculosis*

Mycobacterium tuberculosis (*Mtb*) is the causative agent of TB in humans. It is a fairly large nonmotile rod-shaped bacterium with an average length of 2-4 µm and width of 0.2-0.5 µm. *Mtb* is

an obligate aerobe, which is why its complexes are commonly found in the well-aerated upper lobes of the lungs. The bacterium is a facultative intracellular parasite, usually of macrophages, and replicates within 15-20 hours. Its slow generation time is a physiological characteristic that may contribute to its virulence.[38]

Mycobacterium species are classified as acid-fast bacteria due to the impermeability of their cell walls by certain dyes and stains. They do, however, retain dyes once stained. The Ziehl-Neelsen[51] staining method is a commonly used characterization technique that uses carbol-fuchsin (a pink dye) to stain the mycobacteria before decolourizing the fixed *Mtb* smear with acid-alcohol. The smear is subsequently counterstained with methylene-blue, resulting in the acid-fast bacilli appearing pink in a contrasting background as exemplified in Figure 2.1.[38]

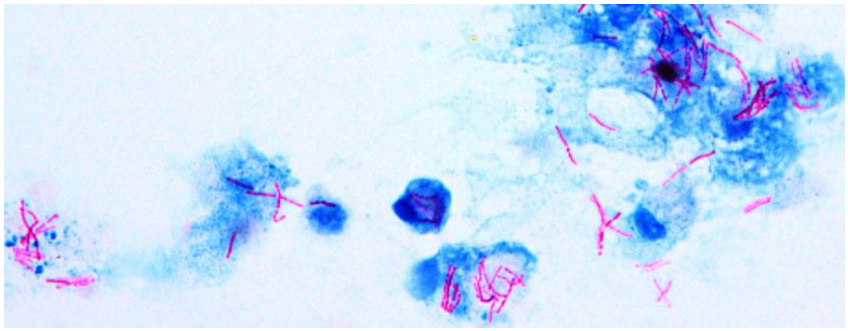

Figure 2.1 Acid-fast staining image of Mtb using the Ziehl-Neelsen stain, carbol-fuchsin.

The mycobacterial cell wall is a complex structure that is required for cell growth, resistance to antibiotics and virulence.[52-54] It is composed of three distinct macromolecules, namely peptidoglycan, arabinogalactan and mycolic acids, which are surrounded by a non-covalently linked outer capsule of proteins and polysaccharides[51-53,55] Refer to Figure 2.2 for a schematic illustration of the cell wall. The mycobacterial cell wall mainly consists of hydrophobic mycolic acids, contributing to the following properties of the bacterium:

- Impermeability to stains and dyes
- Resistance to many antibiotics
- Resistance to killing by acidic and alkaline compounds
- Resistance to osmotic lysis via complement deposition
- Resistance to lethal oxidations and survival inside the macrophages[38,52]

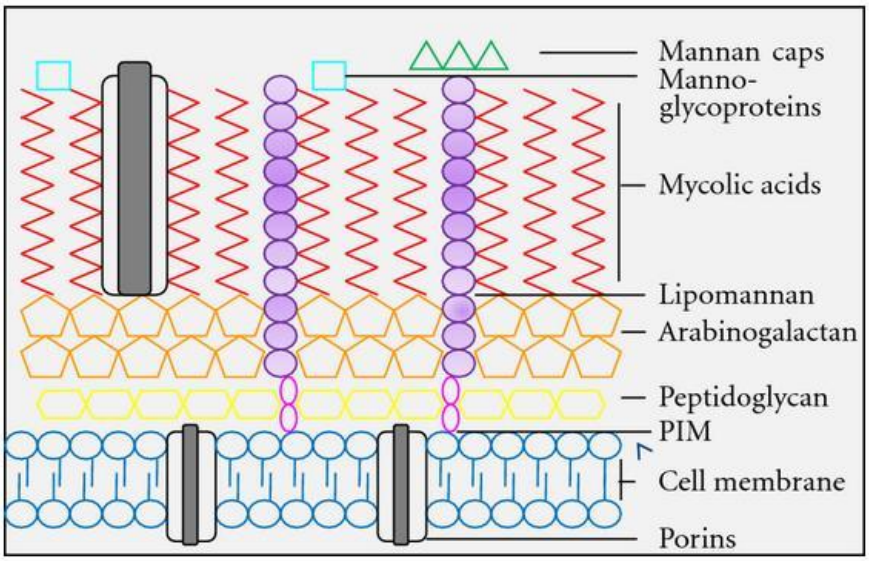

Figure 2.2 The structure of the Mycobacterium tuberculosis cell wall.[56]

The mycolic acids are distributed as a thick layer mostly at the external portions of the cell wall, while the internal layers of mycobacteria consist mostly of arabinogalactan, phosphatidyl-*myo*-inositol mannosides (PIMs) and peptidoglycans (Figure 2.2).[57] Next to the mycolic acid layer, other components include mannose-containing biomolecules including mannose-capped lipoarabinomannan (Man-LAM), the related lipomannan (LM) and mannoglycoproteins. Man-LAM, one of the most abundant mannans present on the cell surface, is an important virulence factor for *Mtb*.[58] Mannan and arabinomannan are present on the surface and form the outer capsule of this bacterium. Man-LAM, LM and PIMs all share a conserved mannosyl-phosphatidyl-*myo*-inositol (MPI) domain that presumably anchors the structures into the plasma membrane.[59]

Based on the *Mtb* cell wall structure, various chemical compounds can be used as modification agents on the polymer substrate to enable the binding and concentration of *Mtb* for imporved specimen collection.

2.8 Polymers

Styrene and maleic anhydride are known to produce alternating copolymers[60,61] that have been used in a variety of applications.[62] Whereas maleic anhydride (MAnh) does not homopolymerize under mild reaction conditions due to the monomer being a strong electron acceptor,[63] it does copolymerize with styrene, forming a strongly alternating copolymer.[64] The resulting styrene-maleic anhydride copolymer (SMA) was chosen as parent polymer for this study due to its ease of synthesis,[65]solubility in a variety of solvents and reactive anhydride functional groups that can easily undergo imidization,[66] esterification[67] and hydrolysis. It is thus fitting to use SMA as the polymer backbone for modification via imidization.

In this study, SMA was synthesized and modified with various *N*-alkylamine compounds before electrospinning these derivatives into nanofibrous substrates. These compounds have the simple formula as schematically illustrated in Figure 2.3 in which R is selected to impart hydrophobic, ionic or polar characteristics to the polymer backbone. The goal was to synthesize polymers with an affinity for the cell wall of *Mtb* so that the polymer substrates can function as capturing surfaces for *Mtb*.

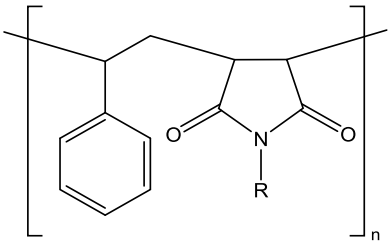

Figure 2.3 Representative structure of SMA copolymer derivatives.

Some of the modification agents that were chosen to modify SMA with have a known affinity for *Mycobacterium tuberculosis*[68] and should facilitate interaction with the *Mtb* cell wall, whereas others have been chosen based on possible affinity for the mycobacterial cell wall. The most preferred substituents R are quaternary ammonium compounds, phenol and tertiary amines.[69] Concanavalin A, a mannose binding lectin,[70] has also proved its affinity to bind with the mannose terminals of the BCG strain when the protein was covalently bound to SMA nanofibers and was also investigated in this study. Refer to Figure 2.4 for the various modification agents used in this study.

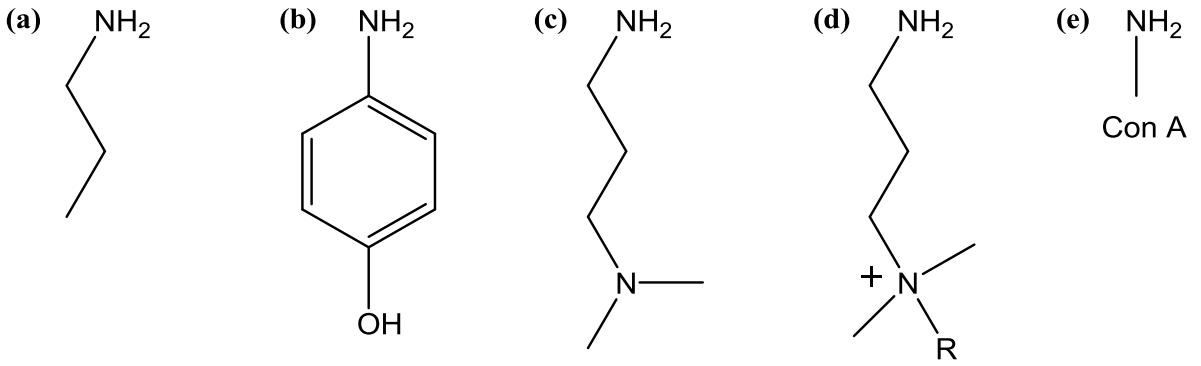

Figure 2.4 Modification agents for the synthesis of styrene maleimide copolymer derivatives: (a) propylamine, (b) 4-aminophenol, (c) 3-(N,N-dimethylamino)-1-propylamine, (d) quaternary ammonium alkyl conjugates and (e) Concanavalin A.

2.9 Electrospinning

Electrospinning is a straightforward, convenient and inexpensive method that allows for the production of continuous fibers with submicron diameters.[71] It is a simple and versatile technique and can produce nanofibers from various polymers within a short time.[72] A syringe containing the polymer solution is connected to a syringe pump to ensure a constant flow rate of the solution through a blunt needle tip. A high-voltage is applied to the polymer-filled syringe using an electrode. The electrode induces a charge on the surface of the polymer droplet. Electrospinning occurs when a

charged polymer solution, possessing sufficient polymer chain entanglements, emits a charged fluid jet in the presence of an applied electric field. The charged polymer jet emanates from a suspended droplet emerging from the needle tip as soon as a Taylor cone forms, which is when the mutual electrostatic charges overcome the surface tension of the droplet.[73] The path of the ejected jet is straight for several millimetres from the Taylor cone, and then the jet enters a region of instability where it undergoes a whipping process. During this whipping process electrical forces bend and stretch the jet significantly during this spiralling trajectory[74] resulting in a continuous decrease of the jet diameter. In combination with solvent evaporation, the electrospinning process result in dry fibers in the nanometer range being deposited onto the collector plate.[75,76] Refer to Figure 2.5 for a schematic illustration of the electrospinning setup.

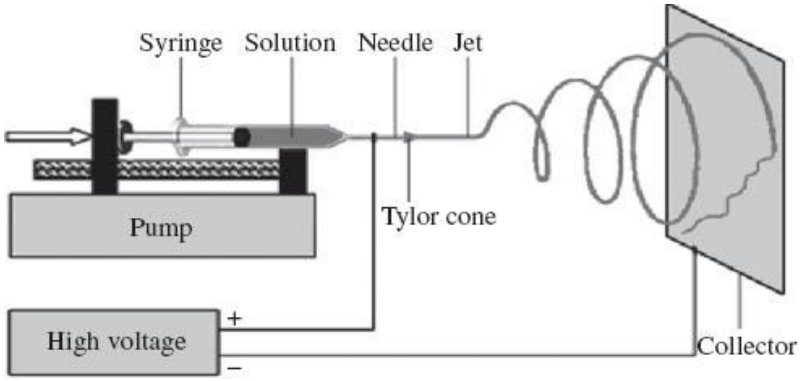

Figure 2.5 Horizontal electrospinning setup.[77]

Nanofibers possess an inherently large specific surface area, rendering them useful in a variety of applications such as tissue engineering scaffolds[76], filtration devices,[78] protective clothing, controlled drug delivery platforms and affinity membranes.[79]

Another application involves the immobilization of proteins, since the electrospun mats may provide a higher loading of proteins per unit mass of nanofibrous support.[80,81] The reduction of the size of carrier materials can effectively improve the efficiency of immobilized proteins.[81] The use of nanofibers to immobilize proteins seems to overcome several limitations often encountered when using other support materials such as membranes, gel matrices, porous particles or nanoparticles.[81] Incorporating Concanavalin A onto polymer nanofibers could therefore provide an affinity membrane that could act as capturing platform for *Mtb* to concentrate bacilli from sputum samples to be used in further diagnostic methods such as sputum smear microscopy or culture.

The structure and morphology of the electrospun fibers depend on a variety of system and process parameters such as viscosity, polymer concentration, solvent effect, spinning distance and voltage application. Electrospun fibers often have beads as "by products"[82] and the formation of beaded fibers have been observed widely.

Various system parameters such as viscosity, molecular weight, surface tension and solvents of the polymer solution affect the electrospinning process and will be discussed in short.

(a) Viscosity

The viscosity of a polymer solution is strongly influenced by its concentration, where an increase in concentration generally leads to an increase in viscosity. The viscosity should be high enough and in synergy with the electrostatic repulsion to overcome the forces due to the surface tension. A certain level of viscosity must be maintained to be stretched by the viscous drag during the electrospinning process. If not, fibers would break up at a rate faster than the solidification of the stretched fiber, resulting in beaded fibers.[82]

There are four different concentration categories for polymer solutions:

(a) Dilute
(b) Semidilute unentangled
(c) Semidilute entangled
(d) Concentrated

The critical chain overlap concentration (C*) is marked by the transition from dilute to semidilute unentangled, where the individual chains, which were initially separated by solvent molecules (a) now begin to overlap even though they still remain largely unentangled (b). With an increase in polymer concentration, the chain overlapping increases even more. Chain entanglement is crucial for fiber formation and thus electrospinning. This transition between (b) and (c) is known as the entanglement concentration (C_e) and is marked by the topological constrains of the polymer chains, resulting in entanglement. At concentrations exceeding C_e smooth, bead-free fibers are produced.[83,84] Viscosity is therefore concentration dependant and the latter should be adjusted accordingly to obtain smooth, bead free nanofibers.

(b) Surface tension

With the application of an electric field to low molecular weight compounds, an electrically driven jet undergoes capillary break-up into droplets that is driven by surface tension, a phenomena known as electrospraying.[85] Fong *et al*. [82] stated that surface tension drives towards the formation of beads, hence reduced surface tension favours the formation of fibers without beads. Therefore, as the molecular weight of the polymer solution is increased (and consequently the viscosity), the beads become bigger, the average distance between the beads becomes longer, the fiber diameter increases and the shape of the beads changes from spherical to spindle-like. A further increase in polymer solution is accompanied by the formation of smooth, bead-free fibers.

(c) Molecular weight and molecular weight distribution

Gupta *et al*. [83] investigated the influence of molecular weight (MW) and molecular weight distribution (MWD) on the electrospinning process and the morphology of the fibers obtained,

which is governed by an interplay with the surface tension. They found that polymers with a higher MW favoured the formation of bead free fibers due to the topological constraints caused by the increased viscosity. In other words, the polymer chains occupied a larger hydrodynamic volume that tends to resist the contraction of the jet due to surface tension. Therefore, polymer chain overlap for low MW polymers is barely sufficient to induce fiber formation at a concentration where the higher MW analogue would produce bead free fibers.

The effect of MWD has also been studied by Gupta *et al*.[83] Polymer droplets and some thin and discontinuous beaded fibers were observed to form when solutions corresponding to a broad MWD and high MW were electrospun. They hypothesized that in a narrow MWD (Đ = 1.00), all the polymer chains in solution have the same hydrodynamic volume.

(d) Solvent effect

In the electrospinning process, solvent is one of the main contributors to solution properties such as conductivity. Wannatong *et al*.[86] investigated the effect of six solvents with different properties (e.g. density, boiling point, solubility parameter, dipole moment and dielectric constant) on the morphology of electrospun polystyrene (PS) fibers. They found that fiber diameters decreased with increasing density and boiling points of the solvents. Beaded fibers were obtained if the solubility parameters of PS and the solvent differed greatly. The productivity of the fibers (number of fiber webs formed per unit area per unit time) increased with increasing dielectric constant and dipole moment of the solvent. Among the solvents that they studied, dimethylformamide (DMF) was found to be the best solvent that provided PS fibers with the highest productivity and optimal morphological characteristics.

The evaporation rate of a polymer solution in a high boiling point solvent can be increased and subsequently improved by adding a low boiling point solvent, e.g. adding ethanol (low boiling point) to a polyethylene oxide (PEO) in water (high boiling point) solution,[82,87,88] it prevented the formation of beaded fibers. Another example where using a mixed solvent system was found to be superior to a single solvent system was when dichloromethane and DMF was used for the solution of biodegradable poly(*p*-dioxanone-*co*-L-lactide)-block-poly(ethylene glycol) copolymer, instead of using just one of the two solvents. [89]

2.10 Conclusion

To conclude, this chapter discussed the various diagnostic approaches to paediatric TB and highlighted the difficulties in obtaining suitable samples from young children with suspected TB infection. Briefly, improved specimen collection methods were discussed, but the lack of a gold standard to correctly diagnose children with TB remains a challenge. The gold standard for the diagnosis of active pulmonary disease is a positive *Mtb* culture from a clinical specimen. However, children younger than 5 years with pulmonary TB rarely produce sputum.[24] Even when specimens

are obtained from children, fewer than 20% are smear positive for AFB[43] and culture results are frequently negative and usually too late to effect initial management. Without accurate diagnostic tools for children, both underdiagnosis and overdiagnosis are common.[45]

A polymer, SMA, has been identified to undergo modification with suitable chemical moieties for increased affinity between the modified polymer and the cell wall of *Mtb* to act as *Mtb*-capturing platforms. Electrospinning was chosen as technique to produce polymer nanofibers with a high surface to volume ratio in order to increase the area available for binding to *Mtb*.

In summary, the production of modified nanofibers with chemical moieties that can facilitate affinity binding to *Mtb* could concentrate bacilli in samples to be used in existing microscopy protocols for the accurate and timely diagnosis of TB in children.

2.11 References

1. Jacobs W.R. *HS Talks: Biomedical & Life Sciences Collection* **2009**, 2-4.

2. Baddeley, A; *et al*. *WHO Report: Global tuberculosis report* **2014***,* 17-23.

3. Raviglione, M.C.; Snider, D.E.; Kochi, A.G. *JAMA*. **1995,** *3*, 220-226.

4. Hartman-Adams, H.; Clark, K.; Juckett, G. *Am. Fam. Phys*. **2014**, *11*, 889-896.

5. Mack, U.; Migliori, G.B.; Sester, M.; *et al*. *Eur. Respir. J*. **2009**, *33*, 956-973.

6. Salgame, P.; Geadas, C.; Collins, L.; Jones-López, E.; Ellner, J.J. *Tuberculosis* **2015**, *95*, 373-384.

7. Dannenberg, Jr. A.M. *Immunobiology* **1994**, *191*, 461-473.

8. Riley, R.L. *Am. Rev. Tuberc*. **1957**, *76*, 931-941.

9. Smith, D.W.; Wiegeshaus, E.H. *Rev. Inf. Dis*. **1989**, *11*, S385-S393.

10. Mosser, D.M. *J Leukoc. Biol*. **2003**, *73*, 209-212.

11. Khan, E.A.; Starke, J.R. *Emerg. Infect. Dis*. **1995**, *1*, 115-123.

12. Ghandi, N.R.; Moll, A. *Lancet* **2006**, *368*, 1575-1580.

13. Nicol, M.P.; Zar, H.J. *Paediatr. Resp. Rev*. **2011**, *12*, 16-21.

14. Nelson, L.J.; Wells, C.D. *Sem.Pediatr. Inf. Dis.* **2004**, *15*, 150-154.

15. Nelson, L.; Wells, C. *Int. J. Tuberc. Lung Dis*. **2004**, *8*, 636-647.

16. Mubarik, M.; Nabi, B.; Ladakhi, G.; Sethi, A. *Jk. Prac*. **2000**, *7*, 12-15.

17. Harries, A.; Hargreaves, N.; Graham, S.; *et al*. *Int J.Tuberc. Lung Dis*. **2002**, *6*, 424-431.

18. Starke, J. *Chest* **1993**, *104*, 329-330.

19. Eamranond, P.; Jaramillo, E. *Int. J. Tuberc. Lung Dis*. **2001**, *5*, 594-603.

20. Starke, J.R. *Tuberculosis* **2003**, *83*, 208-212.

21. Graham, S.M. *Lancet Infec. Dis*. **2010**, *10*, 581-582.

22. Pai, M.; O'Brien, R. *Semin. Respir. Crit. Care. Med*. **2008**, *29*, 560.

23. Butt, T.; Ahmed, R.; Kazmi, S.Y.; Afzal, R.K.; Mahmood, A. *J. Coll. Phys. Surg. Pak*. **2003**, *13*, 728-734.

24. Lalvani, A.; Millington, K.A. *Curr. Opin. Infect. Dis*. **2007**, *20*, 264-271.

25. Shingadia, D.; Novelli, V. *Lancet* **2003**, *3*, 624-632.

26. Menzies, D.; Pai, M.; Comstock, G. *Ann. Intern. Med*. **2007**, *146*, 340-W88.

27. Cohn, D.L.; O'Brien, R.J.; Geiter, L.J.; Gordin, F.; Hershfield, E.; Horsburgh, C. *MMWR Morb. Mortal Wkly. Rep*. **2000**, *49*, 1-54.

28. Lalvani, A.; Pathan, A.A.; Mcshane, H.; *et al*. *Am. J. Resp. Crit. Care Med*. **2001**, *163*, 824-828.

29. Mori, T.; Sakatani, M.; Yamagishi, F.; *et al*. *Am. J. Resp. Crit. Care Med*. **2004**, *170*, 59-64.

30. Mahairas, G.G.; Sabo, P.J.; Hickey, M.J.; Singh, D.C.; Stover, C.K. *J Bacteriol*. **1996**, *178*, 1274-1282.

31. Harboe, M.; Oettinger, T.; Wiker, H.G.; Rosenkrands, I.; Andersen, P. *Infect. Immun*. **1996**, *64*, 16-22.

32. Burrill, J.; Williams, C.J.; Bain, G.; Conder, G.; Hine, A.L.; Misra, R.R. *Radiographics* **2007**, *27*, 1255-1273.

33. Woodring, J.H.; Vandiviere, H.M.; Fried, A.M.; Dillon, M.L.; Williams, T.D.; Melvin, I.G. *AJR Am. J. Roentgenol*. **1986**, *146*, 497-506.

34. American Thoracic Society. *Am. J. Respir. Crit. Care Med*. **2000**, *161*, 1376-1395.

35. Haas, D. *Prac. Infec. Dis*. **2000**, *4*, 2576-2607.

36. Ahmed, M.; Aziz, S. *J. Pak. Med. Assoc.* **1998**, *48*, 183-184.

37. Aber, V.R.; Allen, B.W.; Mitchison, D.A.; Ayuma, P.; Edwards, E.A.; Keyes, A.B. *Tubercle* **1980**, *61*, 123-133.

38. Todar, K. *Onl. Textb. Bact*. **2011**, 1-4.

39. Parry, C.M. *Trop. Doct*. **1993**, *23*, 145-146.

40. Kim. T.C.; Blackman, R.S.; Heatwole, K.M.; Kim, T.; Rochester, D.F. *Am. Rev. Respir. Dis*. **1984**, *129*, 264-268.

41. Levy, H.; Feldman, C.; Sacho, H.; Van der Meulen, H.; Kallenbach, J.; Koornhof, H. *Chest* **1989**, *95*, 1193-1197.

42. Ba, F.; Rieder, H. *Int. J. Tuberc. Lung Dis*. **1999**, *3*, 1101-1105.

43. Strumpf, I.J.; Tsang, A.Y.; Sayre, J.W. *Am. Rev. Respir. Dis*. **1979**, *119*, 599-602.

44. Marais, B.J.; Gie, R.P.; Schaaf, H.S.; Beyers, N.; Donald, P.R.; Starke, J.R. *Am. J. Resp. Crit. Care Med*. **2006**, *173*, 1078-1090.

45. Coovadia, H.; Jeena, P.; Wilkinson, D. *Int. J. Tuberc. Lung Dis*. **1998**, *2*, 844-851.

46. Palme, I.B.; Gudetta, B.; Bruchfeld, J.; Eriksson, M.; Giesecke, J. *Acta. Paediatrica* **2004**, *93*, 311-315.

47. Zar, H.J.; Hanslo, D.; Apolles, P.; Swingler, G.; Hussey, G. *Lancet* **2005**, *365*, 130-134.

48. Franchi, L.M.; Cama, R.I.; Gilman, R.H.; Montenegro-James, S.; Sheen, P. *Lancet* **1998**, *352*, 1681-1682.

49. Owens, S.; Abdel-Rahman, I.E.; Balyejusa, S.; *et al*. *Arch. Dis. Child*. **2007**, *92*, 693-696.

50. Vargas, D.; García, L.; Gilman, R.H.; *et al*. *Lancet* **2005**, *365*, 150-152.

51. Hett, E.C.; Rubin, E.J. *Microbiol. Mol. Biol. Rev*. **2008,** *72*, 126-56.

52. Barry, C.E.; Crick, D.C.; McNeil, M.R. *Inf. Dis. Drug Targ*. **2007**, *7*, 182-202.

53. Kaur, D.; Guerin, ME.; Škovierová, H.; Brennan, PJ.; Jackson, M. *Adv. Appl. Microbiol*. **2009**, *69*, 23-78.

54. Bansal-Mutalik, R.; Nikaido, H. *Proc. Nat. Acad. Sci. (U S A)*. **2014**, *111*, 4958-4963.

55. Sani, M.; Houben, E.; Geurtsen, J.; *et al*. *PLoS. Pathog*. **2010**, *6*, 1-10.

56. Kleinnijenhuis, J.; Oosting, M.; Joosten, L.A.; Netea, M.G.; Van Crevel, R. *Clin. Dev. Immunol*. **2011**, *2011*, 1-12.

57. Torrelles, J.B.; Schlesinger, L.S. *Tuberculosis* **2010**, *90*, 84-93.

58. Strohmeier, G.R.; Fenton, M.J. *Microb. Infect*. **1999**, *1*, 709-717.

59. Briken, V.; Porcelli, S.A.; Besra, G.S.; Kremer, L. *Mol. Microbiol*. **2004**, *53*, 391-403.

60. Ha, N.T.H. *Polymer* **1999**, *40*, 1081-1086.

61. Ha, N.; Fujimori, K. *Acta. Polymerica* **1998**, *49*, 404-410.

62. Shulkin, A.; Stöver, H.D. *J. Membr. Sci*. **2002**, *209*, 421-432.

63. Trivedi, B.C.; Culbertson, B.M. *Maleic anhydride* **1982**, 239.

64. Hill, D.J.T.; O'Donnell, J.J.; O'Sullivan, P.W. *Progr. Pol. Sci*. **1982**, *8*, 215-275.

65. Jeong, J.; Byoun, Y.; Ko, S.; Lee, T.Y. *J. Ind. Eng. Chem.* **2001**, *7*, 310-315.

66. Vermeesch, I.; Groeninckx, G. *J. Appl. Polym. Sci*. **1994**, *53*, 1365-1373.

67. Hou, S.; Kuo, P.; *Polymer* **2001**, *42*, 2387-2394.

68. Cronje, L.; Warren, R.; Klumperman, B. *J. Mat. Chem. B.* **2012**, *48*, 6608-6618.

69. Bshena, O.; Heunis, T.D.J.; Dicks, L.M.T.; Klumperman, B. *Fut. Med. Chem.* **2011**, *3*, 1821-1847.

70. Scott, J.K.; Loganathan, D.; Easley, R.B.; Gong, X.; Goldstein, I.J. *Proc. Nat. Acad. Sci. (U S A)*. **1992**, *89*, 5398-5402.

71. Reneker, D.H.; Chun, I. *Nanotechnology* **1996**, *7*, 216.

72. Kim, B.C.; Nair, S.; Kim, J.; *et al*. *Nanotechnology* **2005**, *16*, S382.

73. Wilm, M.S.; Mann, M. *Int. J. Mass Spec. Ion Proc*. **1994**, *136*, 167-180.

74. Reneker, D.H.; Yarin, A.L.; Fong, H.; Koombhongse, S. *J. Appl. Phys*. **2000**, *87*, 4531.

75. Yao, L.; Haas, T.W.; Guiseppi-Elie, A.; Bowlin, G.L.; Simpson, D.G.; Wnek, G.E. *Chem. Mat*. **2003**, *15*, 1860-1864.

76. Matthews, J.A.; Wnek, G.E.; Simpson, D.G.; Bowlin, G.L. *Biomacromolecules* **2002**, *3*, 232-238.

77. Mottaghitalab, V.; Farjad, M. *J. Pol. Eng*. **2013**, *33*, 857-873.

78. Qin, X.; Wang, S. *J. Appl. Polym. Sci*. **2006**, *102*, 1285-1290.

79. Kenawy, E.; Bowlin, G.L.; Mansfield, K.; *et al*. *J. Control. Rel*. **2002**, *81*, 57-64.

80. Huang, X.; Xu, Z.; Wan, L.; Innocent, C.; Seta, P. *Macromol. Rap. Comm*. **2006**, *27*, 1341-1345.

81. Jia, H.; Zhu, G.; Vugrinovich, B.; Kataphinan, W.; Reneker, D.H.; Wang, P. *Biotechnol. Prog*. **2002**, *18*, 1027-1032.

82. Fong, H.; Chun, I.; Reneker, D. *Polymer* **1999**, *40*, 4585-4592.

83. Gupta, P.; Elkins, C.; Long, T.E.; Wilkes, G.L. *Polymer* **2005**, *46*, 4799-4810.

84. Graessley, W.W. *Polymer* **1980**, *21*, 258-262.

85. Bailey, A.G. *Phys. Bull*. **1988**, *35*, 146.

86. Wannatong, L.; Sirivat, A.; Supaphol, P. *Polym. Int*. **2004**, *53*, 1851-1859.

87. Jaeger, R.; Schönherr, H.; Vancso, G.C. *Macromolecules* **1996**, *29*, 7634-7636.

88. Shin, Y.; Hohman, M.; Brenner, M.; Rutledge, G. *Polymer*. **2001**, *42*, 9955-9967.

89. Bhattarai, S.R.; Bhattarai, N.; Yi, H.K.; Hwang, P.H.; Cha, D.I.; Kim, H.Y. *Biomaterials* **2004**, *25*, 2595-2602.

Chapter 3: Synthesis, electrospinning and characterization of styrene maleimide copolymers

3.1 Introduction

Styrene maleic anhydride (SMA) copolymer is a very versatile intermediate polymer that can be easily functionalized with various low molecular weight compounds containing amine and hydroxyl groups.[1] These active agents can be covalently linked to SMA via ring-opening of the maleic anhydride residue.[2] In this chapter the initial coupling reaction of SMA with various primary amine compounds to obtain its maleimide derivatives (SMI) is detailed. One such derivative underwent further functionalization with various bromoalkane compounds of different chain lengths; yielding SMI quaternary ammonium alkyl conjugates (SMI-qC_x).

Electrospinning has been recognized as an efficient technique for the fabrication of polymer nanofibers with average diameters in the range of micro- to nanometers,[3,4] yielding fibers with a high specific surface area. The electrospinning process is driven by the electrical forces on free charges on the surface or inside a polymeric liquid.[5] Even though the SMI polymers were non-ionic, the SMI-qC polymers were modified to contain a quaternary ammonium moiety, resulting in a charged polymer chain. The selection of a suitable solvent or solvent system as the carrier of a particular polymer is fundamental for optimisation of the electrospinning process.[6] Many factors influence the morphology of the collected fibers, of which polymer concentration and choice of solvent are two of the main contributors.[4,6]

This chapter describes the synthesis and modification of SMA and its modified derivatives, and the characterization thereof using ^{1}H-NMR and ^{13}C-NMR spectroscopy. All synthesized and modified copolymers were utilized in the electrospinning process for producing nanofibers. The nanofibers were characterized using scanning electron microscopy (SEM) and attenuated total reflectance Fourier transform infrared spectroscopy (ATR-FTIR). IR was useful in determining the degree of chemical modification of the SMI-qC_x polymers. Brunauer-Emmett-Teller (BET) surface analysis was conducted to evaluate the available surface area of the nanofibrous substrate, and water contact angle measurements were conducted to evaluate the hydrophobic/hydrophilic nature of the nanofibrous substrates.

3.2 Synthesis of functionalized SMI nanofibers

3.2.1 Modification of SMA

It is well known that both styrene and maleic anhydride copolymerize in an alternating manner at temperatures below 90 °C,[7] yielding poly(styrene-*alt*-maleic anhydride) (SMA). SMA was synthesized using conventional radical copolymerization[1] to yield an alternating copolymer (M_w = 15 901 g/mol, $Đ$ = 2.15, MAnh content: 50%) (Figure 3.1).

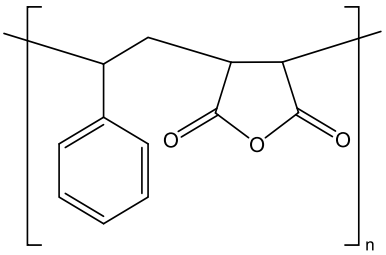

Figure 3.1 Repeating unit of SMA.

Due to its reactivity towards amines and alcohols, the anhydride moiety constitutes a versatile handle to modify the polymer.[8] The covalent attachment of primary *N*-alkylamine or *N*-arylamine compounds to SMA commences through a ring-opening reaction of the cyclic maleic anhydride moiety, resulting in the formation of carboxyl and amide groups.[2] This is a relatively fast and reversible step, followed by irreversible ring-closure that takes place at elevated temperatures,[9] yielding the imidization product poly(styrene-*alt*-maleimide) (SMI) that is stable in aqueous solution.[10,11] The equilibrium of this reaction is shifted towards the imide formation in the presence of an excess of the primary amine compound, at a temperature exceeding 140 °C and with the accompanying elimination of the condensation water.[12] The chemical modification of SMA via the imidization reaction is schematically illustrated in Scheme 3.1.

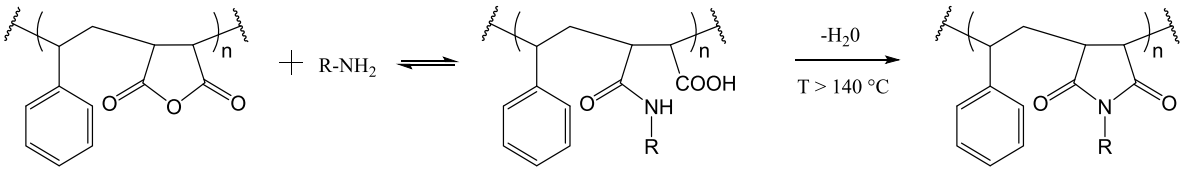

Scheme 3.1 Schematic representation of the imidization reaction.[13]

Three amino compounds, namely propylamine (Pr), 4-aminophenol (AP) and 3-(*N,N*-dimethylamino)-1-propylamine (DMAPA) were used for the modification of SMA. The nucleophilic addition of the commercially available primary amines occurred at room temperature in a suitable solvent, followed by heating under reflux at 170 °C to facilitate ring-closure.[9,13] After imidization, the corresponding maleimide copolymers were precipitated in diethyl ether or ethyl acetate and dried under vacuum for 24 hours. These modified SMI compounds were electrospun using suitable solvent systems. Further modification of SMA functionalized with DMAPA was achieved using bromoalkane compounds yielding the corresponding quaternary ammonium SMI polymers (SMI-qC_x), which were subsequently electrospun into nanofibrous mats using tetrahydrofuran (THF) and DMF as solvent.

(a) Synthesis of SMI-Pr

The ring-opening reaction of SMA with propylamine at room temperature in DMF followed by ring-closure at 170 °C yielded the corresponding poly(styrene-*N*-propylmaleimide) copolymer (SMI-Pr).[13,14] The polymer was cooled, precipitated in diethyl ether and dried under vacuum at 60 °C overnight to remove residual solvents. The net reaction is schematically illustrated in Scheme 3.2.

The resultant maleimide derivative was electrospun into nanofibers using a 1:2 solvent system of DMF and acetone.

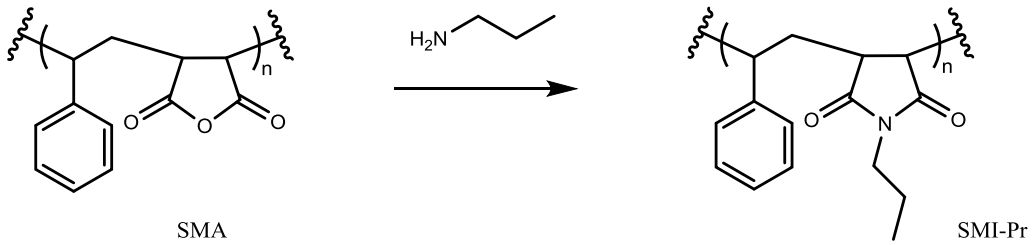

Scheme 3.2 Schematic illustration of the chemical modification of SMA with propylamine.

(b) Synthesis of SMI-AP

Similarly, the imidization reaction of SMA with an *N*-arylamine, namely 4-aminophenol, commenced at 170 °C in DMSO to yield the stable, ring-closed poly(styrene-*N*-[4-hydroxyphenyl] maleimide) (SMI-AP). The net reaction is schematically illustrated in Scheme 3.3. The resultant maleimide derivative was electrospun using a 1:1 solvent system of DMF and ethanol.

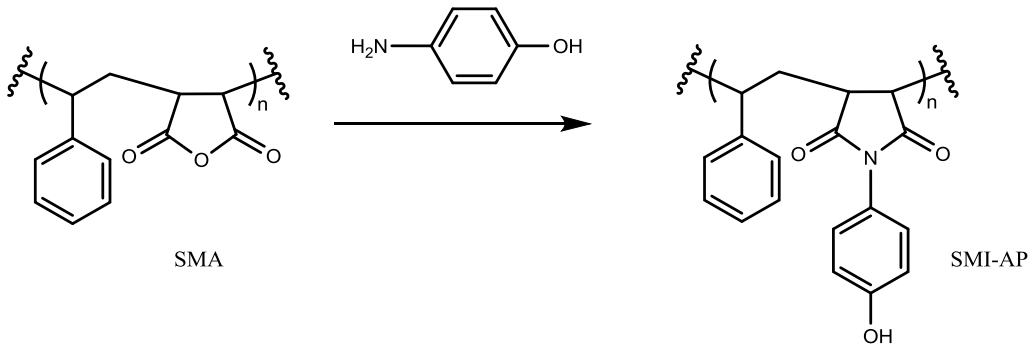

Scheme 3.3 Schematic illustration of the chemical modification of SMA with 4-aminophenol.

(c) Synthesis of SMI-tC

The preparation of styrene-[*N*-3-(*N',N'*-dimethylamino)propyl maleimide] copolymer (SMI-tC) entailed a straightforward imidization reaction of the maleic anhydride residues of SMA with 3-(*N,N*-dimethylamino)-1-propylamine in DMF at 170 °C. The synthesized polymer was electrospun using a 1:1 solvent system of DMF and ethanol. SMI-tC also served as precursor for the synthesis of its quaternized derivatives.[15] Refer Scheme 3.4 for the schematic illustration of the synthesis and modification of SMI.

(d) Synthesis of SMI-qC$_8$, SMI-qC$_{10}$, SMI-qC$_{12}$ and SMI-qC$_{14}$

SMI-qC$_8$ (Scheme 3.4 (a)), SMI-qC$_{10}$ (Scheme 3.4 (b)), SMI-qC$_{12}$ (Scheme 3.4(c)) and SMI-qC$_{14}$ (Scheme 3.4 (d)) were synthesized via the precursor polymer SMI-tC. Quaternization of the tertiary amine moiety with an excess of the bromoalkane compounds of various alkane chain lengths yielded the corresponding functionalized copolymers which were electrospun into nanofibers using a 1:1 solvent system of DMF and methanol.

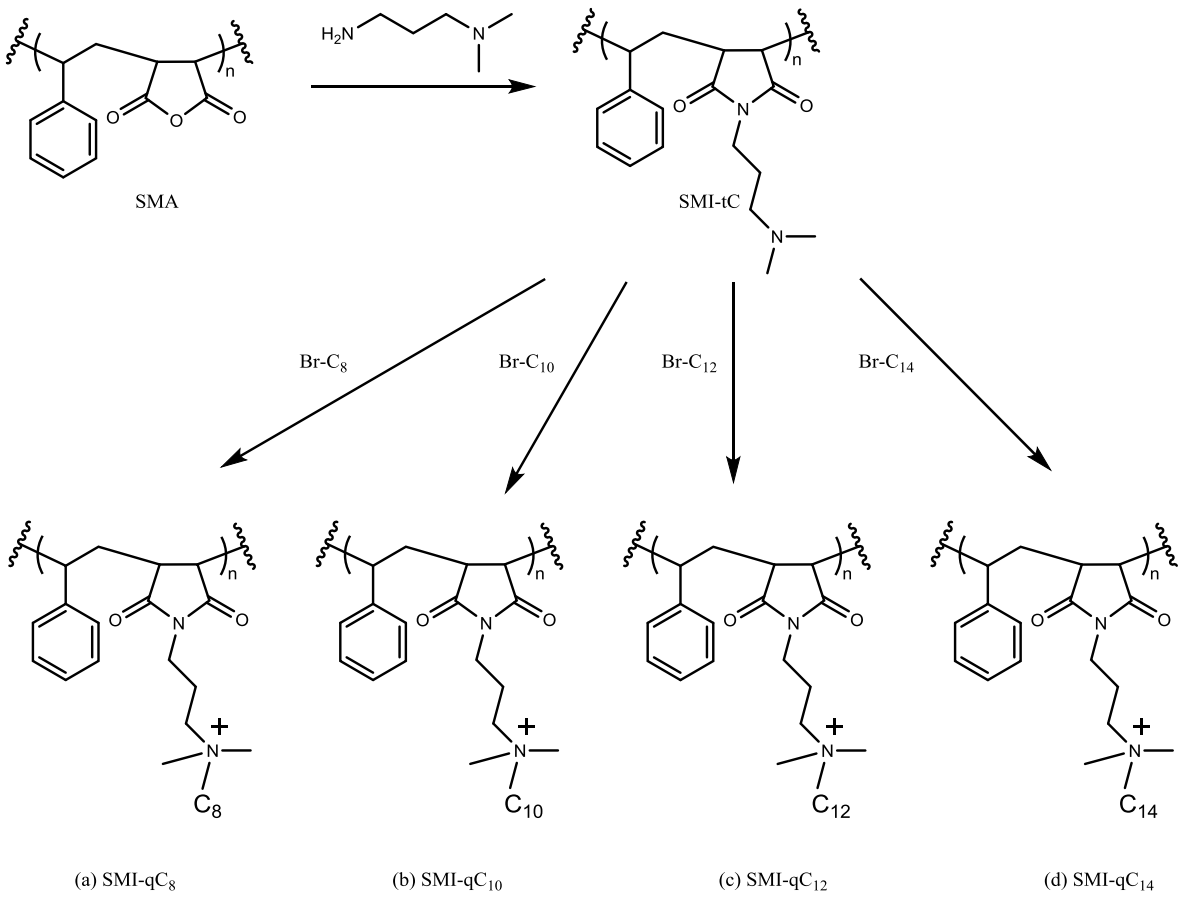

Scheme 3.4 Schematic illustration of the modification route followed to synthesize SMI-qC$_x$ polymers.

3.3 Electrospinning of functionalized polymers

Single needle electrospinning employs a syringe filled with polymer solution that can be charged by an electrode clamped to the needle tip and an oppositely charged collector plate, typically covered with foil. A syringe pump is set at a constant flow rate and initiates the formation of a droplet at the needle tip. Two opposing forces work in on the droplet, namely the electrostatic repulsive force caused by the same charge as introduced by the electrode and the polymer solution surface tension. The charge repulsion force will aim to expand the surface area of the droplet and the solution surface tension that is a contractive force will aim to reduce the surface area of the droplet. As the

intensity of the electric field is increased, the accumulated mutual charge repulsion on the surface of the polymer droplet overcomes the surface tension forming a Taylor cone from which a jet ejects and accelerates towards the collector plate.[16,17] During jet acceleration, solvent evaporation in combination with a whipping process stretches the fiber, thus reducing its diameter and forming a non-woven nanofibrous mat.[18] Refer Table 3.1 for the electrospinning conditions of the functionalized polymers.

Table 3.1 Electrospinning conditions used for the functionalized polymers.

	Solvent system	Solvent ratio	Polymer weight %	Tip to collector distance (cm)	Flow rate (mL/min)
SMA	DMF: acetone	1:2	14	15	0.090
SMI-Pr	DMF: acetone	1:2	15	18	0.080
SMI-AP	DMF: EtOH	1:1	22	15	0.065
SMI	DMF: EtOH	1:1	20	18	0.085
SMI-qC$_8$	DMF: MeOH	1:1	32	15	0.025
SMI-qC$_{10}$	DMF: MeOH	1:1	30	15	0.027
SMI-qC$_{12}$	DMF: MeOH	1:1	25	15	0.027
SMI-qC$_{14}$	DMF: MeOH	1:1	23	15	0.029

Binary solvent systems were used for all polymers in various ratios. DMF was used as common solvent for all polymers and had the function of stabilizing and sustaining the electrospinning jet.[19,20] The high boiling point of DMF (152-154 °C) prevents fast evaporation of the solvent and facilitates jet elongation, thereby reducing the diameters of the collected fibers.[18] However, using a single solvent system comprising only of a high boiling point solvent has the distinct disadvantage of forming beaded fibers as well as fusion of adjacent fibers on the collector plate, having the appearance of "wet" fibers due to insufficient solvent evaporation.[4] This problem was circumvented by the addition of a low boiling point solvent, such as methanol, ethanol or acetone, depending on the solubility of the respective polymer. As a result, the addition of a low boiling point solvent aided the solvent evaporation process without inhibiting jet elongation.

Bead formation is often observed within electrospun nanofibers as a result of low solution viscosity, resulting in instability of the polymer solution jet.[20] Solution viscosity is a function of both concentration and polymer molecular weight;[21] therefore by adjusting the solution concentration stable jet formation could be achieved. The SMA copolymer synthesized in this study had sufficiently high molar mass for proper polymer chain entanglements to yield smooth, bead-free nanofibers in the submicron diameter range.

3.4 Characterization of SMA and SMI derivatives

SMA and its derivatives were characterized using ^{1}H-NMR and ^{13}C-NMR spectroscopy, as well as ATR-FTIR. Characterization of the electrospun nanofibers to evaluate fiber morphology and average fiber

diameters was accomplished using SEM. Brunauer-Emmett-Teller (BET) surface analysis was conducted to evaluate the available surface area of the nanofibrous substrates, and water contact angles measurements were employed to investigate the hydrophilic or hydrophobic character of the electrospun substrates.

3.4.1 Characterization of SMA

SMA was synthesized using conventional radical copolymerization.[22]

(a) ^{1}H-NMR

The ^{1}H-NMR spectrum of SMA is shown in Figure 3.2 with the assignments of the relevant peaks.

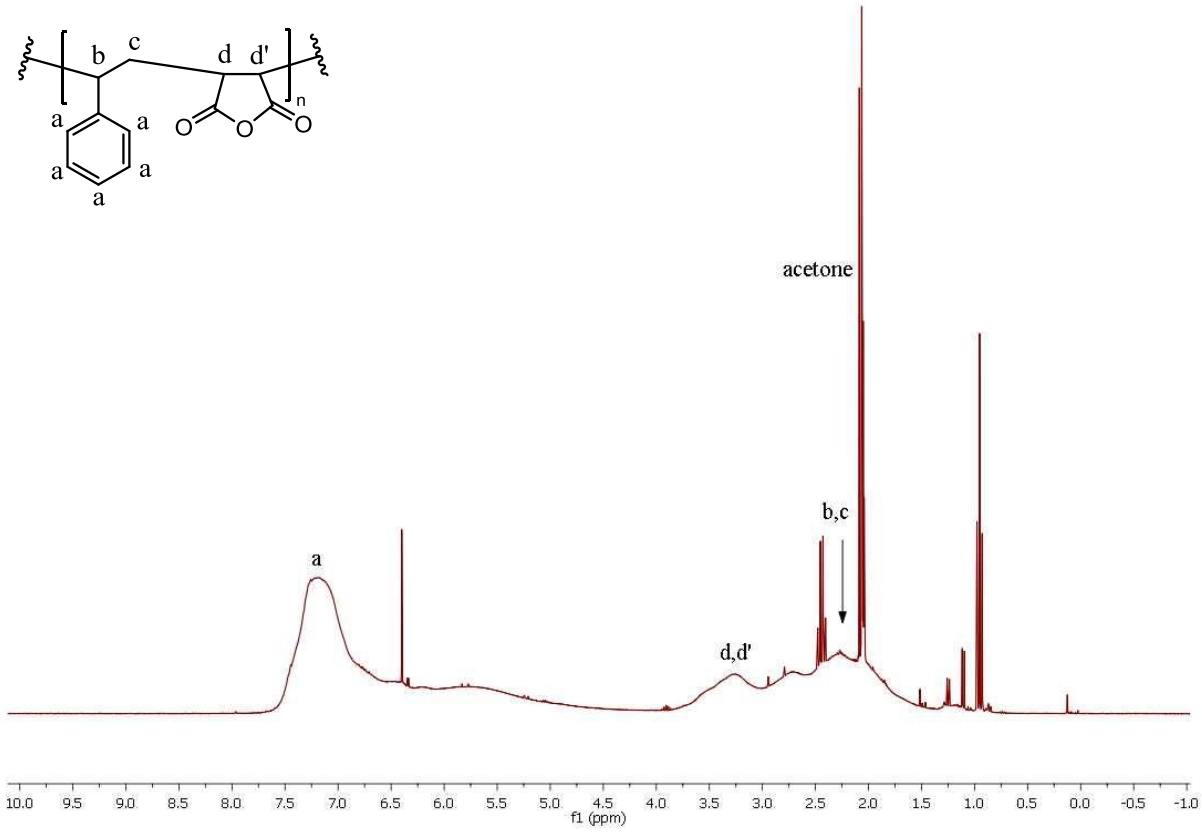

Figure 3.2 ^{1}H-NMR spectrum of SMA.

A broad peak at 2.26 ppm in the ^{1}H-NMR spectrum of SMA corresponds to the chemical shift of the methylene (–CH_2–) and methine (–CH–) protons of the copolymer backbone (b, c). Due to the electronegative nature of oxygen atoms, the hydrogens attached to a carbon next to a carbonyl group (C=O) give absorptions in a downfield region, i.e. at higher ppm value. This deshielding effect is illustrated by the broad peak at δ = 3.26 ppm attributed to the methine protons (d, d'). Hydrogens attached to an aromatic ring have large chemical shifts due to deshielding caused by the large

anisotropic field.[23] The aromatic protons (a) are therefore present as a broad peak in the range δ = 7.0 – 7.5 ppm, which is characteristic of proton signals from styrene residues.[24,25]

To determine the styrene/maleic anhydride ratio, the peaks of the aromatic protons (a, 5H) and the methine protons (d,d', 2H) were integrated and the mole ratios calculated. The ratio obtained was approximately 1:1 of styrene to maleic anhydride units, concluding that an alternating copolymer was synthesized (MAnh content = 50%).[7,25,26]

(b) ^{13}C-NMR

Figure 3.3 shows the representative ^{13}C-NMR spectrum of SMA and the assignments of the relevant peaks. The ^{13}C-NMR spectrum confirmed the results obtained by ^{1}H-NMR spectroscopy.

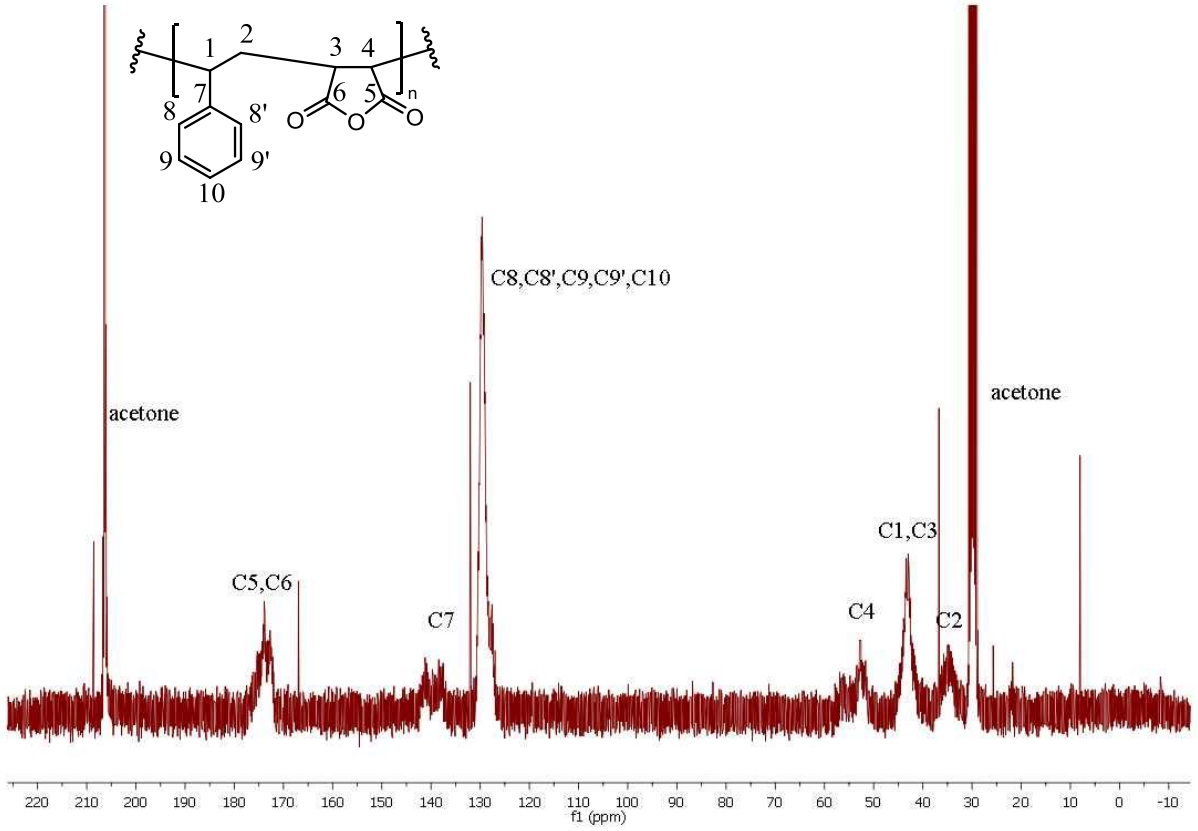

Figure 3.3 ^{13}C-NMR spectrum of SMA.

The ^{13}C-NMR spectrum of SMA is characterized by the methylene (C2) and methine (C1, C3, C4) carbon peaks appearing between 32 – 54 ppm, with overlapping of the C1 and C3 peaks observed. The quaternary aromatic carbon (C7) appears at 139 ppm, adjacent to the aromatic ring carbons (C8, C8', C9, C9', C10) at 129 ppm.

As reported by Ha[27], triad sequences of styrene (S) and maleic anhydride (M) in a copolymer could be determined by ^{13}C-NMR. Using this technique, it can be determined whether the copolymer microstructure is alternating (SMS), semi-alternating (SSM or MSS) or non-alternating (SSS). The two predominant markers are C7 and C2. A perfectly alternating sequence (SMS) will have a C7 resonance at δ = 137 – 140 ppm and a C2 resonance at δ = 33 – 37 ppm. As the styrene content

increases (sequences such as SSM and SSS), these resonances will shift upfield to values of δ = 145 – 147 ppm for C7 and δ = 42 – 47 ppm for C2. The SMA synthesized in this experiment had resonance values of δ = 139 ppm for C7 and δ = 34 ppm for C2, indicating that an alternating styrene maleic anhydride copolymer was synthesized.[28] Finally, the peaks at δ = 172 and 173 ppm are designated to the carbonyl carbons (C5, C6) which appear more downfield due to the deshielding effect of the electronegative oxygen atoms.[27]

3.4.2 Characterization of SMI-Pr

SMA was modified with propylamine via a ring opening reaction with the reactive maleic anhydride residue, followed by ring closure at elevated temperatures to yield the stable maleimide derivative, poly(styrene-*N*-propylmaleimide) (SMI-Pr).[13]

(a) ^{1}H-NMR

The ^{1}H-NMR spectrum of SMI-Pr is shown in Figure 3.4 with the assignment of the relevant peaks.

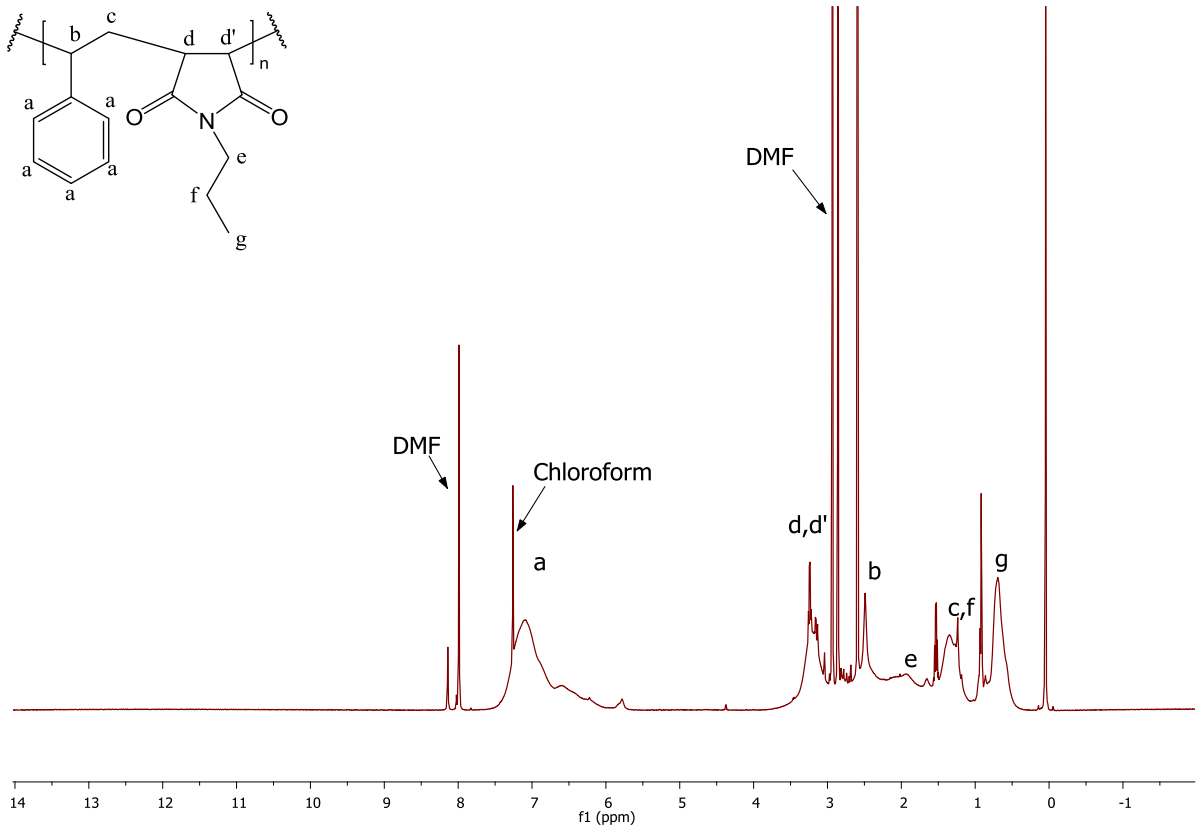

Figure 3.4 ^{1}H-NMR spectrum of SMI-Pr.

The broad peak at δ = 7.17 ppm in the ^{1}H-NMR spectrum of SMI-Pr corresponds to the hydrogens attached to the aromatic ring (a). They are deshielded by the large anisotropic field generated by

the electrons in the ring's π system, resulting in a large chemical shift. Benzylic hydrogens (b) are also deshielded by the anisotropic field of the ring, but to a lesser extent and can be found at δ = 2.49 ppm. Methylene (–CH_2 –) absorptions appear in the region δ = 1.2–1.4 ppm, giving rise to the proton signal at 1.33 ppm (c,f). The methine hydrogens in the polymer backbone (d, d') are deshielded by the anisotropy of the adjacent C = O group, appearing more downfield at δ = 3.19 ppm. The α hydrogen (e) is slightly deshielded due to the electronegativity of the attached nitrogen, giving rise to a proton signal at 2.03 ppm. Methyl groups are often recognizable as tall peaks in the region 0.7–1.3 ppm. The peak at δ = 0.69 ppm with an integral value of three thus confirms the presence of the methyl group (g) at the end of the propyl chain.[23]

The ^{1}H-NMR spectrum of SM-Pr thus confirms the successful imidization of SMA with propylamine to yield SMI-Pr.

(b) ^{13}C-NMR

Figure 3.5 shows the representative ^{13}C-NMR spectrum of SMI-Pr and the assignments of the relevant peaks. The ^{13}C-NMR spectrum confirmed the results obtained by ^{1}H-NMR spectroscopy.

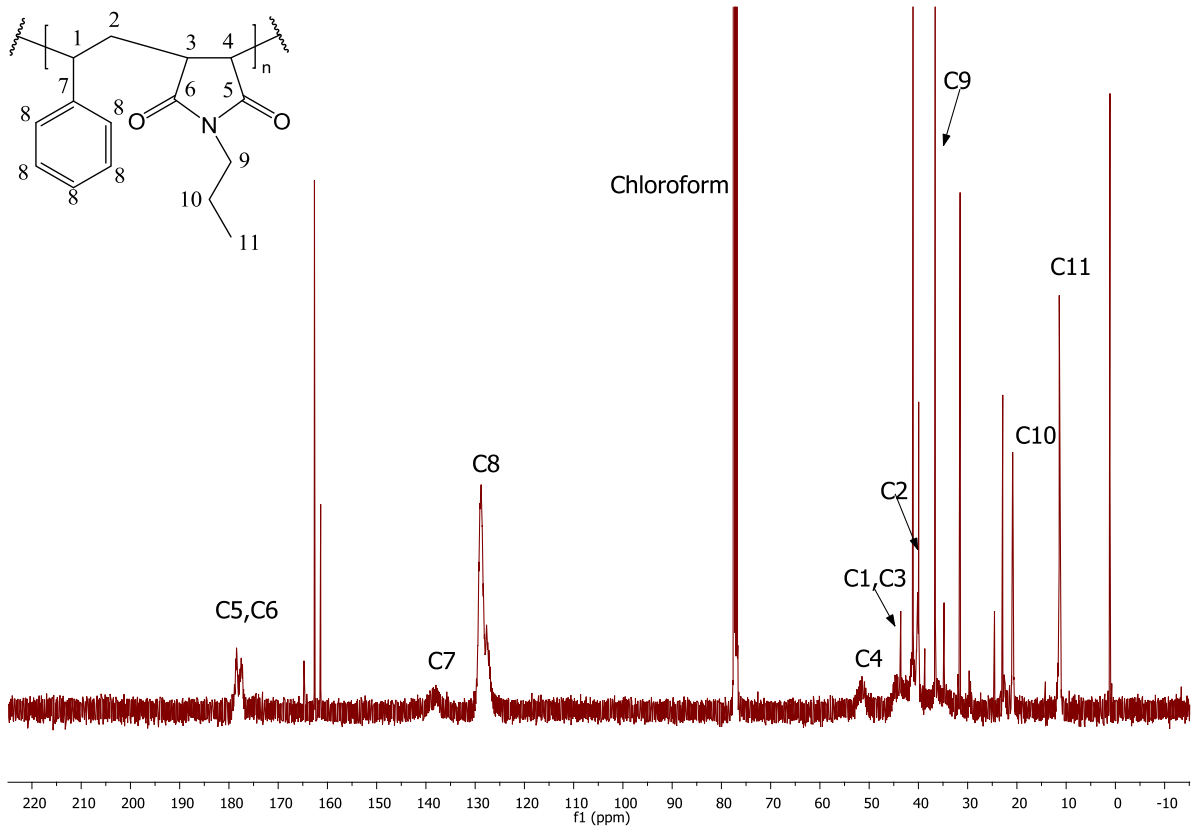

Figure 3.5 ^{13}C-NMR spectrum of SMI-Pr.

Electronegativity and anisotropy affect ^{13}C chemical shifts in nearly the same fashion as they affect ^{1}H chemical shifts. The ^{13}C-NMR spectrum of SMI-Pr is characterized by a peak at δ = 178 ppm, indicative of the resonance signals of the carbonyl carbons (C5, C6) of the imide group. The quaternary aromatic carbon (C7) gives rise to a signal at δ = 138 ppm, adjacent to the aromatic carbon signal (C8) at 128 ppm. In addition to the methylene signal at δ = 40 ppm (C2) and the methine signals at 43 and 51 ppm (C1, C3 and C4) arising from the polymer backbone, new peaks are observable in the upfield region. These include the α carbon (C9) next to the electronegative nitrogen atom at δ = 36 ppm and the methylene β carbon (C10) at 20 ppm. Finally, the methyl group of the propyl chain appears most upfield at δ = 11 ppm giving rise to a sharp peak in the distinct region associated with methyl carbons.[23]

The ^{13}C-NMR spectrum of SM-Pr thus confirms the successful imidization of SMA with propylamine to yield SMI-Pr.

3.4.3 Characterization of SMI-AP

SMA was modified with 4-aminophenol via imidization to yield its maleimide derivative, poly(styrene-*N*-[4-hydroxyphenyl] maleimide) (SMI-AP).[25]

(a) ^{1}H-NMR

The ^{1}H-NMR spectrum of SMI-AP is shown in Figure 3.6 with the assignment of the relevant peaks.

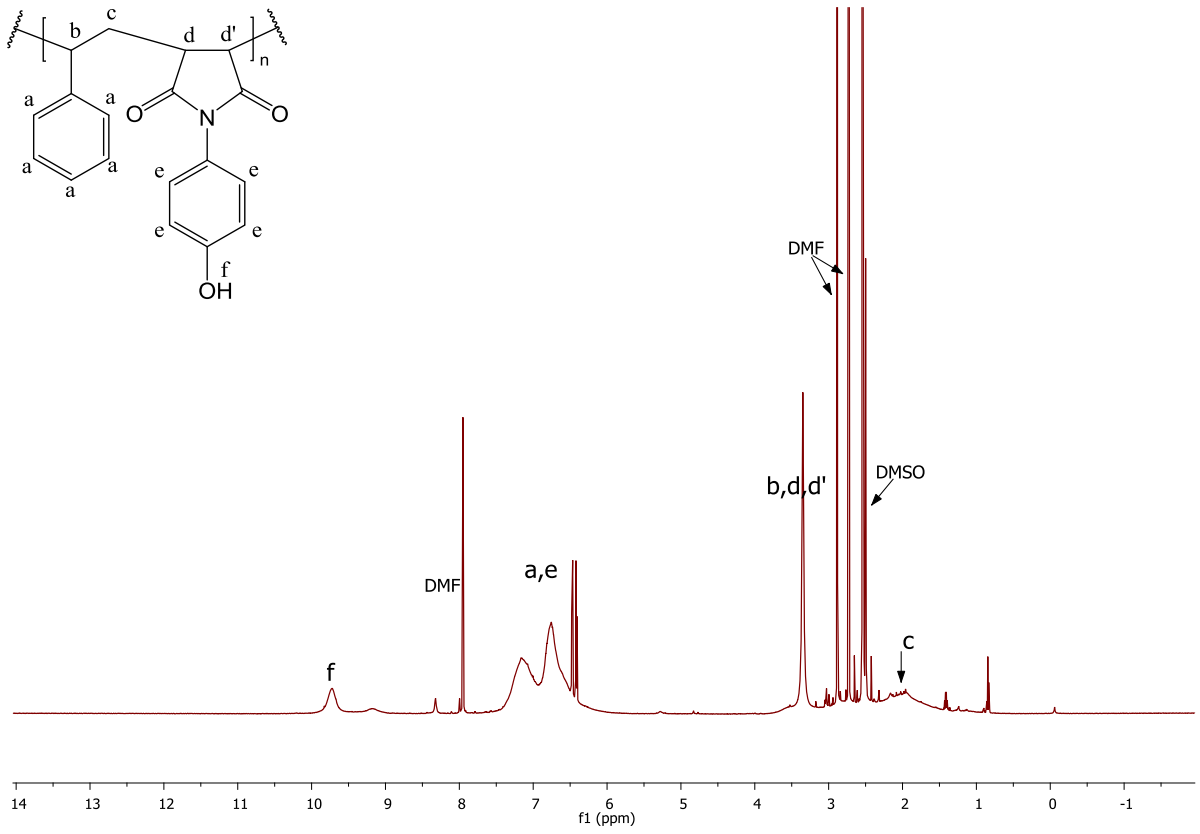

Figure 3.6 ^{1}H-NMR spectrum of SMI-AP.

The broad bimodal peak at δ = 7.14 and 6.77 ppm in the ^{1}H-NMR spectrum of SMI-AP corresponds to the hydrogens attached to the aromatic ring of the styrene unit (a) of the polymer backbone and those of the attached aminophenol group (e). The chemical shift of the methine (–CH–) proton appears at an upfield value of δ = 1.99 (c), whilst the methylene ($–CH_2–$) protons (b, d and d') appear more downfield as an overlapping peak at 3.35 ppm. Deshielding due to the anisotropy of the carbonyl groups (C = O) and styrene unit accounts for this phenomenon. The phenolic proton (f) is deshielded due to the electronegative oxygen atom and is shifted downfield to δ = 9.73 ppm.[23]

The ^{1}H-NMR spectrum of SM-AP thus confirms the successful imidization of SMA with 4-aminophenol to yield SMI-AP.

(b) ^{13}C-NMR

Figure 3.7 shows the representative ^{13}C-NMR spectrum of SMI-AP and the assignments of the relevant peaks. The ^{13}C-NMR spectrum confirmed the results obtained by ^{1}H-NMR spectroscopy.

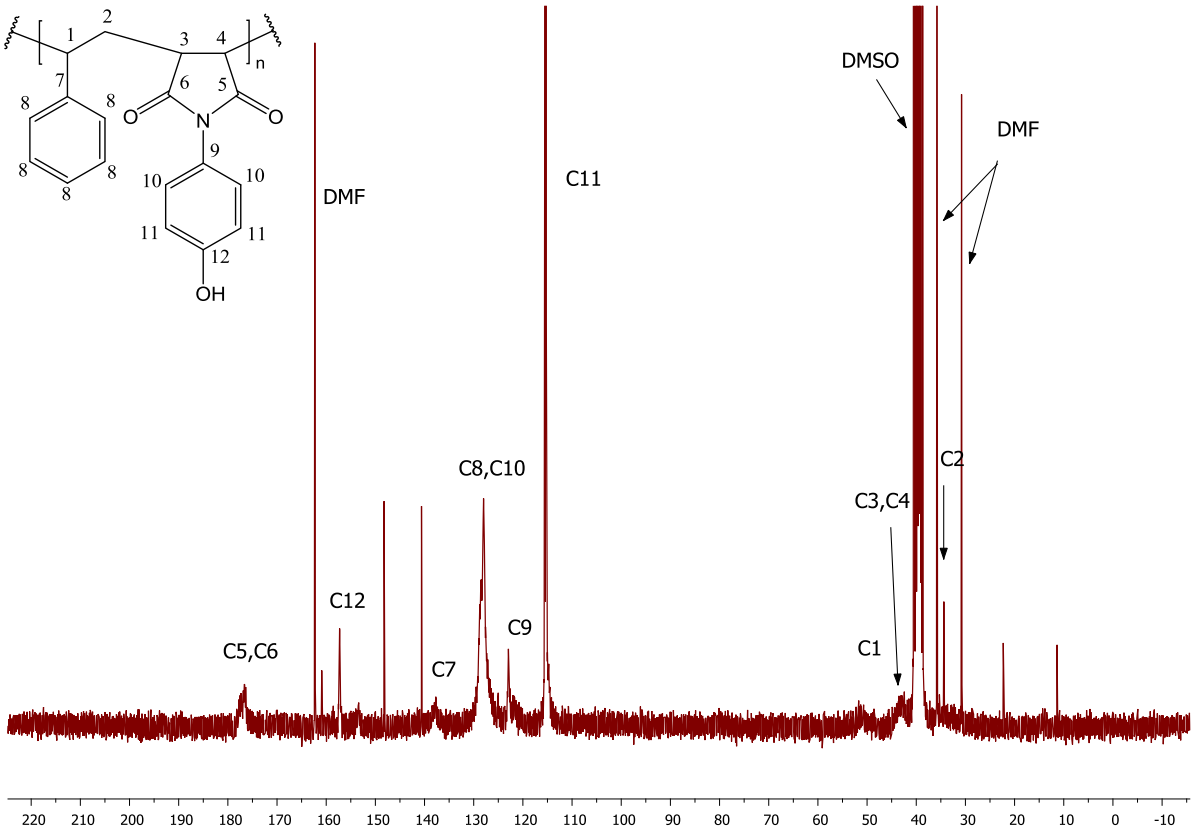

Figure 3.7 ^{13}C-NMR spectrum of SMI-AP.

The ^{13}C spectrum of SMI-AP is characterized by a peak at δ = 176 ppm which corresponds to the resonance signal of the carbonyl carbons (C5, C6) of the imide group. The quaternary aromatic carbon (C7) gives rise to a signal at δ = 137 ppm, adjacent to the overlapping aromatic carbon signal (C8, C10) at 128 ppm. Due to their difference in chemical environment, the phenolic aromatic carbons (C11) appear more upfield in the spectrum at δ = 115 ppm, whereas the α phenolic carbon (C12) appears more downfield at 157 ppm due the electronegative oxygen atom which deshields the electron density on the carbon atom. Both values are in good agreement with literature.[23] The quaternary imide aromatic carbon (C9) accounts for the resonance signal at δ = 122 ppm.

The methylene signal at δ = 34 ppm (C2) and the methine signals at 43 and 51 ppm (C1, C3 and C4) are observed in the upfield region and arises from the polymer backbone resonance signals.

The ^{13}C-NMR spectrum of SM-AP thus confirms the successful imidization of SMA with 4-aminophenol to yield SMI-AP.

3.4.4 Characterization of SMI-tC

SMA was modified with 3-(*N,N*-dimethylamino)-1-propylamine via a ring opening reaction of the reactive maleic anhydride residue, followed by ring closure at elevated temperatures to yield the imidization product SMI-tC.[13]

(a) ^{1}H-NMR

Figure 3.8 shows the representative ^{1}H-NMR spectrum of SMI-tC and the assignments of the relevant peaks.

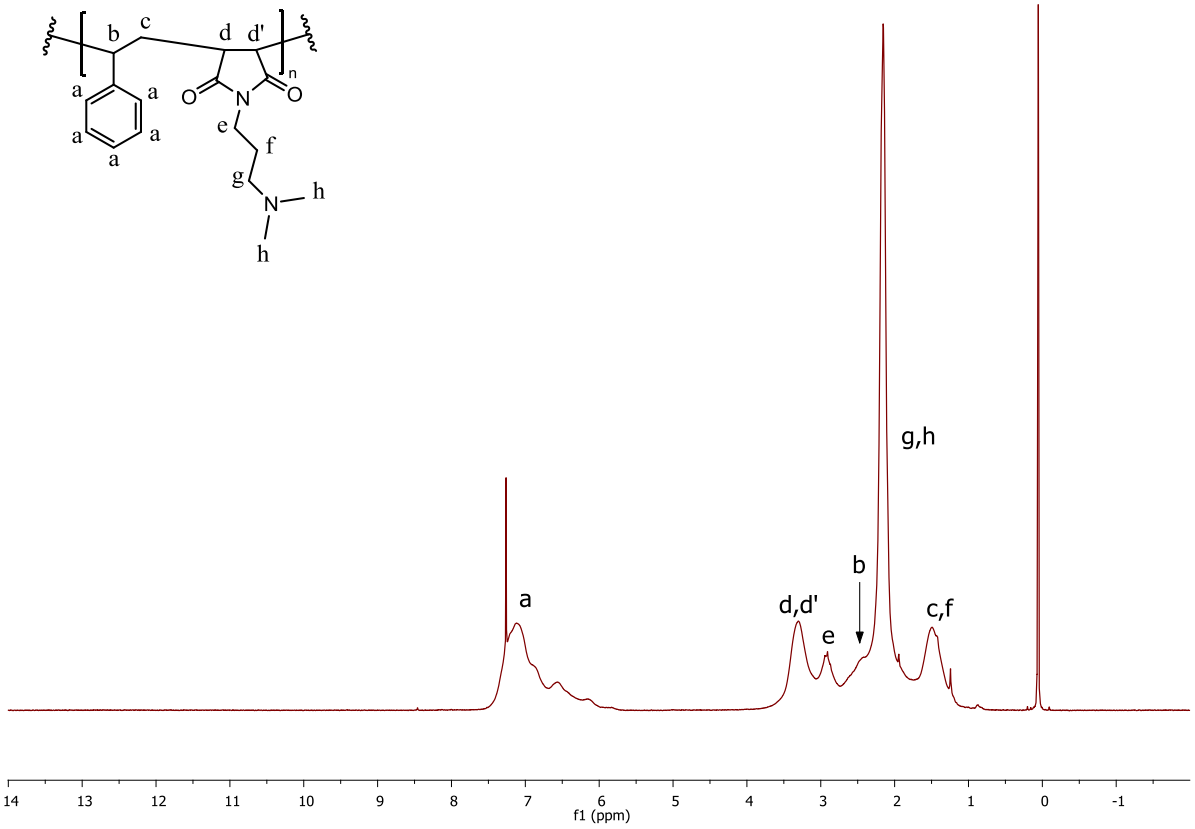

Figure 3.8 ^{1}H-NMR spectrum of SMI.

The broad peak at δ = 7.12 ppm in the ^{1}H-NMR spectrum of SMI-tC corresponds to the deshielded hydrogens attached to the aromatic ring (a). The benzylic hydrogens (b) are also deshielded by the anisotropic field of the ring, but to a lesser extent and can be found at δ = 2.48 ppm. Methyl groups are often recognizable as tall peaks in the upfield region between δ = 0.7–1.3 ppm.[23] The nitrogen atom adjacent to the terminal methyl groups, however, has an electron withdrawing effect on the methyl groups (h), which shifts the peak upfield to δ = 2.15 ppm, overlapping with the methylene hydrogens (g). The anisotropic effect of the carbonyl groups (C = O) adjacent to the methine hydrogens in the polymer backbone (d, d') are responsible for the proton signal appearing downfield at δ = 3.32 ppm. The α hydrogen (e) is highly deshielded to the adjacent nitrogen atom in combination with the electronegative carbonyl groups, giving rise to a proton signal at δ = 2.93 ppm.

Finally, methylene (–CH_2 –) absorptions arising from the polymer backbone (c) and the attached *N*-alkylamine (f) appear as an overlapping peak in the upfield region at δ = 1.49 ppm.

The ^{1}H-NMR spectrum of SMI thus confirms the successful imidization of SMA with 3-(*N,N*-dimethylamino)-1-propylamine to yield SMI-tC.

(b) ^{13}C-NMR

Figure 3.9 shows the representative ^{13}C-NMR spectrum of SMI-tC and the assignments of the relevant peaks.

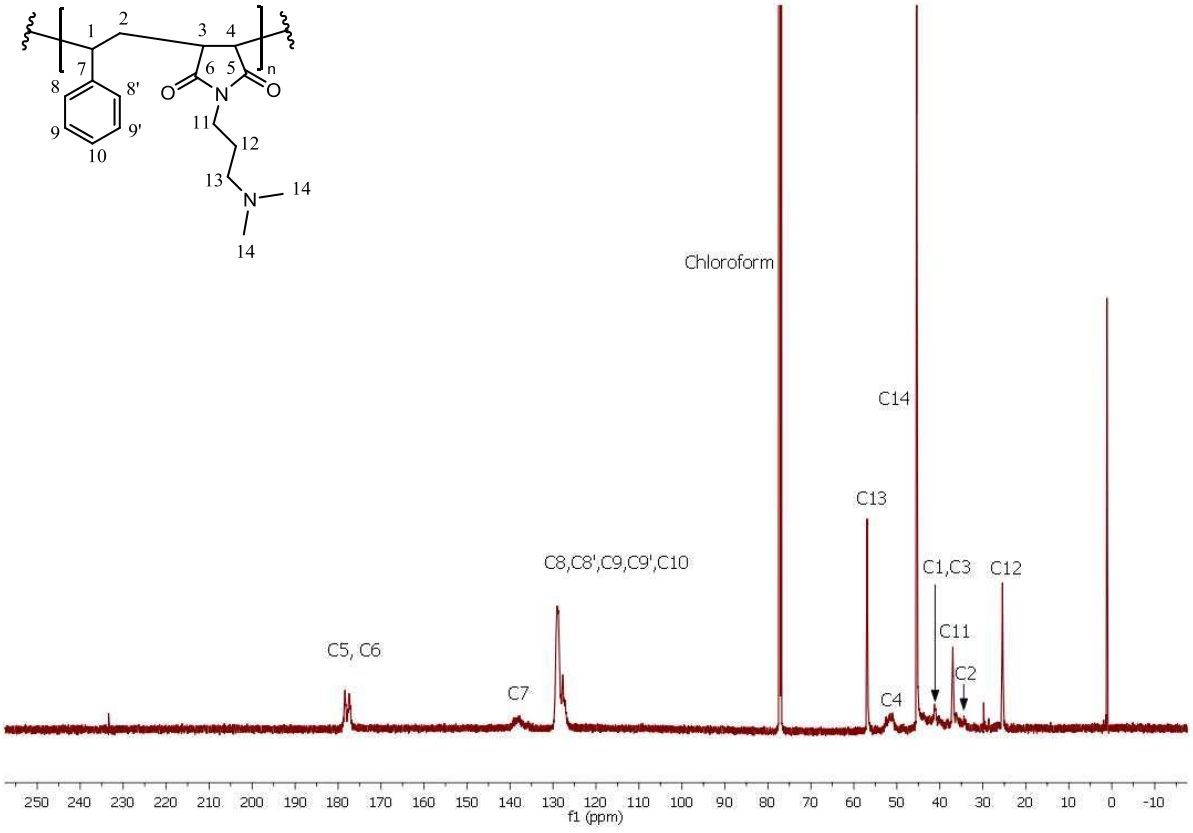

Figure 3.9 ^{13}C-NMR spectrum of SMI.

The ^{13}C-NMR spectrum of SMI-tC is characterized by the methylene (C2) and methine (C1, C3, C4) carbon peaks of the polymer backbone appearing between δ = 34 – 51 ppm, as was observed in the ^{13}C-NMR spectrum of SMA (Figure 3.3). The peaks at δ = 172 and 173 ppm (SMA) shifted downfield after conversion of the anhydride to an imide as can be seen in the lower spectrum at δ = 177 and 178 ppm.[25] The aromatic ring carbon peak (C7) appears at 137 ppm adjacent to the aromatic ring carbons (C8, C8', C9, C9', C10) at 129 ppm.

In addition, new peaks appeared in the spectrum corresponding to the aliphatic signals of the methyl group (C14) at δ = 45 ppm and methylene groups (C11, C12 and C13) at δ = 36, 25 and 56 ppm. These peaks are indicative of the imidization reaction that took place between the maleic anhydride residue of SMA and 3-(*N,N*-dimethylamino)-1-propylamine. The ^{13}C-NMR spectrum of SMI-tC thus confirms the results obtained by ^{1}H-NMR spectroscopy.

3.4.5 Characterization of SMI-qC$_8$, SMI-qC$_{10}$, SMI-qC$_{12}$ and SMI-qC$_{14}$

SMI-tC was modified with an excess of various bromoalkane compounds to facilitate the quaternization reaction of the tertiary amine moiety of SMI-tC to yield the corresponding modified SMI-qC$_x$ polymers, namely SMI-qC$_8$, SMI-qC$_{10}$, SMI-qC$_{12}$ and SMI-qC$_{14}$.[15] Since the ^{1}H-NMR and ^{13}C-NMR spectra of these polymers are similar, only one ^{1}H-NMR and ^{13}C-NMR spectrum will be discussed as representative example, namely that of SMI-qC$_{12}$.

(a) ^{1}H-NMR

Figure 3.10 shows the representative ^{1}H-NMR spectrum of SMI-qC$_{12}$ and the assignments of the relevant peaks.

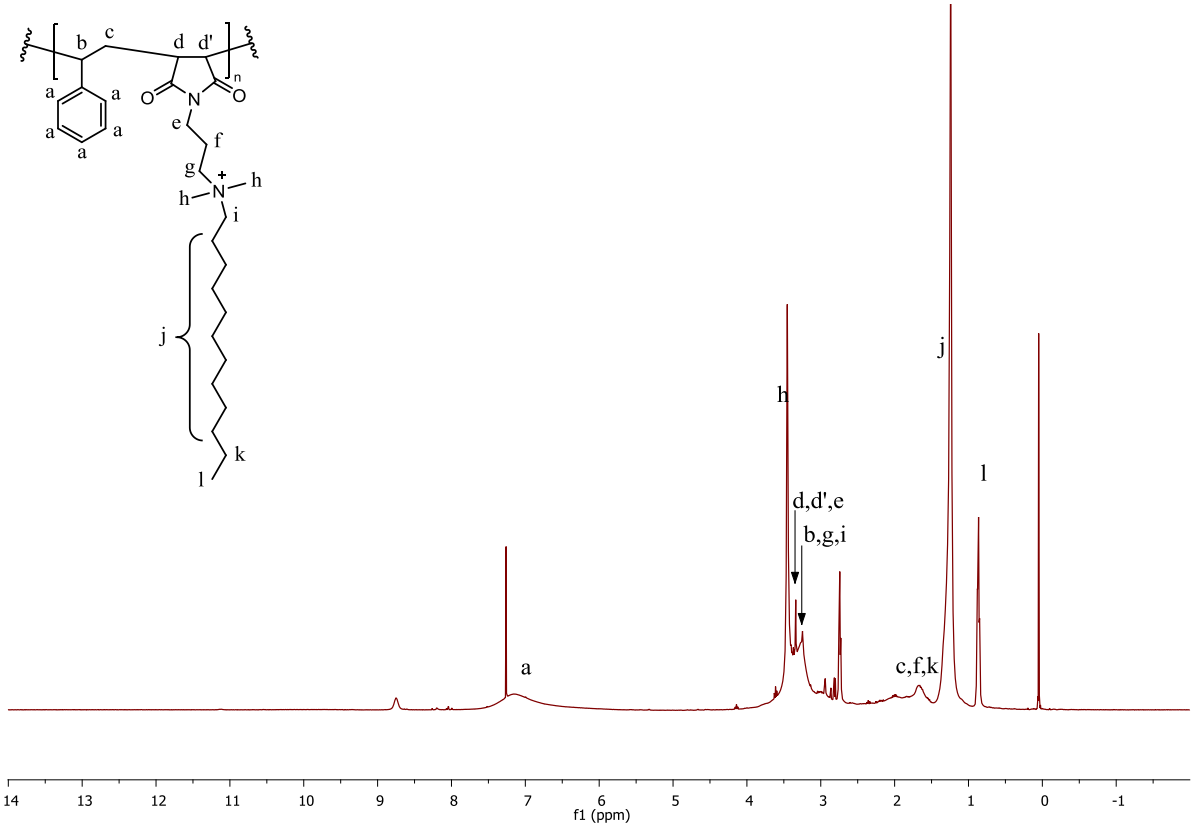

Figure 3.10 ^{1}H-NMR spectrum of SMI-qC12.

The ^{1}H-NMR spectrum of SMI-qC$_{12}$ is characterized by a sharp signal appearing upfield at δ = 0.86 ppm, corresponding to the terminal methyl groups of the C$_{12}$ chain. A sharp signal at δ = 1.24 ppm can be attributed to the methylene protons (–CH$_2$–) of the carbon chain (j). Aliphatic methylene protons of the polymer backbone (c), the C$_{12}$ chain (k) and the *N*-alkylamine (f) appear as a broad peak at δ = 1.69 ppm. Protons adjacent to the quaternized ammonium moiety (e, g, h, i) and imide carbonyl groups (d, d') appear as overlapping peaks between 2.94 – 3.45 ppm, as indicated in the spectrum.[25] These peaks appear more downfield due to the deshielding effect of the

electronegative nitrogen and carbonyl groups. The broad peak at δ = 7.14 ppm arises from the deshielded aromatic protons.[23]

The ^{1}H-NMR spectrum of SMI-qC_{12} thus confirms the successful quaternization of SMI using 1-bromododecane to yield SMI-qC_{12}.

(b) ^{13}C-NMR

Figure 3.11 shows the representative ^{13}C-NMR spectrum of SMI and the assignments of the relevant peaks.

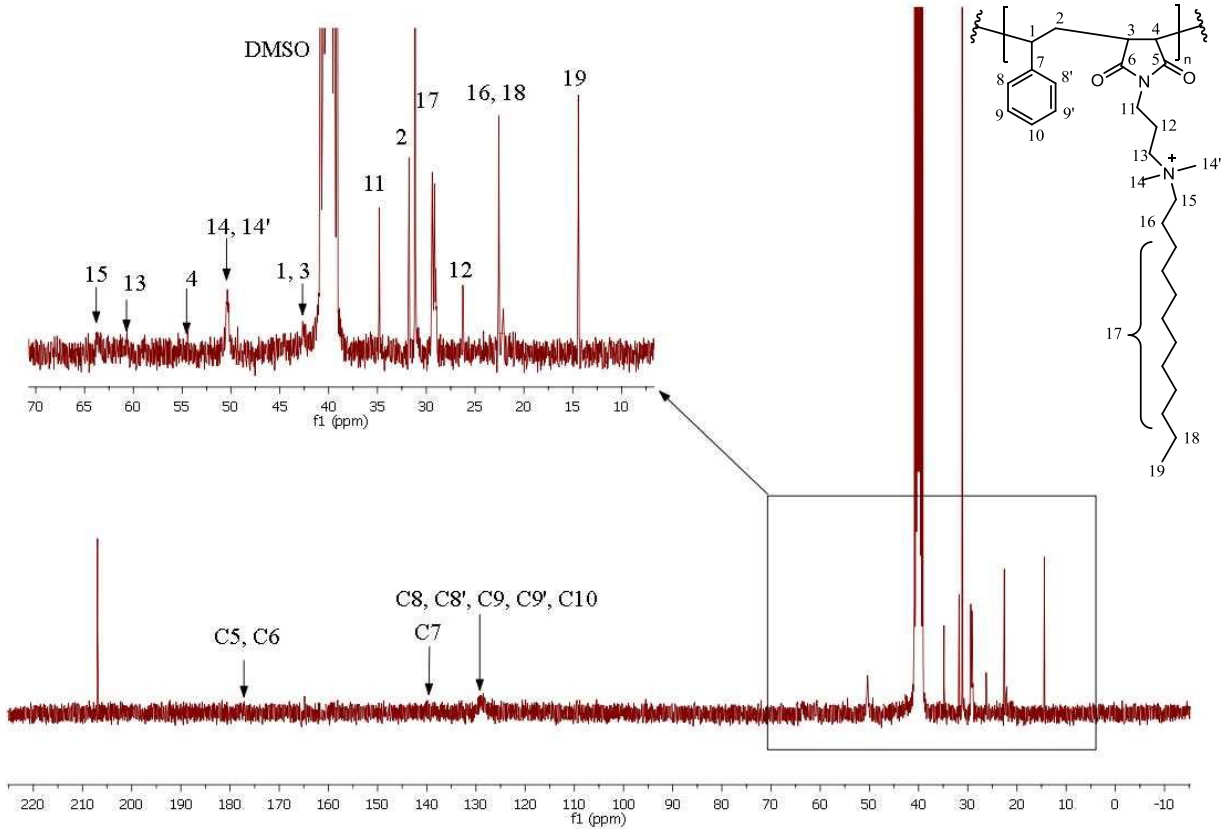

Figure 3.11 ^{13}C-NMR spectrum of SMI-qC_{12}.

In addition to the peaks observed in the ^{13}C-NMR spectrum of SMI-tC (refer Figure 3.9), the ^{13}C-NMR spectrum of SMI-qC_{12} also displayed new peaks between δ = 14 – 63 ppm. These peaks can be attributed to the methyl and methylene carbons of the C_{12} alkyl chain that have been attached to the tertiary amine moiety of SMI-tC via a nucleophilic substitution reaction, as indicated in the spectrum. The peak at δ = 31.16 ppm corresponds to the methylene carbon signals arising from the alkyl chain (C17). In addition, the methyl group (C19) of the C_{12} alkyl chain exhibits a characteristic peak in the upfield region at δ = 14.43 ppm. Furthermore, methylene carbon signals are present at δ = 22.48 ppm, which originates from the attached alkyl chain (C16, C18). The presence of these peaks thus confirms that nucleophilic substitution took place at the tertiary amine moiety of SMI-tC to yield SMI-qC_{12}.

The ^{13}C-NMR spectrum of SMI-qC_{12} thus confirms the results obtained by ^{1}H-NMR spectroscopy.

3.4.6 ATR-FTIR

The nanofibrous mats of SMA, SMI-Pr, SMI-AP, SMI-tC and SMI-qC_8, SMI-qC_{10}, SMI-qC_{12} and SMI-qC_{14} were further characterized and compared using ATR-FTIR.

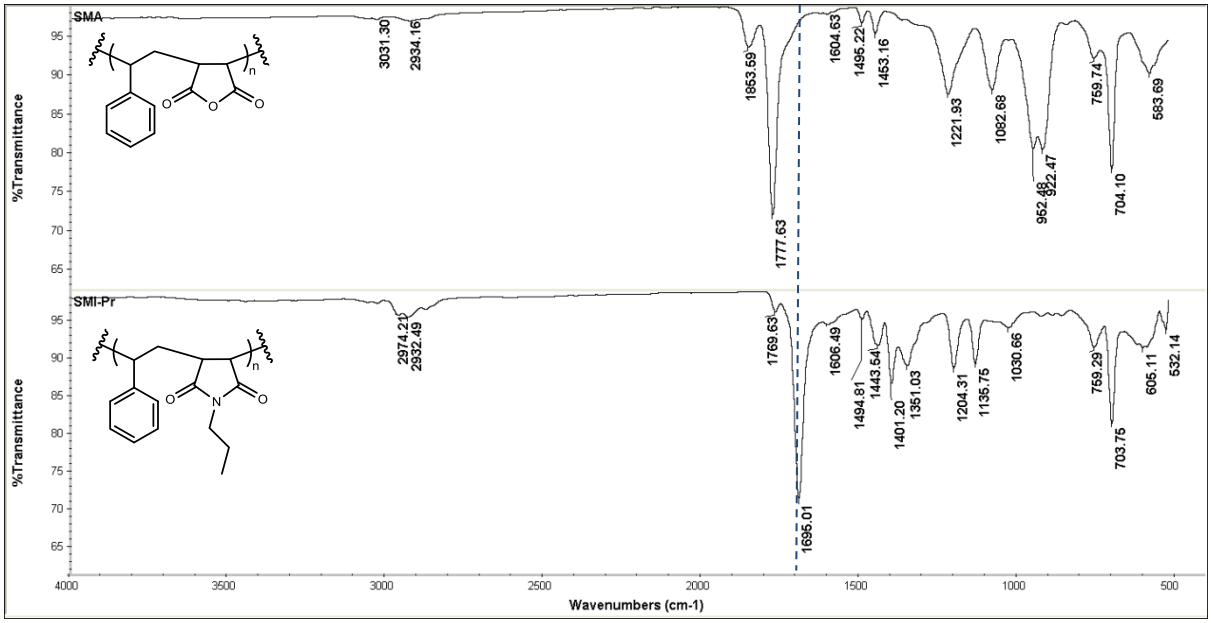

Figure 3.12 IR spectra of SMA and SMI-Pr copolymers.

In the IR spectrum of SMA (refer to Figure 3.12), the absorption bands at 1853 and 1777 cm^{-1} are characteristic of the asymmetric and symmetric C=O stretch vibration of the five membered cyclic anhydride unit, and the strong, broad absorption band at 1204 cm^{-1} is due to the cyclic ring ether (–C–O–C–) of the maleic anhydride residue.[29] Aromatic =C– (sp^2) and aliphatic –CH_2– (sp^3) stretch vibrations occur at 3031 and 2934 cm^{-1}, respectively, with the ring stretch absorptions (C=C) appearing at 1604 and 1453 cm^{-1}. Finally, the out-of-plane C–H bending vibrations of the monosubstituted aromatic ring gives rise to two bands at 952 and 922 cm^{-1}.[23]

The IR spectrum of SMI-Pr has similar bands to that of SMA, but with shifting of the C=O bands from 1853 and 1777 cm^{-1}, respectively, to 1769 and 1695 cm^{-1}, respectively, which indicates the formation of an imide bond and thus confirms that imidization took place.[13] The C–N stretch absorption is visible as a medium intensity band at 1135 cm^{-1}, but without N–H stretch vibrations in the range 3500 – 3300 cm^{-1}, confirming that the ring-closed product was obtained. The methyl group of the attached propyl chain has a characteristic C–H bending absorption band at 1351 cm^{-1}, which is absent in the spectrum of SMA. An increase in the intensity of the absorption band at 2932 cm^{-1} can be ascribed to the methyl (–CH_3) and methylene (–CH_2–) stretch vibrations originating from the propyl chain of the modification agent, propylamine.[23]

The degree of conversion (DC) to the modified product can be calculated by using a reference peak in the spectra. In this instance, the peak at 704 cm^{-1} exhibits the out-of-plane bending motion of the monosubstituted benzene ring[23] which does not produce any change during the reaction due to the benzene ring not partaking in the modification reaction. Using the ratio of peak heights at 1777 cm^{-1}

and 704 cm^{-1} in the spectrum of SMA and SMI-Pr, the percentage of unreacted maleic anhydride (MA) was calculated using Eq. 3.1:[30]

$$(\%\ MA) = \frac{[Abs\ (1769\ cm^{-1})/Abs\ (703\ cm^{-1})]_{SMI-Pr}}{[Abs\ (1777\ cm^{-1})/Abs\ (704\ cm^{-1})]_{SMA}} \times 100 \qquad (3.1)$$

The % MA was calculated to be 11.3 %, and the DC was calculated to be 88.7 % using Eq. 3.2:[30]

$$\%\ DC = 100 - (\%\ MA) \qquad (3.2)$$

The results obtained from the IR spectra suggest that SMA was successfully modified via an imidization reaction between propylamine and the reactive maleic anhydride residue of SMA with 88.7 % conversion, yielding SMI-Pr.

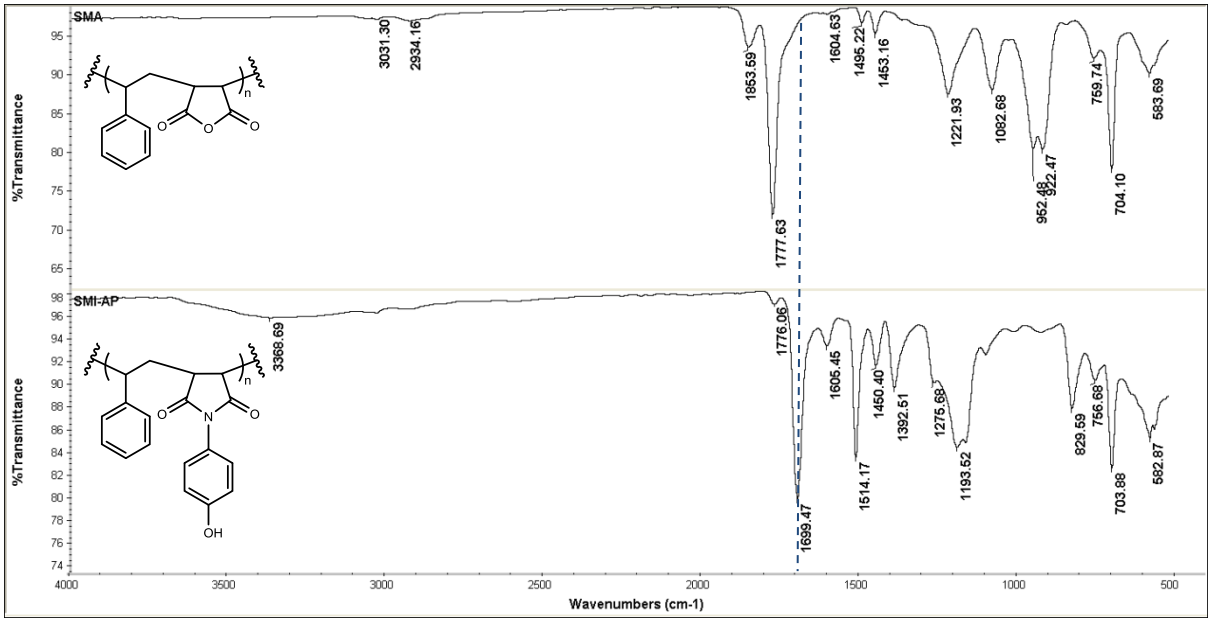

Figure 3.13 IR spectra of SMA and SMI-AP copolymers.

The IR spectrum of SMI-AP is characterized by several new absorption bands when compared to that of SMA, such as the imide carbonyl stretch vibration (C=O) at 1699 cm^{-1} in combination with the C–N stretch vibration at 1392 cm^{-1}, as can be seen in Figure 3.13. The presence of these peaks confirms that imidization of SMA took place. A broad peak is visible at 3368 cm^{-1}, resembling the absorption signal of hydrogen bonded O–H, whereas the phenolic C–O stretch vibration occurs at 1193 cm^{-1}. In addition to the out-of-plane C–H bending vibrations of the styrene unit at 704 and 759 cm^{-1} (present in both SMA and SMI-AP), a new weak absorption band at 829 cm^{-1} is characteristic of the out-of-plane C–H bending of the para-substituted aromatic ring of 4-aminophenol. Both spectra exhibit C=C ring stretch absorptions of the aromatic rings in the range of 1600 – 1450 cm^{-1}.[23] The degree of conversion was calculated to be 95.0 % using Eq. 3.1 and 3.2.

Comparison of the ATR-FTIR spectra of SMA and SMI-AP confirmed that SMA was successfully modified with 4-aminophenol to yield the SMI-AP copolymer with 95.0 % degree of conversion.

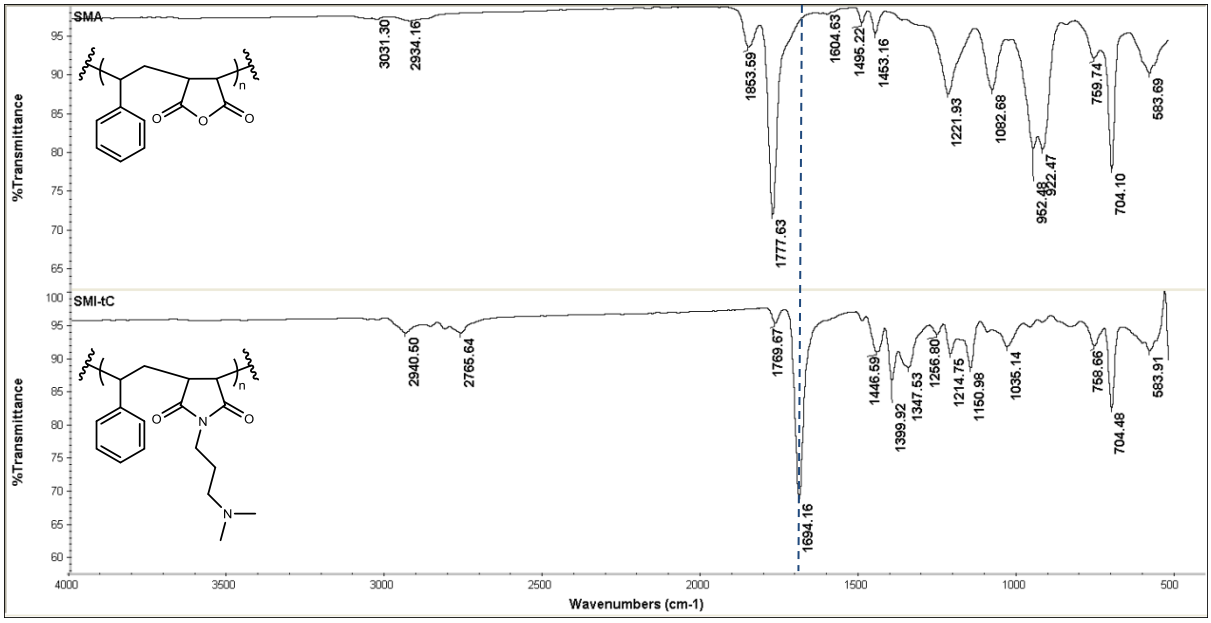

Figure 3.14 IR spectra of SMA and SMI-tC copolymers.

The IR spectrum of the SMI-tC copolymer has similar bands to that of SMA except for the disappearance of the bands at 1853 cm^{-1} and 1777 cm^{-1} indicative of the maleic anhydride residue, and the appearance of the imide carbonyl (C=O) asymmetric and symmetric stretch vibrations at 1769 and 1694 cm^{-1}, respectively. In addition, a new peak at 1150 cm^{-1} can be assigned to the C–N stretch vibration of the new imide bond which can clearly be seen in Figure 3.14. Note also the disappearance of the strong, broad peak at 1221 cm^{-1} (–C–O–C–) which is now only visible as a small peak at 1214 cm^{-1}, indicating that some maleic anhydride groups did not undergo imidization. The peaks at 2940 and 2765 cm^{-1} can be attributed to the asymmetric and symmetric methyl ($–CH_3$) and methylene ($–CH_2–$) stretching vibrations due to the C_{12} alkyl chain and methyl groups present in SMI.[23] No bands were observed in the 3500 – 3100 cm^{-1} region, indicating the absence of N–H bonds; thus confirming that ring closure took place at elevated temperatures yielding a cyclic imide moiety with 88.7 % conversion (Eq. 3.1 and 3.2).[13]

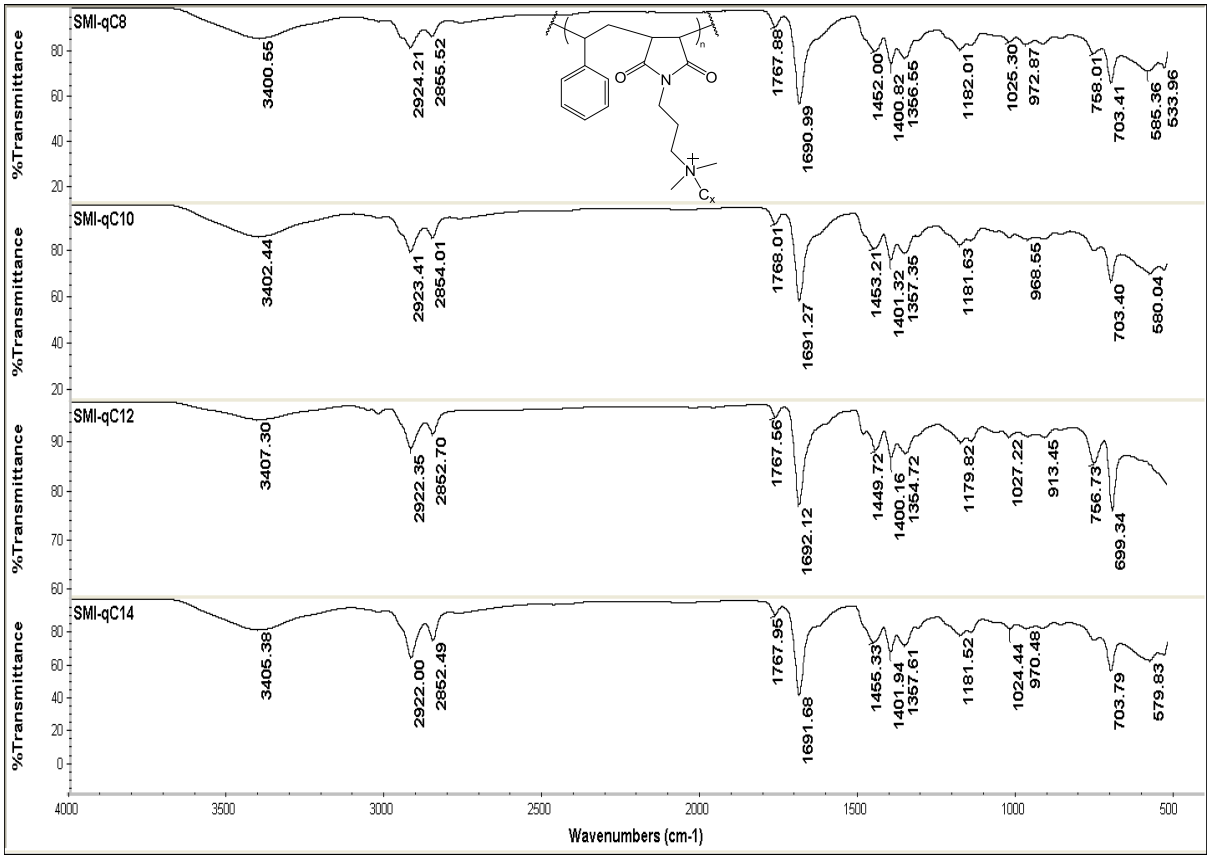

Figure 3.15 IR spectra of the SMI-qC polymers.

When comparing the IR spectrum of SMI (Figure 3.14) to that of the functionalized SMI-qC$_x$ polymers (Figure 3.15), a broad band appears at ~3400 cm^{-1} which can be attributed to the quaternary ammonium nitrogen[23] of the salt that formed via the nucleophilic substitution reaction between the tertiary amine moiety of SMI-tC and the bromoalkane compounds. Furthermore, an increase in the intensity of the bands at ~2855 and ~2924 cm^{-1} can be attributed to the methyl (-CH$_3$) and methylene (-CH$_2$-) stretch vibrations of the alkyl chains that have been attached to the tertiary amine functional group via a nucleophilic substitution reaction. This confirms the successful quaternization of SMI-tC to yield the various SMI-qC$_x$ copolymers.

The degree of quaternization (DQ) can be calculated by using a reference peak in the spectra. In this instance, the peak at ~703 cm^{-1} exhibits the out-of-plane bending motion of the monosubstituted benzene ring[23] which does not produce any change during the reaction[30] due to the benzene ring not partaking in the modification reaction. The methyl groups of the attached *N*-alkylamine moiety exhibit a characteristic C–H bending absorption band at ~1356 cm^{-1}, which increases in intensity with the introduction of the alkyl chains in the quaternized copolymers. Using the ratio of peak heights at 703 and 1356 cm^{-1} in the spectra of SMI-tC (refer Figure 3.14) and SMI-qC$_8$, SMI-qC$_{10}$, SMI-qC$_{12}$ and SMI-qC$_{14}$ (refer to Figure 3.15) the DQ was calculated using Eq. 3.3.

$$(\%DQ) = \frac{[Abs\ (703\ cm^{-1})/Abs\ (1356\ cm^{-1})]_{SMI-qC_x}}{[Abs\ (704\ cm^{-1})/Abs\ (1347\ cm^{-1})]_{SMI}} \times 100 \qquad (3.3)$$

The DQs of the corresponding quaternized copolymers were calculated using Eq. 3.3 to be 84.8 %, 74.2 %, 86.2% and 93.5 % for SMI-qC$_8$, SMI-qC$_{10}$, SMI-qC$_{12}$ and SMI-qC$_{14}$, respectively.

3.4.7 SEM analysis

The polymers were dissolved in a binary solvent system with DMF being the common solvent for all systems with the addition of acetone, methanol or ethanol as the secondary low boiling point solvents. All polymers were electrospun using a single-needle technique in a horizontal setup. Nanofibers with an average diameter in the range of 218 – 468 nm were obtained. These nanofibrous mats were cross-linked with heat treatment at 130 °C under vacuum to render them water insoluble and thus viable to undergo affinity studies with mycobacteria as described in Chapter 5.

Analysis of the SEM images with regard to fiber morphology revealed that all the nanofibers were bead-free, round and had a smooth fiber surface. Using higher polymer concentrations ensured that bead-free fibers are formed during electrospinning.[20] Refer to Figure 3.16 and Figure 3.17 for the SEM images of the polymer nanofibers.

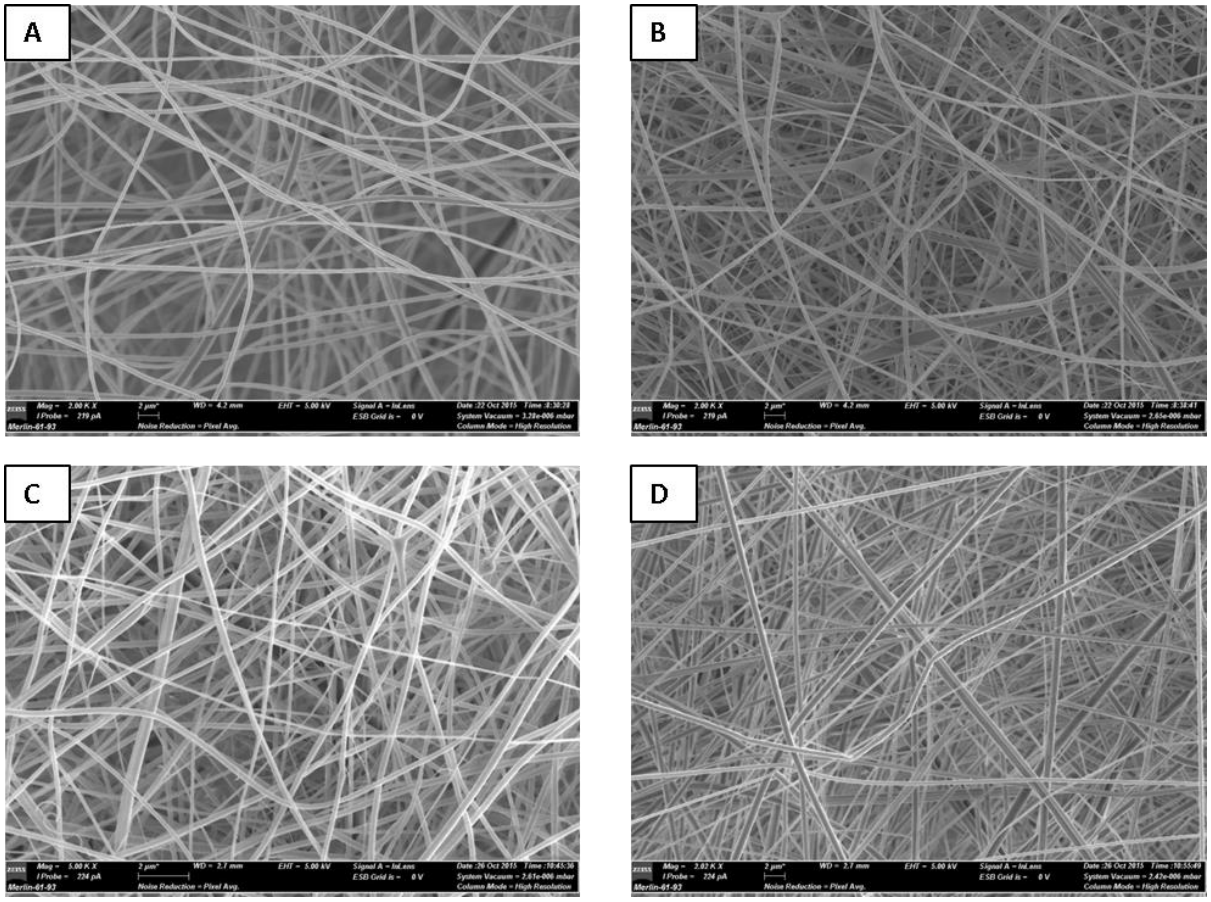

Figure 3.16 SEM images obtained for (A) SMA, (B) SMI-Pr, (C) SMI-AP and (D) SMI-tC.

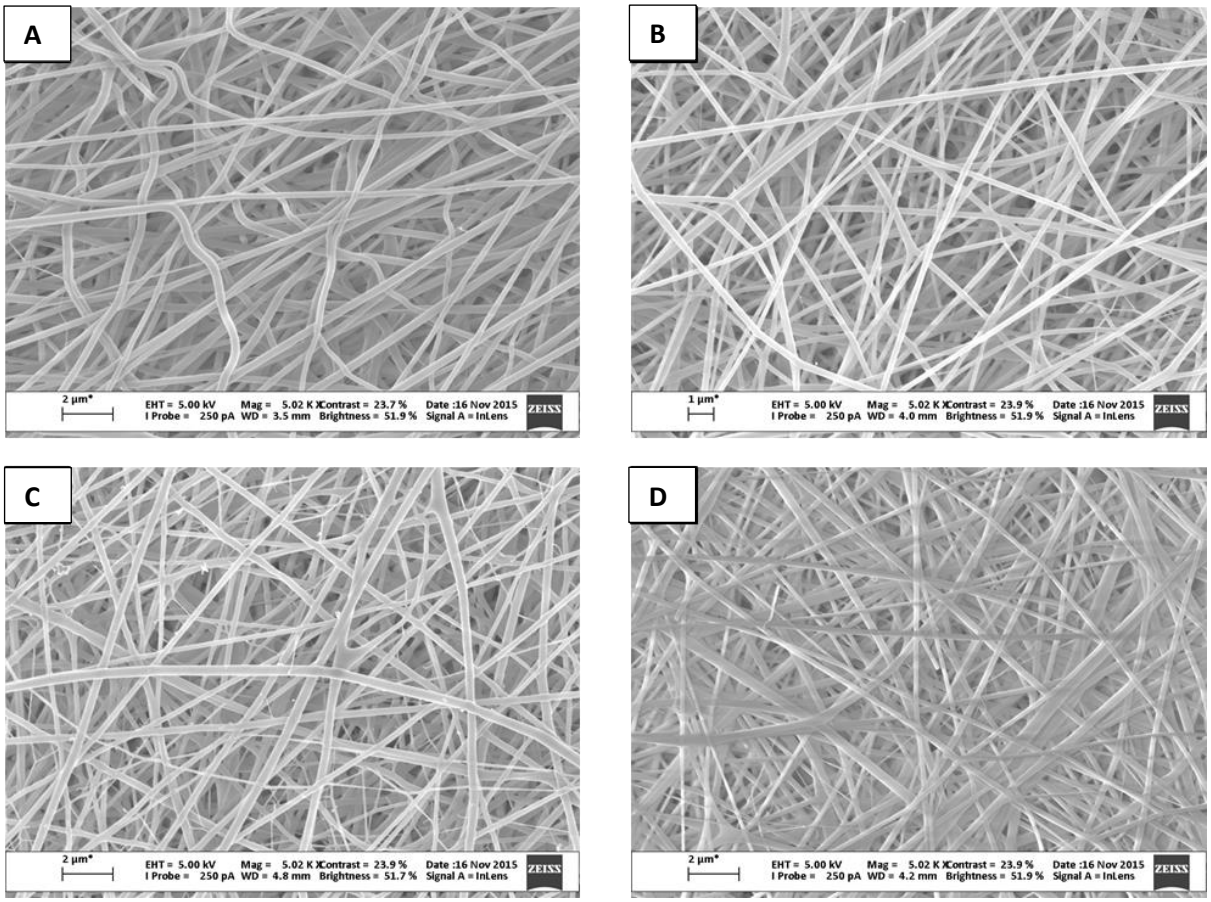

Figure 3.17 SEM images obtained for (A) SMI-qC$_8$, (B) SMI-qC$_{10}$, (C) SMI-qC$_{12}$ and (D) SMI-qC$_{14}$.

Refer to Table 3.2 in the following section for the average fiber diameters and standard deviations of the copolymer nanofibers.

3.4.8 BET surface area analysis

Surface characteristics of a material refer to the properties associated with its surface. Typical measurements include surface area, pore size and porosity. Information on surface characteristics is of importance when considering substrates with a large surface to volume ratio. A substrate with a large surface to volume ratio, such as nanofibers, has the advantage that a high proportion of chemical groups are available to undergo chemical reactions.[31]

Brunauer *et al*.[32] have established the most widely used method for the determination of the surface area of solids (the BET method). They showed that molecules are adsorbed layer by layer. The linear BET plot for the N_2 adsorption isotherm leads to the monolayer capacity, which provides the specific surface area using the molecular area of an N_2 molecule (0.162 nm^2).[33]

Nitrogen adsorption/desorption measurements were employed to measure the specific surface areas of the modified SMI copolymer nanofibers using the Brunauer-Emmet-Teller (BET) method.[34] The measured BET surface areas of the copolymers are summarized in Table 3.2.

Table 3.2 Average fiber diameters and measured BET surface areas of the synthesized copolymers.

	Average fiber diameter (nm)	BET surface area (m^2/g)
SMA	468 ± 111	363.77
SMI-Pr	270 ± 96	547.89
SMI-AP	225 ± 50	699.63
SMI-tC	440 ± 147	377.77
SMI-qC$_8$	259 ± 60	569.42
SMI-qC$_{10}$	218 ± 50	892.72
SMI-qC$_{12}$	239 ± 63	667.13
SMI-qC$_{14}$	222 ± 66	748.18

The surface area per unit mass of nanofibrous substrate is inversely proportional to the average fiber diameter. This relationship is illustrated in Figure 3.18.[35] The smallest fiber diameters with the corresponding highest BET surface area value was obtained for SMI-qC$_{10}$.

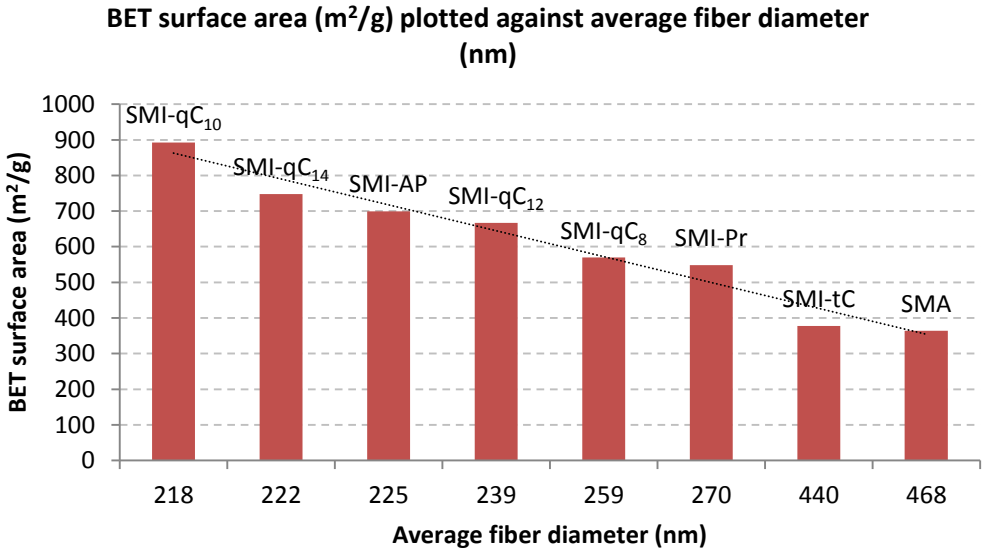

Figure 3.18 Measured BET surface area (m^2/g) plotted against average fiber diameter (nm) for the various polymers.

3.4.9 Water contact angle measurements

Water contact angle measurements can be used to determine the wettability of a surface, which provides an indication of how effectively a liquid will spread over a surface. Contact angle, θ, is defined as the angle between the substrate surface and the tangent line at the point of contact of the liquid droplet with the substrate. The contact angle is a good indicator of the relative hydrophobicity or hydrophilicity of a substrate.[36] Contact angles exceeding 90° (Figure 3.19(A)) are

typically observed for hydrophobic surfaces and show poor wettability, whereas contact angles below 90° (Figure 3.19(C, D)) represent hydrophilic surfaces that exhibit good wettability.

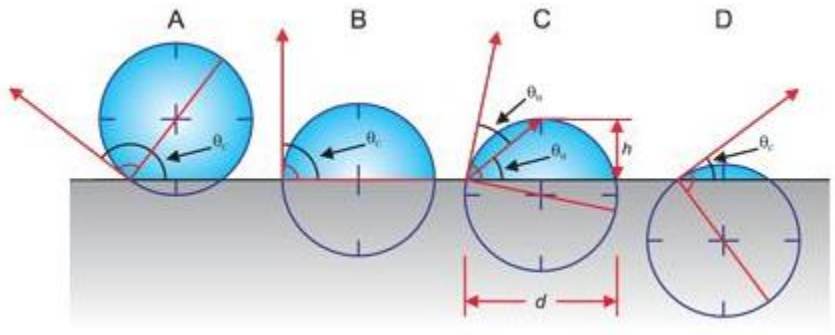

Figure 3.19 Illustration of water contact angle measurements for (A) θ > 90°, (B) θ = 90°, and (C, D) θ < 90°.[37]

Measurements of the height (h) and the base diameter (d) of the captured images allow the half-angle (θ/2) method to be used (Figure 3.20). A correction factor of 2 is applied to obtain the full angle (θ) (Eq. 3.4).[37]

$$\theta = 2\tan^{-1}\left(\frac{2h}{d}\right) \qquad (3.4)$$

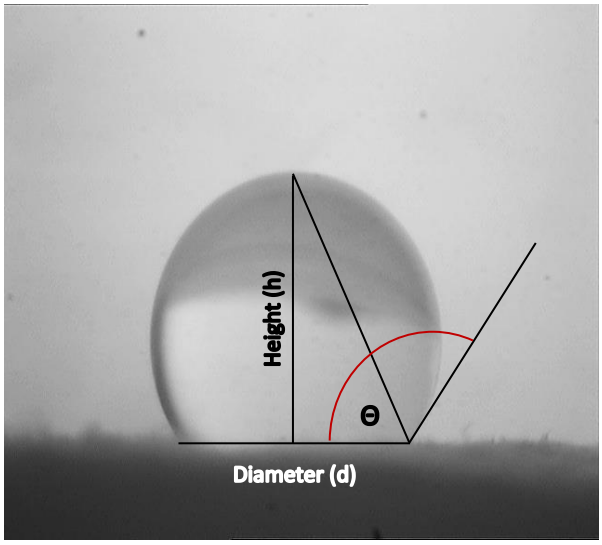

Figure 3.20 Schematic illustration of measurements obtained to calculate water contact angles.

Static water contact angles measured on the nanofibrous substrates of SMA and its SMI derivatives are visualized in the captured images as seen in Figure 3.21.

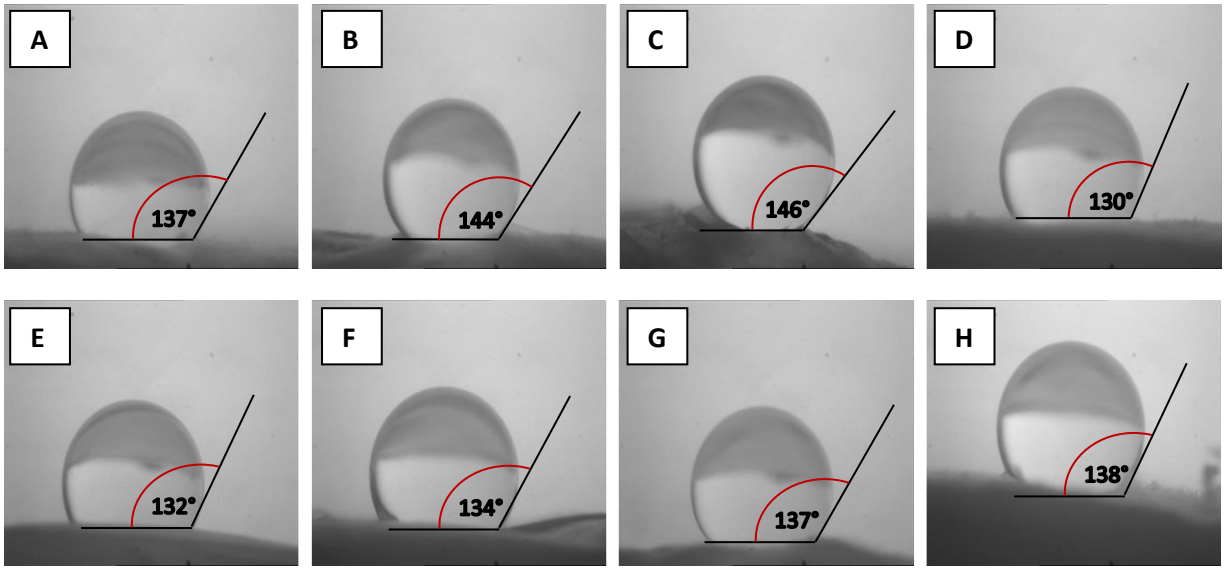

Figure 3.21 Captured images of water droplets on (A) SMA, (B) SMI-Pr, (C) SMI-AP, (D) SM-tC, (E) SMI-qC$_8$, (F) SMI-qC$_{10}$, (G) SMI-qC$_{12}$ and (H) SMI-qC$_{14}$ nanofibers and the corresponding static water contact angles (θ).

The measured contact angle values reflect the hydrophobicity or hydrophilicity of the electrospun substrates (Figure 3.22), since a more hydrophobic surface will exhibit a larger contact angle. All of the nanofibrous substrates have contact angles exceeding 90° and can therefore be classified as hydrophobic substrates which exhibit poor wettability. Considering that these substrates could provide a capturing platform for mycobacteria in aqueous solution, wettability is of utmost importance[15] and the lack thereof could impede their suitability to be used for this purpose. The extent of hydrophilicity, however, cannot be too high (θ < 90°), as it can reduce the mechanical strength of the substrate.[38]

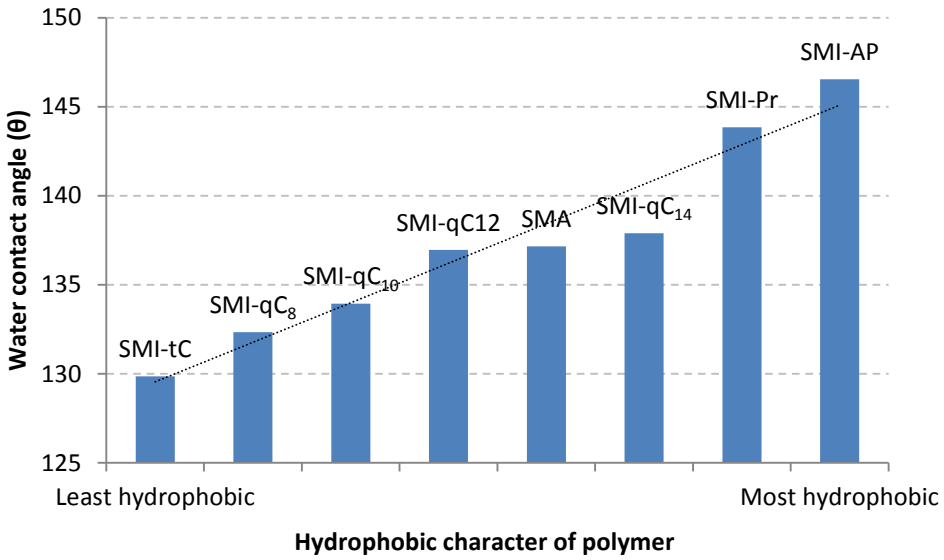

Figure 3.22 Measured water contact angles as a function of hydrophobic nanofibrous substrates of the various polymers.

The origin of hydrophobicity can be explained by examining the chemical composition of the various polymers and their ability to form hydrogen bonds with water molecules. Ion-dipole interactions between polar water molecules and the cationic ammonium moieties (refer to Figure 3.23) of the

quaternized polymers (SMI-qC$_x$) enable water solubility. Their alkyl chains, however, are non-polar hydrocarbons that repel water molecules, increasing the polymer's hydrophobic character.[39] The longer alkyl chain of SMI-qC$_{14}$ renders it more hydrophobic in nature than SMI-qC$_8$. This is observed in Figure 3.22, where θ = 138° for SMI-qC$_{14}$ and θ = 132° for SMI-qC$_8$. The same argument of alkyl-related hydrophobicity applies for the large contact angle observed for SMI-Pr.

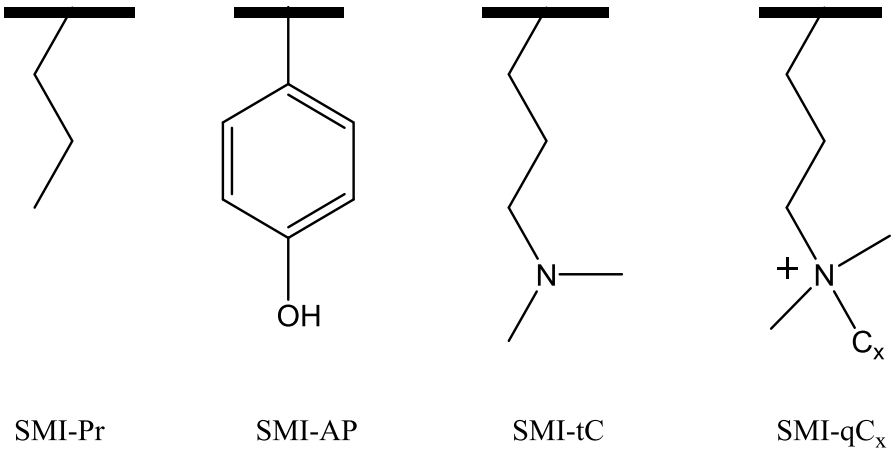

Figure 3.23 Chemical composition of the various SMA derivatives.

Hydrogen interactions between the electron lone pairs of the dimethylamino-group of SMI-tC (Figure 3.23) and water molecules account for the favourable interaction resulting in hydrophilic behaviour to some extent.[39] SMI-tC nanofibers are the least hydrophobic of the electrospun polymers. The highest degree of hydrophobicity was observed for SMI-AP which was expected due to the anisotropic effect of the phenol ring, which reduces the net dipole moment of the O – H bond, thus attenuating the interaction with water molecules.[23]

3.5 Conclusion

An alternating styrene-maleic anhydride copolymer (SMA) was synthesized via conventional radical copolymerization and served as the parent polymer that underwent chemical modification at its reactive maleic anhydride residue. Various primary amine compounds were used to facilitate the *N*-alkylation of SMA via a ring opening reaction at the maleic anhydride residue, followed by ring closure at elevated temperatures. One such maleimide derivative, SMI-tC, underwent additional substitution reactions with various bromoalkane compounds that yielded the corresponding SMI-qC$_x$ polymers containing quaternary ammonium moieties and an aliphatic hydrocarbon tail of various lengths (C$_8$-C$_{14}$).

All polymers were electrospun using binary solvent systems by means of a single needle technique in a controlled humidity atmosphere to yield nanofibers with average fiber diameters in the range of 463-575 nm.

Characterization using ^{1}H-NMR-, ^{13}C-NMR- and ATR-FTIR spectroscopy confirmed the successful synthesis and modification of pristine SMA to yield the various SMI derivatives. SEM was used to characterize the surface morphology and fiber diameters obtained for the various electrospun polymers. The BET method for surface area measurements were conducted to obtain the corresponding surface areas of the nanofibrous substrates. Lastly, the hydrophobic / hydrophilic character of the various polymers was investigated by means of water contact angle measurements to predict their suitability as capturing platforms for mycobacteria in aqueous solution.

3.6 Experimental

3.6.1 Chemicals

Styrene monomer (Sigma Aldrich, ≥99%) was passed through a column of aluminium oxide (Sigma Aldrich, ≥98%), a treatment which adsorbed the inhibitors and impurities. Maleic anhydride (Sigma Aldrich, 99%) was recrystallized from benzene. Methyl ethyl ketone (MEK), isopropanol, hexane, dimethylformamide (DMF), diethyl ether, dimethylsulfoxide (DMSO), ethanol, methanol and tetrahydrofuran (THF) were all purchased from Kimix and distilled prior to use. Acetone (Kimix), propylamine (Sigma), 4-aminophenol 97% (ACROS Organics), 3-(*N,N*-dimethylamino)-1-propylamine (Sigma), 1-bromooctane (Sigma), 1-bromodecane (Sigma), 1-bromododecane (Sigma) and 1-bromotetradecane (Sigma) was used without further purification. 2,2'-Azobis(2-methylpropionitrile) (AIBN) (Riedel-de Haën) was recrystallized from methanol, dried under vacuum and refrigerated before use. THF Chromasolv® Plus (for HPLC, ≥99.9%) was used for SEC. Deuterated acetone (acetone-d6) (Sigma Aldrich, 99.9 atom % D), deuterated chloroform ($CDCl_3$) (Sigma Aldrich, 99.8 atom % D) and deuterated dimethyl sulfoxide (d-DMSO) (Merck, 99.8 atom % D) was used as solvents for NMR spectroscopy.

3.6.2 Characterization techniques

(a) Nuclear magnetic resonance spectroscopy (NMR)

A Varian ^{Unity}*Inova* 600- and VNMRS 300 Liquid State NMR Spectrometer with VnmrJ 2.1B software was used to obtain the ^{1}H-NMR and ^{13}C-NMR spectra of all samples.

Deuterated chloroform ($CDCl_3$) and deuterated dimethyl sulfoxide (d-DMSO) were used as solvents. Tetramethylsilane (TMS) was used as internal standard (δ = 0 ppm).

(b) Size exclusion chromatography (SEC)

The molar mass (M_n) and polydispersity index (Đ) of SMA were obtained by size exclusion chromatography (SEC). The SEC instrument consists of a Waters 1515 isocratic HPLC pump, a Waters 717plus auto-sampler, Waters 600E system controller (run by Breeze Version 3.30 SPA) and a Waters in-line Degasser AF. Tetrahydrofuran (THF, HPLC grade, stabilized with 0.125% butylated hydroxytoluene (BHT)) was used as eluent at flow rates of 1 mL/min. The column was kept at 30 °C and the injection volume was 100 µL. Two PLgel (Polymer Laboratories) 5 µm Mixed-C (300x7.5 mm) columns and a pre-column (PLgel 5µm Guard, 50x7.5 mm) were used. Calibration was done using narrow dispersity polystyrene standards ranging from 580 to $2x10^6$ g/mol. All molecular weights were reported as polystyrene equivalents.

Samples were dissolved in THF (2 mg/mL) and filtered through 0.45 µm nylon filters before being subjected to analysis.

(c) Attenuated total reflectance Fourier transform infrared (ATR-FTIR) spectroscopy

All spectra were obtained using a Thermo Scientific Nicolet iS10 Smart iTR spectrometer that was operated in transmission mode from 4000 to 400 cm^{-1} with a resolution of 2 cm^{-1}. A background spectrum was collected before sample collection. Omnic 8.1 software from Thermo Fisher Scientific Inc. was used for data acquisition and data processing.

(d) Scanning electron microscopy (SEM)

Nanofiber samples were cut into 0.5 x 0.5 cm square pieces and mounted onto stubs using double sided carbon tape prior to being coated with gold sputter under vacuum using an Edwards S15OA Sputter Coater in order to make the sample surfaces electrically conducting.

Imaging of the samples was accomplished using a Leo® 1430VP Scanning Electron Microscope. The stubs with nanofiber samples were loaded into the imaging chamber. The scanning electron (SE) images show the surface of the nanofibers. Beam conditions under vacuum during surface analysis were 7 kV and approximately 1.5 nA, with a spot size of 150 d_p.

(e) Brunauer-Emmet-Teller (BET) surface area analysis

Specific surface area determinations were performed using a Micromeritics ASAP 2020 V3.03 Surface Area and Porosity Analyzer. The surface area of activated SMA and SMI-derivative nanofibers (100 mg sample each) were determined by N_2 absorption using Brunauer-Emmet-Teller (BET) method at 100 °C.

(f) Water contact angle measurments

The hydrophobic/hydrophilic character of SMA and SMI-derivative nanofibers were investigated by means of static water contact angle measurements. A Zeiss microscope unit was used for magnification. The test entailed placing a 1.0 µL drop of Milli-Q water on the nanofibrous surface and immediately capturing images using a Nikon SMZ-2T camera (Japan). Image analysis software (SEM Image Studio v7.1) was used to determine the contact angle. A minimum of 10 measurements, taken at different positions on the film, was carried out. The contact angles were measured on both sides of the drop and averaged.

3.6.3 Synthesis of poly(styrene-*alt*-maleic anhydride) (SMA)

A 1:1 molar ratio of styrene:maleic anhydride was used to synthesize an alternating copolymer via conventional radical copolymerization.[1]

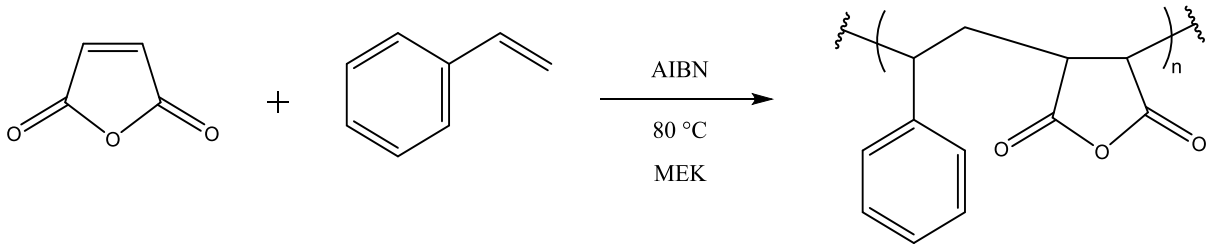

Scheme 3.5 Synthesis of poly(styrene-alt-maleic anhydride) (SMA).

Styrene monomer (15 g, 0.14 mol), maleic anhydride (MAnh) (14 g, 0.14 mol) and 2,2'-azobis(2-methylpropionitrile) (AIBN, 0.1182 g, 7.20 x 10^{-4} mol) were dissolved in 200 mL methyl ethyl ketone (MEK) at room temperature. The reaction mixture was purged with argon for 30 min, placed in a heated oil bath at 60 °C for 1 hour and refluxed for 16 hours at 80 °C without argon flow. The reaction mixture was cooled to room temperature, precipitated in isopropanol and washed with heptane. Any unreacted monomer and residual solvent was removed under vacuum at 50 °C overnight. SEC was used to analyse the molecular weight and polydispersity index. M_w = 15 901 g/mol, Đ = 2.15.

Major IR absorptions: 3030, 1849, 1775, 1711, 1219, 762, 701 cm^{-1}.

^{1}H NMR (300 MHz, acetone): δ (ppm) = 7.19 (s, broad, 5H, aromatic), 2.93 (dd, 2H, -C**H**-C**H**-), 2.41 (s, 3H, -C**H**-, -C**H$_2$**-).

^{13}C NMR (75 MHz, acetone): δ (ppm) = 174.15 (s, 2C, -N-**C**=O), 139.62 (s, 1C, -**C**H-), 129.69 (s, 5C, aromatic), 54.77 (s, 1C, -**C**H-), 42.97 (s, 2C, -**C**H-, -**C**H-), 32.11 (s, 1C, -**C**H$_2$-).

3.6.4 Synthesis of poly(styrene-*N*-propylmaleimide) (SMI-Pr)

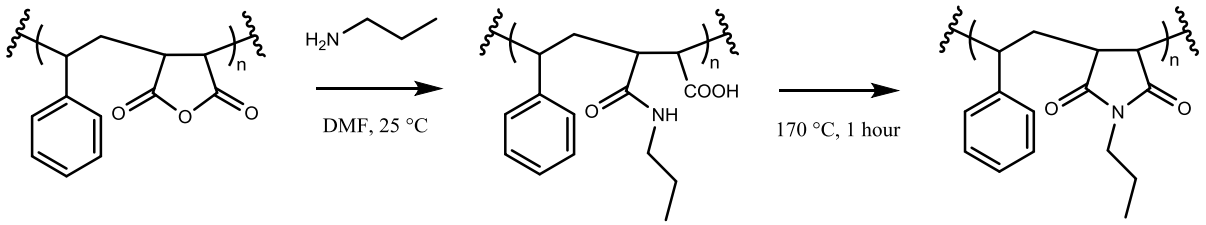

Scheme 3.6 Synthesis of poly(styrene-N-propylmaleimide) (SMI-Pr).

Propylamine (1.75 g, 29.6 mmol) was added dropwise to a solution of SMA (2 g, 9.89 mmol MAnh) in 20 mL dimethylformamide (DMF) at room temperature. The reaction was placed in a heated oil bath at 170 °C for one hour, where after it was precipitated into diethyl ether, filtered and dried under vacuum at 60 °C overnight to remove residual solvent.

Major IR absorptions: 2932, 1769, 1695, 1494, 1443, 1401, 1351, 1204, 1135, 759, 703 cm^{-1}.

^{1}H-NMR: (600 MHz, $CDCl_3$): δ (ppm) = 7.17 (s, broad, 5H, aromatic), 3.19 (m, 2H, -C**H**-C**H**-), 2.49 (s, 2H, $(CO)_2N$-C**H$_2$**-), 2.03 (s, 2H, -C**H$_2$**-), 1.33 (s, 3H, -C**H**-, -C**H$_2$**-), 0.69 (s, 3H, -C**H$_3$**-).

^{13}C NMR: (101 MHz, $CDCl_3$): δ (ppm) = 178.46 (d, 2C, -N-**C**=O), 138.60 (s, 1C, -**C**-aromatic), 128.80 (s, 5C, aromatic), 51.12 (s, 1C, -**C**H-), 43.59 (s, 2C, -**C**H-, -**C**H-), 40.12 (s, 1C, -**C**H_2-), 36.58 (s, 1C, -N-**C**H_2-), 20.87 (s, 1C, -**C**H_2-), 11.35 (s, -**C**H_3-).

3.6.5 Synthesis of poly(styrene-*N*-[4-hydroxyphenyl] maleimide) (SMI-AP)

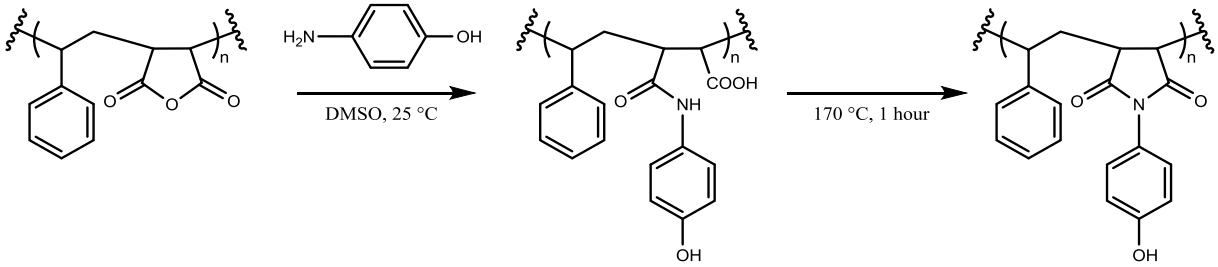

Scheme 3.7 Synthesis of poly(styrene-N-[4-hydroxyphenyl]maleimide) (SMI-AP).

A solution of 4-aminophenol (3.24 g, 29.6 mmol) in 10 mL dimethylsulfoxide (DMSO) was added dropwise to a solution of SMA (2 g, 9.89 mmol MAnh) in 20 mL DMSO. The reaction was placed in a heated oil bath at 170 °C for one hour. After cooling, the polymer was precipitated into ethyl acetate, filtered and dried under vacuum at 60 °C overnight to remove residual solvent.

Major IR absorptions: 3368, 1669, 1605, 1514, 1450, 1392, 1193, 829, 756, 703 cm^{-1}.

^{1}H NMR: (600 MHz, DMSO): δ = 9.73 (s, 1H, -O**H**-), 6.95 (d, broad, 9H, aromatic), 3.35 (s, 3H, -C**H**-, -C**H**-, -C**H**-), 1.99 (s, 2H, -C**H$_2$**-).

^{13}C NMR: (75 MHz, DMSO): δ = 176.66 (d, 2C, -N-**C**=O-), 157.27 (s, 1C, -**C**-OH), 137.63(s, 1C, -CH-**C**-aromatic), 127.99 (s, 7H, aromatic), 122.94 (s, 1C, -N-**C**-aromatic), 115.39 (s, 2C, aromatic), 51.51 (s, 1C, -**C**H-), 43.54 (s, 2C, -**C**H-, -**C**H-), 34.38 (s, 1C, -**C**H$_2$-).

3.6.6 Synthesis of poly(styrene-[*N*-3-(*N'*,*N'*-dimethylamino)propyl maleimide) (SMI-tC)

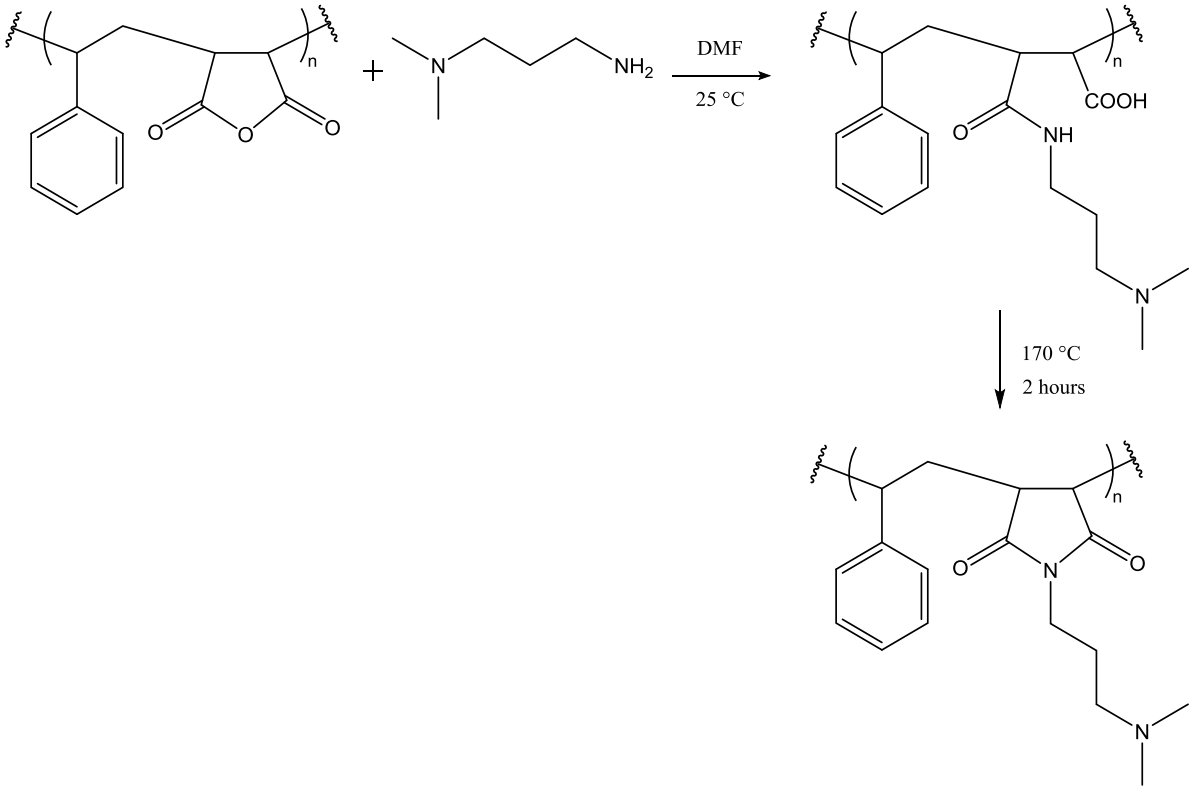

Scheme 3.8 Synthesis of poly(styrene-[N-3-(N',N'-dimethylamino)propyl maleimide) (SMI-tC).

3-(*N,N*-dimethylamino)-1-propylamine (DMAPA) (15 g, 147 mmol) was added dropwise to a solution of SMA (10 g, 49 mmol MAnh) in 50 mL DMF at room temperature. The reaction was placed in a heated oil bath at 170 °C for two hours, whereafter it was precipitated into diethyl ether, filtered and dried under vacuum at 60 °C overnight to remove residual solvent.

Major IR absorptions: 2943, 2767, 1768, 1689, 1398, 1344, 1149, 754, 701 cm^{-1}.

^{1}H NMR (400 MHz, $CDCl_3$): δ (ppm) = 6.92 (s, broad, 5H, aromatic), 3.32 (s, 2H, -C**H**-C**H**-), 2.93 (s, 2H, -(CO)$_2$N-C**H$_2$**-), 2.48 (s, 2H, -C**H**-, -C**H$_2$**-), 2.48 (s, 8H, -N-C**H$_2$**-, -N(C**H$_3$**)$_2$), 1.49 (s, 2H, -C**H$_2$**-).

^{13}C NMR (151 MHz, $CDCl_3$): δ (ppm) = 178.00 (d, 2C, -N-**C**=O), 137.91 (s, 1C, -**C**H-), 128.95 (s, 5C, aromatic), 56.94 (s, 1C, -N-**C**H$_2$-), 51.46 (s, 1C, -**C**H-), 45.39 (s, 2C, -N-(**C**H$_3$)$_2$), 41.01 (s, 2C, -**C**H-, -**C**H-), 36.98 (s, 1C, -N-**C**H$_2$-), 34.34 (s, 1C, -**C**H$_2$-), 25.41 (s, 1C, -**C**H$_2$-).

3.6.7 Synthesis of SMI-qC$_x$ polymers

(a) Synthesis of poly(styrene-[*N*-3-(*N'*-octyl-*N',N'*-dimethylammonium)propyl maleimide]) (SMI-qC$_8$)

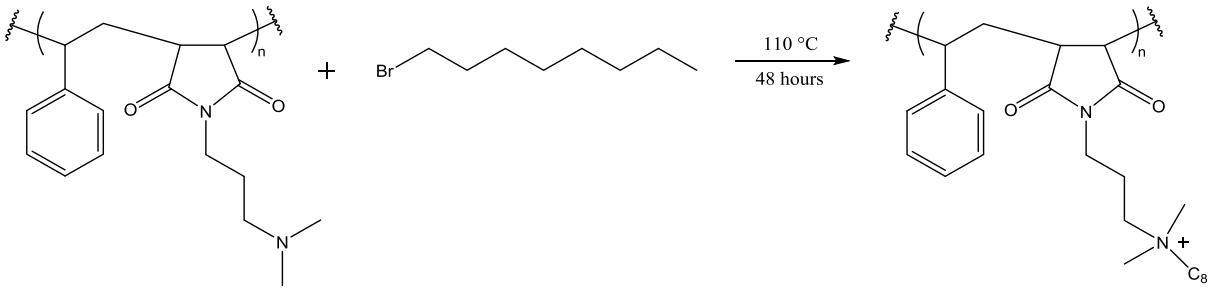

Scheme 3.9 Synthesis of poly(styrene-[N-3-(N'-octyl-N',N'-dimethylammonium)propyl maleimide]).

To a solution of poly(styrene-[*N*-3-(*N',N'*-dimethylamino)propyl maleimide) (1.5 g, 5.2 mmol MAnh) in 25 mL DMF was added dropwise 1-bromooctane (1.26 g, 6.5 mmol) at room temperature. The reaction was stirred at 110 °C for 48 hours, cooled, precipitated in diethyl ether, filtered and washed three times with hexane. The SMI-qC$_8$ polymer was dried under vacuum at 60 °C overnight to remove residual solvent.

Major IR absorptions: 3400, 2924, 2855, 1768, 1690, 1452, 140, 1356, 1182, 1025, 758, 703 cm^{-1}.

^{1}H-NMR (400 MHz, $CDCl_3$): δ (ppm) = 7.13 (s, broad, 5H, aromatic), 3.45 (s, 6H, -N(C**H$_3$**)$_2$), 3.34 (s, 4H, -C**H**-C**H**-, -(CO)$_2$N-C**H$_2$**-), 3.25 (s broad, 7H, -N-C**H$_2$**-, -N-C**H$_2$**-, -C**H**-, -C**H$_2$**-), 1.68 (s, 4H, -C**H$_2$**-, -C**H$_2$**-), 1.24 (s, 10H, -(C**H$_2$**)$_5$-), 0.87 (s, 3H, C**H$_3$**-CH$_2$-).

^{13}C-NMR (75 MHz, DMSO): δ (ppm) = 174.15 (s, 2C, -N-**C**=O), 139.62 (s, 1C, -**C**H-), 129.69 (s, 5C, aromatic), 63.79 (s, 1C, -N-**C**H$_2$-), 61.10 (s, 1C, -N-**C**H$_2$-), 54.77 (s, 1C, -**C**H-), 50.38 (s, 2C, -N(**C**H$_3$)$_2$), 42.55 (s, 2C, -**C**H-, -**C**H-), 31.77 (s, 1C, -**C**H$_2$-), 31.16 (s, 4C, -(**C**H$_2$)$_4$-), 26.32 (s, 1C, -**C**H$_2$-), 22.48 (s, 2C, -**C**H$_2$-, -**C**H$_2$-), 14.43 (s, 1C, -**C**H$_3$).

(b) Synthesis of poly(styrene-[*N*-3-(*N'*-decyl-*N',N'*-dimethylammonium)propyl maleimide]) (SMI-qC_{10})

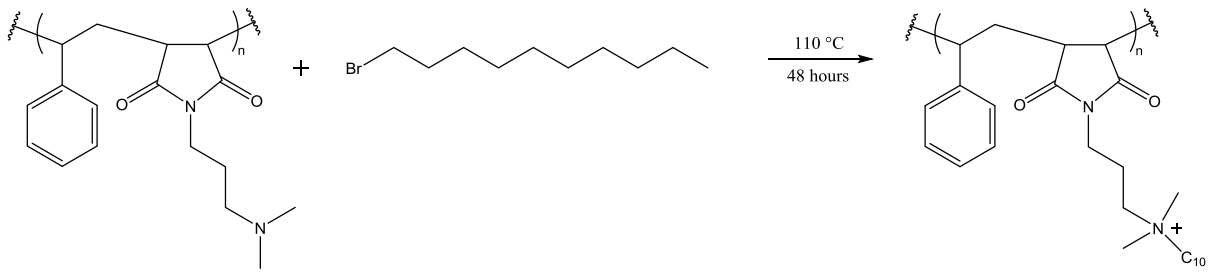

Scheme 3.10 Synthesis of poly(styrene-[N-3-(N'-decyl-N',N'-dimethylammonium)propyl maleimide]).

The same method was followed as with 3.6.7 (a) using 1-bromodecane (1.44 g, 6.5 mmol).

Major IR absorptions: 3402, 2923, 2854, 1768, 1691, 1453, 1401, 1357, 1181, 703 cm^{-1}.

^{1}H-NMR (400 MHz, $CDCl_3$): δ (ppm) = 7.13 (s, broad, 5H, aromatic), 3.45 (s, 6H, -N($C\mathbf{H_3}$)$_2$), 3.34 (s, 4H, -C**H**-C**H**-, -$(CO)_2$N-C$\mathbf{H_2}$-), 3.25 (s broad, 7H, -N-C$\mathbf{H_2}$-, -N-C$\mathbf{H_2}$-, -C**H**-, -C$\mathbf{H_2}$-), 1.68 (s, 4H, -C$\mathbf{H_2}$-, -C$\mathbf{H_2}$-), 1.24 (s, 14H, -($C\mathbf{H_2}$)$_7$-), 0.87 (s, 3H, C$\mathbf{H_3}$-CH_2-).

^{13}C NMR (75 MHz, DMSO): δ (ppm) = 174.15 (s, 2C, -N-**C**=O), 139.62 (s, 1C, -**C**H-), 129.69 (s, 5C, aromatic), 63.79 (s, 1C, -N-**C**H_2-), 61.10 (s, 1C, -N-**C**H_2-), 54.77 (s, 1C, -**C**H-), 50.38 (s, 2C, -N($\mathbf{C}H_3$)$_2$), 42.55 (s, 2C, -**C**H-, -**C**H-), 31.77 (s, 1C, -**C**H_2-), 31.16 (s, 6C, -($\mathbf{C}H_2$)$_6$-), 26.32 (s, 1C, -**C**H_2-), 22.48 (s, 2C, -**C**H_2-, -**C**H_2-), 14.43 (s, 1C, -**C**H_3).

(c) Synthesis of poly(styrene-[*N*-3-(*N'*-dodecyl-*N',N'*-dimethylammonium)propyl maleimide]) (SMI-qC_{12})

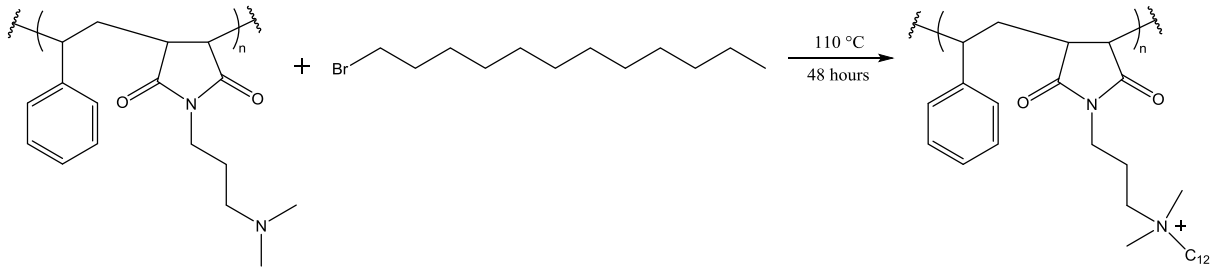

Scheme 3.11 Synthesis of poly(styrene-[N-3-(N'-dodecyl-N',N'-dimethylammonium)propyl maleimide]).

The same method was followed as with 3.6.7 (a) using 1-bromododecane (1.62 g, 6.5 mmol).

Major IR absorptions: 3407, 2922, 2852, 1767, 1692, 1449, 1400, 1354, 1179, 1023, 756, 699 cm^{-1}.

^{1}H-NMR (400 MHz, $CDCl_3$): δ (ppm) = 7.13 (s, broad, 5H, aromatic), 3.45 (s, 6H, -N($C\mathbf{H_3}$)$_2$), 3.34 (s, 4H, -C**H**-C**H**-, -(CO)$_2$N-C$\mathbf{H_2}$-), 3.25 (s broad, 7H, -N-C$\mathbf{H_2}$-, -N-C$\mathbf{H_2}$-, -C**H**-, -C$\mathbf{H_2}$-), 1.68 (s, 4H, -C$\mathbf{H_2}$-, -C$\mathbf{H_2}$-), 1.24 (s, 18H, -(C$\mathbf{H_2}$)$_9$-), 0.87 (s, 3H, C$\mathbf{H_3}$-CH$_2$-).

^{13}C NMR (75 MHz, DMSO): δ (ppm) = 174.15 (s, 2C, -N-**C**=O), 139.62 (s, 1C, -**C**H-), 129.69 (s, 5C, aromatic), 63.79 (s, 1C, -N-**C**H$_2$-), 61.10 (s, 1C, -N-**C**H$_2$-), 54.77 (s, 1C, -**C**H-), 50.38 (s, 2C, -N(**C**H$_3$)$_2$), 42.55 (s, 2C, -**C**H-, -**C**H-), 31.77 (s, 1C, -**C**H$_2$-), 31.16 (s, 8C, -(**C**H$_2$)$_8$-), 26.32 (s, 1C, -**C**H$_2$-), 22.48 (s, 2C, -**C**H$_2$-, -**C**H$_2$-), 14.43 (s, 1C, -**C**H$_3$).

(d) Synthesis of poly(styrene-[*N*-3-(*N'*-tetradecyl-*N',N'*-dimethylammonium)propyl maleimide]) (SMI-qC$_{14}$)

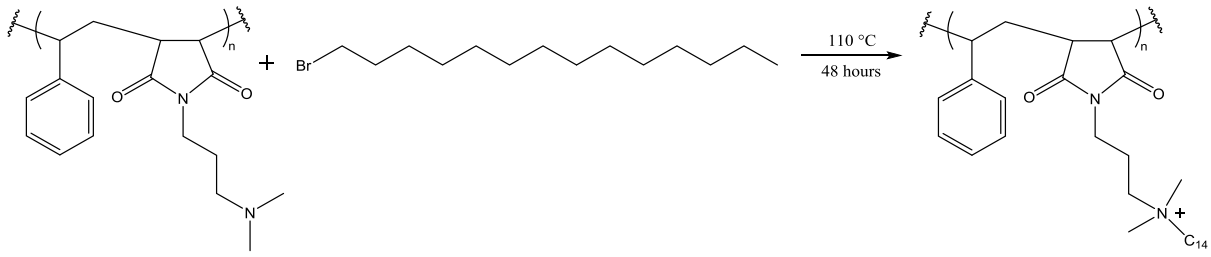

Scheme 3.12 Synthesis of poly(styrene-[N-3-(N'-tetradecyl-N',N'-dimethylammonium)propyl maleimide]).

The same method was followed as with 3.6.7 (a) using 1-bromotetradecane (1.80 g, 6.5 mmol).

Major IR absorptions: 3405, 2922, 2852, 1767, 1691, 1455, 1401, 1357, 1181, 1024, 703 cm^{-1}.

^{1}H NMR (300 MHz, $CDCl_3$) δ (ppm) = 6.91 (s, broad, 5H, aromatic), 4.79 (s, 6H, -N($C\mathbf{H_3}$)$_2$), 3.35 (s, 4H -C**H**-C**H**-, -(CO)$_2$N-C$\mathbf{H_2}$-), 3.22 – 2.86 (s, broad, 7H, -N-C$\mathbf{H_2}$-, -N-C$\mathbf{H_2}$-, -C**H**-, -C$\mathbf{H_2}$-), 1.60 (s, 4H, -C$\mathbf{H_2}$-, -C$\mathbf{H_2}$-), 1.35 (s, 22H, -(C$\mathbf{H_2}$)$_{11}$-), 0.88 (s, 3H, C$\mathbf{H_3}$-CH$_2$-).

^{13}C NMR (75 MHz, DMSO): δ (ppm) = 174.15 (s, 2C, -N-**C**=O), 139.62 (s, 1C, -**C**H-), 129.69 (s, 5C, aromatic), 63.79 (s, 1C, -N-**C**H$_2$-), 61.10 (s, 1C, -N-**C**H$_2$-), 54.77 (s, 1C, -**C**H-), 50.38 (s, 2C, -N(**C**H$_3$)$_2$), 42.55 (s, 2C, -**C**H-, -**C**H-), 31.77 (s, 1C, -**C**H$_2$-), 31.16 (s, 10C, -(**C**H$_2$)$_{10}$-), 26.32 (s, 1C, -**C**H$_2$-), 22.48 (s, 2C, -**C**H$_2$-, -**C**H$_2$-), 14.43 (s, 1C, -**C**H$_3$).

3.6.8 Electrospinning of SMA and SMI derivatives

Each polymer solution was placed in a 1 mL syringe with a blunt needle tip with needle diameter of 21 gauge, which was mounted on a horizontal syringe pump with a tip to collector distance of 15 cm. A positive electrode was connected to the needle tip with a charge set at 15 kV, and the negative electrode was connected to the collector plate covered with foil with a charge of equal magnitude. The flow rates were set accordingly for SMA and the SMI derivatives. Approximately 2 mL of each solution was electrospun at relative humidity ranging between 35 - 37%. The relative humidity of

the electrospinning atmosphere was kept constant by employing a dehumidifier, whereas the temperature of 24 °C was maintained by the air conditioner. The collected fibers were placed under vacuum at 130 °C with a dual purpose: to facilitate crosslinking, rendering the fibers water-insoluble, and to remove any residual solvents.

3.7 References

1. Jeong, J.; Byoun, Y.; Ko, S.; Lee,T.Y. *J. Ind. Eng. Chem.* **2001**, *7,* 310-315.

2. Jeong, J.; Byoun, Y.; Lee, Y. *React. Funct. Polym*. **2002**, *50*, 257-263.

3. Huang, Z.; Zhang, Y.; Kotaki, M.; Ramakrishna, S. *Composites Sci. Technol*. **2003**, *63*, 2223-2253.

4. Wannatong, L.; Sirivat, A.; Supaphol, P. *Polym. Int*. **2004**, *53*, 1851-1859.

5. Reneker, D.H.; Chun, I. *Nanotechnology* **1996**, *7*, 216.

6. Luo, C.J.; Nangrejo, M.; Edirisinghe, M. *Polymer* **2010**, *51*, 1654-1662.

7. Wang, M.; Zhu, X.; Wang, S.; Zhang, L. *Polymer* **1999**, *40*, 7387-7396.

8. Nieuwhof, R.P.; Koudijs, A.; Marcelis, A.T.; Sudhölter, E.J. *Macromolecules* **1999**, *32*, 6499-6506.

9. Soer, W.J.; Ming, W.; Koning, C.E.; van Benthem, R.A.; Mol, J.M.C.; Terryn, H. *Progr. Org. Coat*. **2009**, *65*, 94-103.

10. Fang, H.; Mighri, F.; Ajji, A. *J. Appl. Polym. Sci.* **2008**, *109*, 3938.

11. Schmidt, U.; Zschoche, S.; Werner, C. *J. Appl. Polym. Sci*. **2003**, *87*, 1255-1266.

12. Vermeesch, I.; Groeninckx, G. *J. Appl. Polym. Sci*. **1994**, *53*, 1365-1373.

13. Bourland, L.G.; London, M.E.; Cooper, T.A. *Papers from a two-day seminar* **1972**.

14. Soer, W.J.; Ming, W.; Koning, C.E.; van Benthem, R.A.; Mol, J.; Terryn, H. *Progr. Org. Coat*. **2009**, *65*, 94-103.

15. Cronje, L.; Warren, R.; Klumperman, B. *J. Mat. Chem. B.* **2012**, *48*, 6608-6618.

16. Megelski, S.; Stephens, J.S.; Chase, D.B.; Rabolt, J.F. *Macromolecules* **2002**, *35*, 8456.

17. Shenoy, S.L.; Bates, W.D.; Frisch, H.L.; Wnek, G.E. *Polymer* **2005**, *46*, 3372-3384.

18. Reneker, D.H.; Yarin, A.L.; Fong, H.; Koombhongse, S. *J. Appl. Phys*. **2000**, *87*, 4531.

19. Fong, H.; Reneker, D.H. *J. Polym. Sci.* **1999**, *37*, 3488-3493.

20. Lee, K.H.; Kim, H.Y.; Bang, H.J.; Jung, Y.H.; Lee, S.G. *Polymer* **2003**, *44*, 4029-4034.

21. Ferry, J.D. *J. Am. Chem. Soc*. **1950**, *72*, 3746-3752.

22. Jeong, J.; Byoun, Y.; Ko, S.; Lee, T.Y. *J. Ind. Eng. Chem*. **2001**, *7*, 310-315.

23. Lampman, G.M.; Pavia, D.L.; Kriz, G.S.; Vyvyan, J.R. *Spectroscopy* **2010**, *4*, 15-77.

24. Duan, X.; Xiao, J.; Yin, Q.; Zhang, Z.; Mao, S.; Li, Y. *Int. J. Nanomed*. **2012**, *7*, 4961.

25. Bshena, O.; Heunis, T.D.J.; Dicks, L.M.T.; Klumperman, B. *Fut. Med. Chem.* **2011**, *3*, 1821-1847.

26. Berthier, D.L.; Paret, N.; Trachsel, A.; Fieber, W.; Herrmann, A. *Polymers* **2013**, *5*, 234-253.

27. Ha, N.T.H. *Polymer* **1999**, *40*, 1081-1086.

28. Lessard, B.; Maric, M. *Macromolecules* **2009**, *43*, 879-885.

29. Li, H.; Chen, H.; Shen, Z.; Lin, S. *Polymer* **2002**, *43*, 5455-5461.

30. Moraes, L.G.P.; Rocha, R.S.F.; Menegazzo, L.M.; Araújo, E.B.D.; Yukimito, K.; Moraes, J.C.S. *J. Appl. Or. Sci*. **2008**, *16*, 145-149.

31. Agarwal, S.; Wendorff, J.H.; Greiner, A. *Macromol. Rap. Comm*. **2010**, *31*, 1317-1331.

32. Brunauer, S.; Emmett, P.H.; Teller, E. *J. Am. Chem. Soc*. **1938**, *60*, 309-319.

33. Ismail, I.M.K. *Carbon* **1990**, *28*, 423-434.

34. Yalçın, N.; Sevinç, V. S *Carbon* **2000**, *38*, 1943-1945.

35. Širc, J.; Hobzová, R.; Kostina, N.; *et al*. *J. Nanomat.* **2012**, *2012*, 121.

36. Feng, L.; Li, S.; Li, H.; *et al*. *Ang. Chem*. **2002**, *114*, 1269-1271.

37. Miller, R.N. *Mater. Prot. Perf.* **1973**, *12*, 31-36.

38. Kim, K.; Yu, M.; Zong, X.; *et al*. *Biomaterials* **2003**, *24*, 4977-4985.

39. Williams, L.D. *Instit. Bioeng. Biosci*. **2015**, 1-7.

Chapter 4: Surface functionalization of SMA nanofibers with Concanavalin A

4.1 Introduction

Functional side chains attached to polymer surfaces can be used to incorporate various properties to the polymer surface, such as adhesion, lubrication, biocompatibility and water repellent behaviour[1] to name but a few. Such attachments can be accomplished by either surface grafting methods (sensitizers,[2] plasma treatment,[3] high-energy radiation,[4] etc.) or via direct chemical reactions with functional groups on the backbone of the parent polymer. An example of the latter approach entails the immobilization of two enzymes such as horseradish peroxidase (HRP) and glucose oxidase on a membrane consisting of unmodified SMA nanofibers. Cascade reactions on the immobilized enzymes were performed to confirm the immobilization of HRP with retention of enzymatic activity.[5] These enzymes were covalently linked to SMA via ring-opening of the maleic anhydride residues[6] since both enzymes contain accessible amine functional groups.

Polymer nanofibrous substrates provide high degrees of chemical and physical versatility.[5,7] The high surface-to-volume ratio of nanofibers renders them ideal to immobilize high densities of bioactive molecules.[8] A wide range of biomolecules such as enzymes, antibodies, peptides, and DNA have been immobilized onto various nanomaterials such as inorganic nanoparticles, nanotubes, organic colloids and various fibrous materials such as nanofibers. Using nanomaterials as parent substrates significantly improve the efficiency and sensitivity of immobilized molecules for recognizing their counterparts.[7,9-11]

The lectin Concanavalin A (Con A) comprises a significant fraction of the protein in the jack bean (*Canavalia ensiformis*). It is a tetramer that consists of four identical subunits that bind with moderate affinity (K_d 120-500 μM) to the α anomers of D-mannose and D-glucose.[12] When oligosaccharides containing these sugars are displayed on a cell surface, Con A binds with high avidity as a result of multivalent interactions. Due to this high avidity and its specificity for particular sugars, the function of Con A is presumed to involve binding to D-mannosyl-containing oligosaccharides as part of a specific cell recognition process.[13] To enable binding activity, each monomer needs one transition metal ion, Mn^{2+} in the native form, and one calcium ion to give the necessary conformation of the polypeptide chain at the binding site[14] which is formed from four peptide loops.[15]

Proteins are readily immobilized on a prefabricated nanofibrous substrate. Attempting to obtain a homogeneously dissolved solution of such charged molecules with high molecular weight in an organic phase for electrospinning could potentially be extremely difficult and was not attempted in this study. In addition, the harsh electrospinning conditions could diminish their biological activity. Thus, Con A was immobilized onto prefabricated SMA nanofibers using mild reaction conditions.[16]

This chapter describes the electrospinning and surface functionalization of SMA with Con A, and the characterization thereof using ATR-FTIR, the ninhydrin test as well as the horseradish peroxidase (HRP) assay. The SMA nanofibers were produced by single needle electrospinning, followed by the covalent attachment of Con A. Scanning electron microscopy (SEM) was used to evaluate the fiber morphology before and after immobilization of Con A, whereas attenuated total reflectance Fourier transform infrared spectroscopy (ATR-FTIR) was employed to confirm chemical attachment between Con A and the maleic anhydride residue of SMA. The ninhydrin test was used to determine the

presence of immobilized Con A, whereas the horseradish peroxidase assay was employed to quantify the biological activity of the immobilized protein. Brunauer-Emmett-Teller (BET) surface analysis was conducted to evaluate the surface area of the nanofibrous substrate, and water contact angle measurements were done to evaluate the hydrophobic/hydrophilic nature of the substrate.

4.2 Surface functionalization of SMA nanofibers

SMA can readily undergo nucleophilic substitution reactions with various low molecular weight compounds containing amino groups via ring opening of the maleic anhydride residue.[6,17] A secondary amide and carboxylic acid group forms, also known as maleamic acid.[1] Irreversible ring-closure takes place at elevated temperatures,[18] yielding the imidization product poly(styrene-*alt*-maleimide) (SMI). Refer to Scheme 4.1 for a schematic illustration of this reaction.

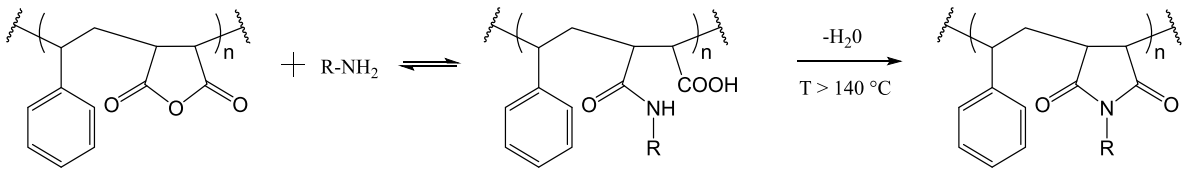

Scheme 4.1 Schematic representation of the imidization reaction.[18]

SMA nanofibers were used as substrate to immobilize Con A via covalent coupling. Heat treatment of pristine SMA nanofibers at 130 °C resulted in preservation of the nanofibrous structure when subjected to the surface functionalization procedure in a buffer solution. Surface functionalization with Con A was accomplished via an imidization reaction between the very reactive and accessible α-amine group present on the N-terminus (of the protein) or the ϵ-amino group of the lysine residues of the protein that react spontaneously with the anhydride groups of SMA under neutral conditions yielding SMI-Con A functionalized nanofibrous mats. A phosphate buffer (PBS) solution containing manganese and calcium ions was chosen as solvent for Con A to preserve its polypeptide conformation and to retain its binding activity.[14,15,19]

In a different approach, the covalent attachment of a monolayer of Con A to prefabricated SMA nanofibers was followed by glutaraldehyde (GA) treatment that cross-linked additional protein molecules and aggregates from the solution onto the covalently attached seed protein molecules.[20] These cross-linked protein aggregates (CLPAs) were expected to improve the biological activity of the immobilized proteins.[20] The immobilization and cross-linking of Con A onto SMA nanofibers using GA yielded SMI-CLPA nanofibers.

The Con A-functionalized SMI nanofibrous mats were washed with buffer solution to remove any unreacted protein, and air dried before characterization using ATR-FTIR. The ninhydrin test was performed to confirm the presence of primary amine groups, thus confirming that Con A was immobilized, and the HRP test was performed to quantify the biological activity of Con A after immobilization. BET surface area analyses were conducted to measure the surface areas of the nanofibers. The hydrophobic/hydrophilic character of SMA, SMI-Con A and SMI-CLPA nanofibrous substrates were evaluated using water contact angle measurements.

4.2.1 Electrospinning of SMA

Previously synthesized SMA (Chapter 3.6.3, Figure 4.1) was electrospun from a 1:2 DMF: acetone solvent system yielding smooth fibers with an average fiber diameter of 468 ± 111 nm, as characterized by SEM. The fibers were dried under vacuum at 130 °C for 24 h to remove residual solvent and to render the fibers water insoluble, a prerequisite to maintain structural integrity during the immobilization of Con A.

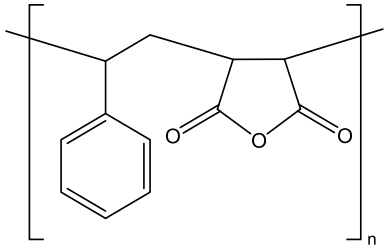

Figure 4.1 Repeating unit of SMA.

4.2.2 Synthesis of SMI-Con A nanofibrous substrate

Concanavalin A (Con A), a lectin from jack beans, are commercially available proteins that contain manganese and calcium near the carbohydrate binding sites. The saccharide binding specificity of Con A has been shown to be directed toward the monosaccharides glucose and mannose.[12] Con A was immobilized onto SMA nanofibers via covalent coupling between the maleic anhydride residue and primary amine groups of Con A (Scheme 4.2).

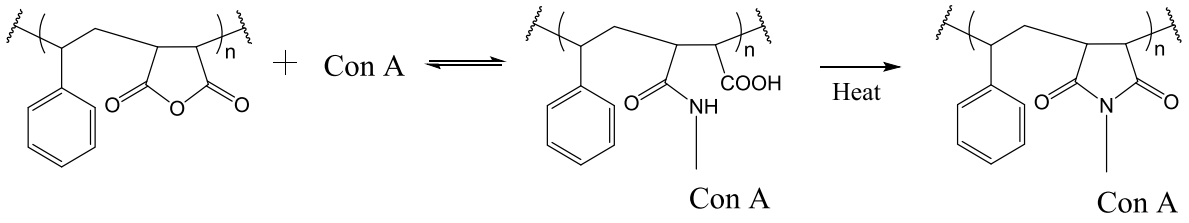

Scheme 4.2 Imidization reaction of SMA with Concanavalin A.

4.2.3 Synthesis of SMI-CLPA nanofibrous substrate

Cross-linked protein aggregates (CLPA) was prepared on SMA nanofibers by immobilizing a monolayer of Con A via covalent coupling between the maleic anhydride residues and the primary amine groups of Con A, followed by treatment with glutaraldehyde (GA) to cross-link additional protein molecules and aggregates from the solution onto the covalently attached seed protein molecules yielding SMI-CLPA nanofibers (Scheme 4.3).

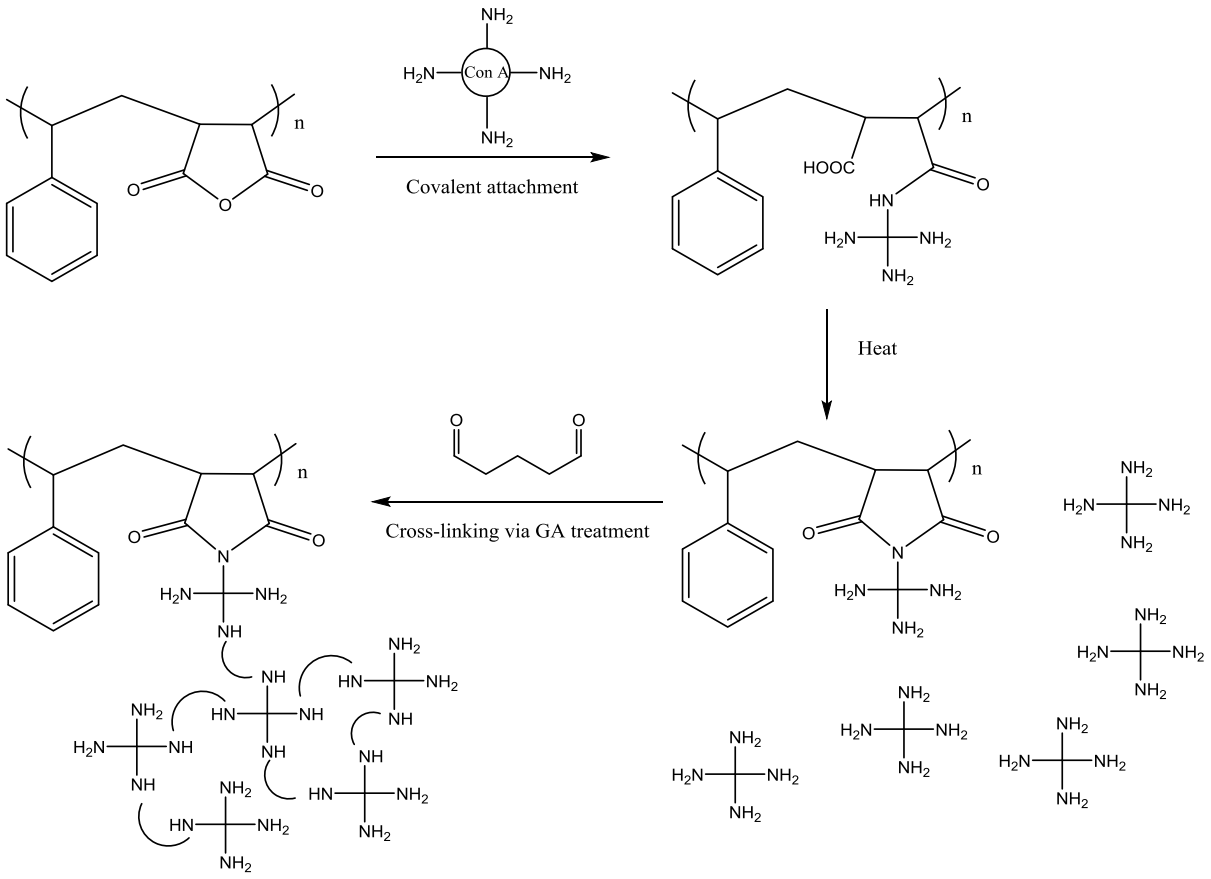

Scheme 4.3 Preparation of CLPAs on SMA nanofibers using Concanavalin A and glutaraldehyde.

4.3 Characterization of SMI-Con A and SMI-CLPA nanofibers

4.3.1 ATR-FTIR

ATR-FTIR was employed in order to confirm that Con A has been covalently immobilized onto the prefabricated SMA nanofibers via imidization. Refer to Figure 4.2 for the representative IR spectra of SMA, SMI-Con A and SMI-CLPA. Due to their shared similarities, only the spectrum of SMI-Con A will be discussed.

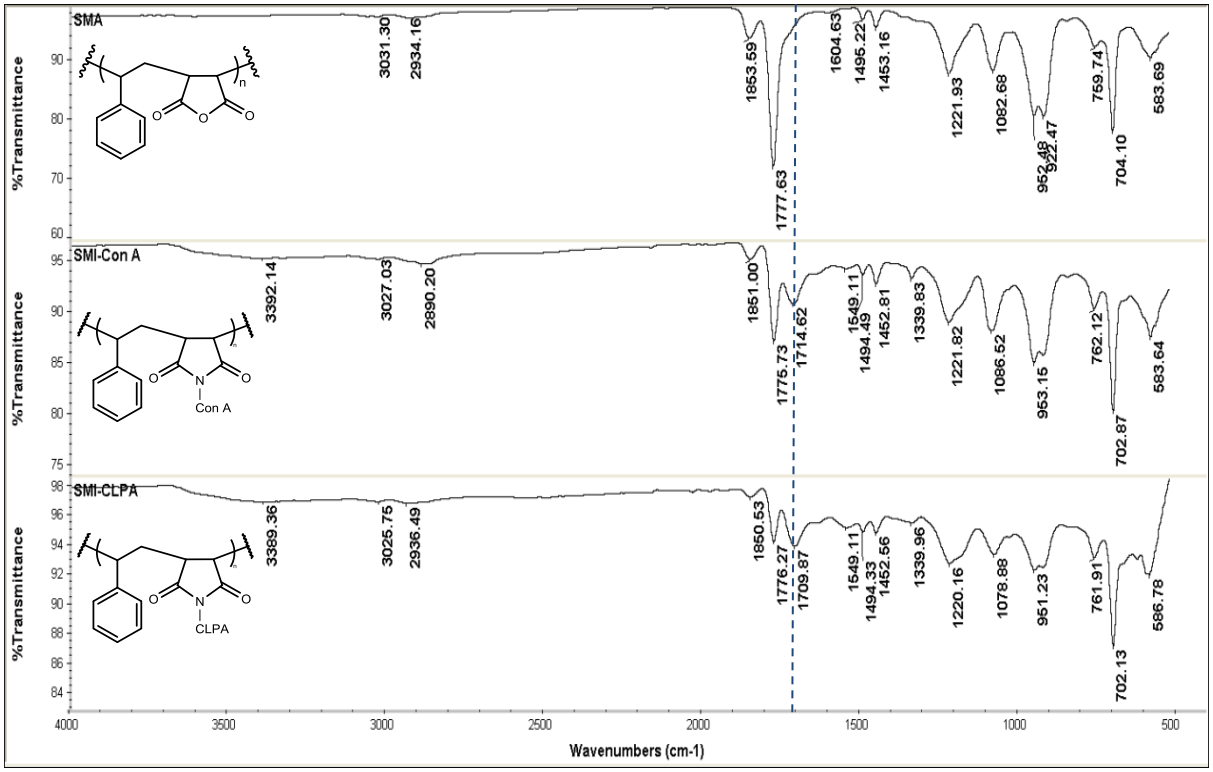

Figure 4.2 IR spectra of SMA and SMA surface functionalized with Concanavalin A (SMI-Con A).

The IR spectrum of SMA is characterized by aromatic =C– (sp^2) and aliphatic –CH_2– (sp^3) stretch vibrations occurring at 3031 and 2934 cm^{-1} with the ring stretch absorptions (C=C) appearing at 1604 and 1453 cm^{-1}. The IR spectrum of SMI-Con A is characterized by a broad absorption band at 3392 cm^{-1} arising from the superposition of O–H and N–H stretching vibrations.[8] A weak absorption band at 1339 cm^{-1} is indicative of a C–N stretch vibration of the newly formed imide bond. Characteristic doublets of the carbonyl (C=O) stretching vibration modes of maleic anhydride can be seen at 1777 and 1853 cm^{-1} in the IR spectrum of SMA.[21] After the reaction of SMA with Con A, a new peak appeared at 1714 cm^{-1}, attributed to the carbonyl stretching vibration of cyclic maleimide.[22] The intensity of the peak at 1775 cm^{-1} decreased, indicating that conversion of cyclic anhydride to cyclic imide via imidization was only partially achieved. The degree of conversion (DC) was calculated by using a reference peak in the spectra. In this instance, the peak at 704 cm^{-1} exhibits the out-of-plane bending motion of the monosubstituted benzene ring[23] which does not produce any change during the reaction. Using the ratio of peak heights at 1777 cm^{-1} and 704 cm^{-1} in both spectra, the percentage of unreacted maleic anhydride (MA) was calculated using Equation 4.1:[24]

$$(\%\ MA) = \frac{[Abs\ (1775\ cm^{-1})/Abs\ (702\ cm^{-1})]_{SMI-Con\ A}}{[Abs\ (1777\ cm^{-1})/Abs\ (704\ cm^{-1})]_{SMA}} \times 100 \qquad (4.1)$$

The height of the absorption bands (*Abs*) of both spectra have been used, and the DC was determined using Equation 4.2:[24]

$$\% DC = 100 - (\% MA) \quad (4.2)$$

The results obtained from the IR spectra indicate that Con A was successfully immobilized onto the SMA nanofibers with 73.6% conversion of the maleic anhydride residue, yielding SMI-Con A nanofibers. SMI-CLPA was successfully functionalized with 68.7% conversion.

4.3.2 Ninhydrin test

The ninhydrin test was employed to further confirm the presence of Con A on the surface of the SMA nanofibers. Ninhydrin (2,2-dihydroxy-1,3-indanedione) reacts with primary amine groups to form the purple dye, Ruhemann's purple (RP). This reaction is unique among chromogenic reactions in that at pH 5.5 it results in the formation of the same soluble chromophore by all primary amines which react, be they amines, amino acids, peptides, proteins, and even ammonia.[25] A colour change from colourless to dark blue was observed for both SMI-Con A and SMI-CLPA nanofibers, which is indicative of a positive test result for the presence of primary amine groups on the surface of the nanofibers and thus confirms that Con A was successfully immobilized. The chemical structure of ninhydrin is shown in Figure 4.3.

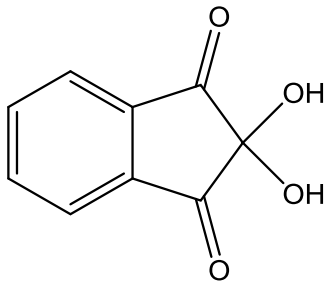

Figure 4.3 Chemical structure of ninhydrin.

4.3.3 Horseradish peroxidase assay

The retention of biological activity of the immobilized Con A was evaluated using a horseradish peroxidase (HRP) assay. HRP is a Con A-binding glycoprotein which is readily detected with a range of chromogenic substrates.[26] For this assay, SMI-Con A and SMI-CLPA fibers were incubated with HRP in a phosphate buffer solution (PBS) for three hours at 25 °C before being rinsed to remove non-binding HRP from the fibers. The substrate 2,2'-azino-bis(3-ethylbenzthiazoline-6-sulfonic acid) (ABTS) was added at room temperature before measuring the change in absorbance at 405 nm ($\Delta A_{405\ nm}$) for three minutes. A colour change from light green to dark blue was observed, confirming that HRP was bound to biologically active Con A immobilized onto SMA nanofibers. The amount of biologically active Con A immobilized onto SMA nanofibers was calculated to be 8.1% for SMI-Con A and 17.3% for SMI-CLPA.[27]

4.3.4 SEM

Pristine SMA nanofibers and surface functionalized SMI-Con A and SMI-CLPA nanofibers were prepared and analysed using SEM to evaluate the fiber morphology and diameters. Prefabricated SMA nanofibers had average fiber diameters of 468 ± 111 nm and that of SMA surface functionalized with Con A was 1077 ± 326 nm for SMI-Con A and 1172 ± 272 nm for SMI-CLPA. The increase in fiber diameters after functionalization was 130% and 150%, respectively, for SMI-Con A and SMI-CLPA. The fiber morphology, however, remained unchanged. The corresponding SEM images are shown in Figure 4.4

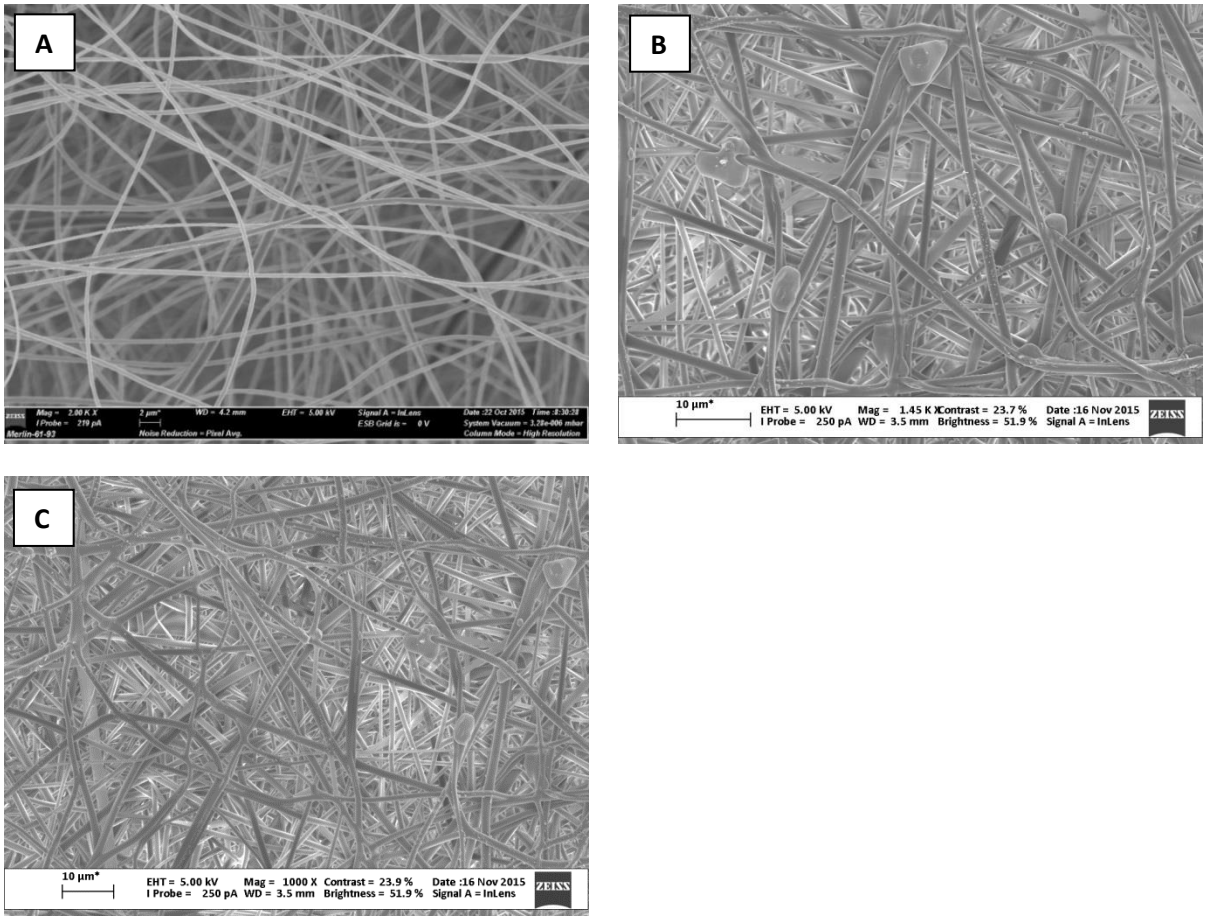

Figure 4.4 SEM images of (A) SMA, (B) SMI-Con A and (C) SMI-CLPA nanofibers.

4.3.5 BET surface area analysis

Surface characteristics of a material refer to the properties associated with its surface. Typical measurements include surface area, pore size and porosity. Information on surface characteristics is of importance when considering substrates with a large surface to volume ratio. A substrate with a large surface to volume ratio, such as nanofibers, has the advantage that more chemical groups are available to undergo chemical reactions. Furthermore, nanofibrous substrates with immobilized enzymes are believed to be able to retain its catalytic activity to a high extent.[28]

Nitrogen adsorption/desorption measurements were employed to measure the specific surface areas of the SMI-Con A and SMI-CLPA nanofibers using the Brunauer-Emmet-Teller (BET) method.[29] The BET surface area of activated SMA nanofibers was measured as 363.8 m^2/g, and that of SMI-Con A and SMI-CLPA nanofibers as 277.6 m^2/g and 225.2 m^2/g, respectively. A decrease of 24% and 38% in the available surface areas of SMI-Con A and SMI-CLPA nanofibers compared to pristine SMA nanofibers was observed. This was expected since the surface area per unit mass of nanofibers is inversely proportional to fiber diameter (refer Figure 4.5). Thus, the increased fiber diameters measured for SMI-Con A and SMI-CLPA as compared to pristine SMA nanofibers accounts for the decrease in surface area obtained by BET measurements.[30]

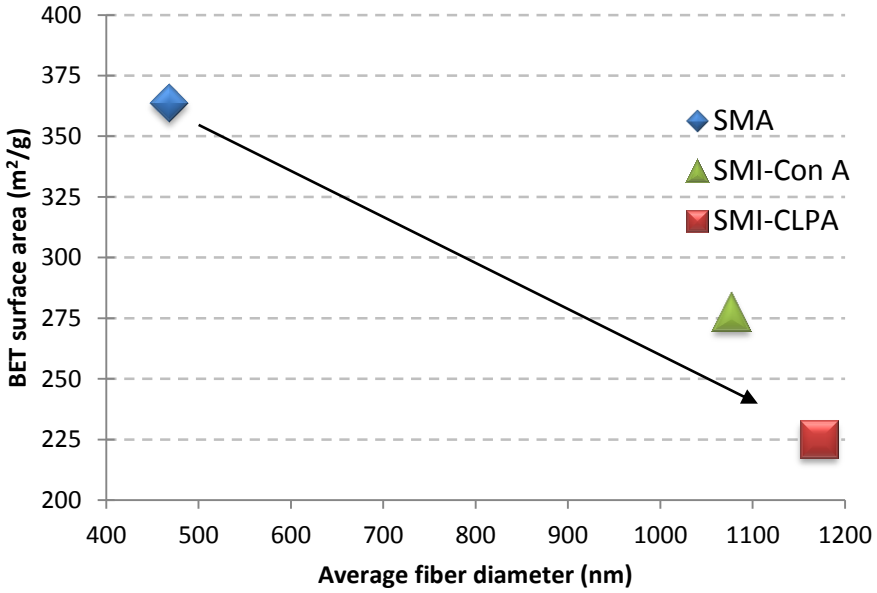

Figure 4.5 Relationship between fiber diameter and surface area for SMA and SMI-Con A nanofibers.

4.3.6 Water contact angle measurements

Water contact angle measurements were used to evaluate the hydrophobic/hydrophilic character of the SMA nanofibers modified with Con A to determine the wettability of the surfaces.

The pristine SMA nanofibers had an average contact angle of θ = 137°, which decreased to θ = 48° after surface functionalization with Con A to yield SMI-Con A nanofibers and to θ = 39° for SMI-CLPA nanofibers (Figure 4.6). The O–H and N–H groups of immobilized Con A allows hydrogen bonding to occur between the amino acid residues and water molecules, rendering SMI-Con A nanofibers hydrophilic in nature. This phenomenon explains the good wettability observed for SMI-Con A substrates when compared to pristine SMA nanofibers, which exhibited hydrophobic behaviour. Considering that SMI-Con A and SMI-CLPA nanofibers could provide a capturing platform for mycobacteria in aqueous solution, wettability is of utmost importance.[16]

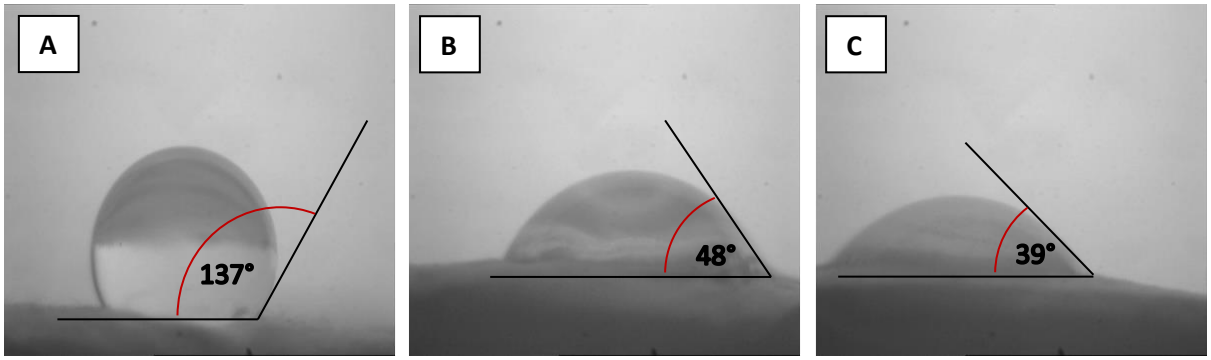

Figure 4.6 Captured images of water droplets on (a) SMA, (b) SMI-Con A and (c) SMI-CLPA nanofibers and their corresponding static water contact angles (θ).

4.4 Conclusion

Prefabricated SMA nanofibrous mats with average fiber diameters of 468 ± 111 nm were surface functionalized with Con A via imidization. Ring closure was achieved by additional heat treatment, yielding a stable cyclic imide with 73.6% conversion,[31] as obtained by integration of peak heights using ATR-FTIR. In a different approach, the covalent attachment of a monolayer of Con A to prefabricated SMA nanofibers was followed by glutaraldehyde (GA) treatment that cross-linked additional protein molecules and aggregates from the solution onto the covalently attached seed protein molecules with 68.7% conversion to yield SMI-CLPA nanofibers. The increase in fiber diameters after functionalization was 130% and 150% for the SMI-Con A and SMI-CLPA nanofibers, respectively, as observed using SEM, with a corresponding decrease in BET surface area by 24% and 38%. The presence of immobilized Con A on the nanofibers was confirmed by a positive test result using ninhydrin, and the biological activity was calculated to be 8.1% and 17.3% for SMI-Con A and SMI-CLPA, respectively, using the horseradish peroxidase assay. An increase in wettability of the nanofibrous substrate, measured by water contact angle, was observed after functionalization, rendering the SMI-Con A and SMI-CLPA nanofibers hydrophilic in nature.

4.5 Experimental

4.5.1 Chemicals

Poly(styrene-*alt*-maleic anhydride) (Chapter 3.6.3) was used without further purification. Dimethyl formamide, acetone and pyridine (Kimix) were distilled and kept on type 4Å Linde molecular sieves prior to use. Sodium chloride (Merck), potassium chloride (Merck), sodium phosphate dibasic (Merck), potassium phosphate monobasic (Merck), calcium chloride (Merck) and manganese(II) chloride beads 99.999% (Sigma) were kept in a moisture-free state prior to use. Concanavalin A (Sigma), glutaraldehyde 50% (Sigma), Tris-HCl (Sigma), Tween 20 (Sigma), ninhydrin (Sigma), 95% absolute ethanol (Sigma), phenol (Sigma), potassium cyanide 98% (Fluka), 2,2'-azino-bis(3-

ethylbenzthiazoline-6-sulfonic acid) (Sigma), hydrogen peroxide 30% (w/w) (Merck), albumin bovine (Sigma), Triton X-100 (Thermo Fisher) and peroxidase from horseradish type VI-A (Sigma) were used without further purification.

4.5.2 Electrospinning of SMA

SMA was dissolved in 2:1 acetone:DMF solvent system (14 wt %). The solution was placed in a 1 mL syringe with a blunt needle tip (21 gauge), which was mounted on a horizontal syringe pump with a tip to collector distance of 15 cm. A positive electrode was connected to the needle tip with a charge set at 15 kV, and the negative electrode was connected to the collector plate covered with foil with a charge of equal magnitude. The flow rate was set at 0.09 mL/min. Approximately 2 mL of solution was electrospun at relative humidity of 40% and temperature of 25 °C. The collected fibers were placed under vacuum at 60 °C to remove any residual solvents.

4.5.3 Immobilization of Concanavalin A on SMA nanofibers

A 10 mM PBS buffer solution (8 g NaCl, 0.2 g KCl, 1.44 g Na_2HPO_4, 0.24 g KH_2PO_4, pH 7.4) was prepared using deionized water. Prefabricated SMA nanofibers (100 mg) were incubated with 10 mL of PBS solution containing Concanavalin A (4 mg/mL), $MnCl_2$ (0.013 mg/mL) and $CaCl_2$ (0.011 mg/mL)[32,33] on a belly dancer laboratory shaker at 37 °C for one hour. The fibers were subsequently washed three times, for 10 min at a time, with PBS-Tween buffer (PBS, 0.01 wt % Tween 20) to remove any unreacted protein adsorbed onto the fiber surface. The fibers were air dried, followed by drying under vacuum at 60 °C for 24 hours.[16]

Major IR absorptions: 3402, 3029, 2890, 1851, 1775, 1714, 1339, 953, 702 cm^{-1}.

4.5.4 CLPA formation of Concanavalin A on SMA nanofibers

Prefabricated SMA nanofibers (100 mg) were incubated with 10 mL of a 10 mM PBS buffer solution (as explained in 4.5.3) containing Convanavalin A (40 mg/mL), $MnCl_2$ (0.013 mg/mL) and $CaCl_2$ (0.011 mg/mL) on a belly dancer laboratory shaker at room temperature for 30 min. The petri dish was moved in to a refrigerator (4° C) for an additional 90 min with rocking, before addition of a glutaraldehyde (GA) solution (final GA concentration was 0.5 % w/v) and the mixture was left to incubate overnight. The cross-linked protein aggregate Con A nanofibers (SMI-CLPA) were subsequently washed with PBS and 100 mM Tris-HCl (pH 7.8). To cap the unreacted aldehyde groups, the nanofibers were incubated in Tris-HCl buffer for 30 min. After capping, the nanofibers were washed three times, for 10 min at a time, with PBS to remove any unreacted protein adsorbed onto the fiber surface. The fibers were air dried, followed by drying under vacuum at 60 °C for 24 hours.[20]

Major IR absorptions: 3389, 3025, 2936, 1850, 1776, 1709, 1549, 1494, 1452, 1339, 1220, 702 cm^{-1}.

4.5.5 Characterization techniques

(a) Attenuated total reflectance Fourier transform infrared (ATR-FTIR) spectroscopy

All spectra were obtained using a Thermo Scientific Nicolet iS10 Smart iTR spectrometer that was operated in transmission mode from 4000 to 400 cm^{-1} with a resolution of 2 cm^{-1}. A background spectrum was collected before sample collection. Omnic 8.1 software from Thermo Fisher Scientific Inc. was used to analyse the spectra.

(b) Ninhydrin test

The ninhydrin test was performed on the SMI-Con A nanofibers to confirm the presence of the immobilized protein on the fiber surface.[25]

To a vial containing a 0.5 mg SMI-Con A nanofiber sample was added 100 µL ninhydrin in ethanol solution (500 mg ninhydrin in 10 mL 95 % absolute ethanol), 100 µL phenol in ethanol solution (40 mg phenol in 10 mL 95 % absolute ethanol) and 50 µL KCN in pyridine solution (2 mL 0.001M KCN solution in distilled water, diluted to 100 mL with distilled pyridine). The vial was heated to 80 °C for 5 min. A colour change was observed from colourless to dark blue, which is indicative of a positive test result for the presence of free amino groups, i.e. protein in this case. Unmodified SMA nanofibers were used as the negative control and Con A was used as the positive control.

The same procedure was followed for SMI-CLPA nanofibers. A colour change from colourless to dark blue was observed, which is indicative of a positive test result for the presence of protein.

(c) Horseradish peroxidase assay

The following assay was used to determine the biological activity of the immobilized Con A on the SMA nanofibers: Enzymatic assay of peroxidase (EC 1.11.1.7) 2,2'-azino-bis (3-ethylbenzthiazoline-6-sulfonic acid) (ABTS) as a substrate.[27]

A 13.6 mg/mL KH_2PO_4 solution was prepared using distilled water, pH 5.0 at 25 °C. To this solution was added ABTS (5.0 mg/mL), hereafter referred to as the *substrate*. A 0.3% (w/w) hydrogen peroxide solution was freshly prepared using a 30% (w/w) hydrogen peroxide solution, hereafter referred to as H_2O_2. The *diluent* was prepared in distilled water using 5.4 mg/mL KH_2PO_4, 2.5 mg/mL albumin bovine and 5.0 mg/mL Triton X-100, pH 6.8 at 25 °C. A 10 mg/mL stock solution of peroxidase enzyme from horseradish type VI-A (HRP) was prepared using cold diluent, hereafter

referred to as *enzy*. SMI-Con A nanofibers (10 mg) were incubated in 1.0 mL of diluted enzy solution (1:10 000 enzy in cold diluent) for 3 hours on a belly dancer laboratory shaker at 25 °C. The SMI-Con A-HRP fibers were subsequently washed with diluent three times, for 10 min at a time, to remove any non-binding HRP. The reagents were pipetted into suitable cuvettes as summarized in Table 4.1.

Table 4.1 Amount of reagents added to the test and blank sample (in millilitres).

	Test	Blank
Substrate	2.90	2.90
H_2O_2	0.10	0.10
Diluent	–	0.05
Enzy	SMI-Con A-HRP (5 mg)	–

The contents were mixed by inversion and the increase in absorbance at 405 nm ($A_{405\ nm}$) was recorded for 3 min at 0.50 second intervals. The fastest rate was observed in the second minute (refer Figure 4.7) for which the change in $A_{405\ nm}$ ($\Delta A_{405\ nm}$) was used as the maximum linear rate for both the test and the blank.

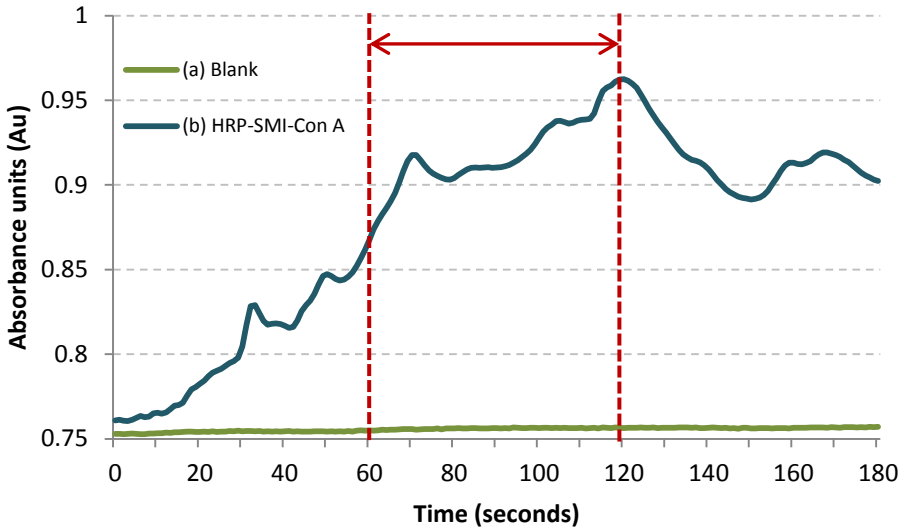

Figure 4.7 Absorbance curve of (a) Blank sample and (b) HRP incubated SMI-Con A fibers vs Time.

The biological activity of the immobilized Con A was quantified by calculating the units of HRP bound per mass of nanofibrous SMI-Con A substrate using Equation 4.4.

$$Units/_{mg\ solid} = \frac{\Delta A_{405\ nm}/\min(test) - \Delta A_{405\ nm}/\min(blank) \times 3.05 * DF}{36.8 * 0.05} \qquad (4.4)$$

3.05 = Final volume (in millilitres) of reaction
DF = Dilution factor of enzyme
36.8 = Millimolar extinction coefficient of oxidised ABTS at $A_{405\ nm}$
0.05 = Volume (in millilitres) of enzyme used

Using this equation, the units/mg solid of HRP bound to SMI-Con A fibers were calculated to be 2 units/mg solid. According to definition, one unit will oxidise 1.0 µmole of ABTS per minute at pH 5.0 at 25°C, therefore 2 units/mg solid will oxidise 2.0 µmole of ABTS per minute. Since the final concentration of ABTS in the cuvette was 8.7 mM, which amounts to 26.5 µmole, of which only 2 µmole was oxidised, it can be concluded that only 8.1% of the immobilized Con A was biologically active.

The same procedure was followed for SMI-CLPA with results indicating that 17.3% of the immobilized Con A was biologically active.

(d) Scanning electron microscopy (SEM)

Nanofiber samples were cut into 0.5 x 0.5 cm square pieces and mounted onto stubs using double sided carbon tape prior to being coated with gold sputter under vacuum using an Edwards S15OA Sputter Coater in order to make the sample surface electrically conducting.

Imaging of the samples was accomplished using a Leo® 1430VP Scanning Electron Microscope. The stubs with nanofiber samples were loaded into the imaging chamber. The scanning electron (SE) images show the surface of the nanofibers. Beam conditions under vacuum during surface analysis were 7 kV and approximately 1.5 nA, with a spot size of 150 d_p.

(e) Brunauer-Emmet-Teller (BET) surface area analysis

Specific surface area determinations were performed using a Micromeritics ASAP 2020 V3.03 Surface Area and Porosity Analyzer. The surface area of activated SMA and SMI-Con A nanofibers (100 mg sample each) were determined by N_2 absorption using Brunauer-Emmet-Teller (BET) method at 100 °C.

(f) Water contact angle

The hydrophobic/hydrophilic character of the pristine SMA, SMI-Con A and SMI-CLPA nanofibers were investigated by means of static water contact angle measurements. A Zeiss microscope unit was used for magnification. The test entailed placing a 1.0 µL drop of Milli-Q water on the nanofibrous surface and immediately capturing images using a Nikon SMZ-2T camera (Japan). Image analysis software (SEM Image Studio v7.1) was used to determine the contact angle. A minimum of 10 measurements, taken at different positions on the film, was carried out. The contact angles were measured on both sides of the drop and averaged.

4.6 References

1. Evenson, S.; Badyal, J. *J. Phys. Chem*. **1998,** *102*, 5500-5502.

2. Ho, R.; Su, A.; Wu, C.; Chen S. *Polymer* **1993**, *34*, 3264-3269.

3. Chilkoti, A.; Ratner, B.D.; Briggs, D. *Chem. Mat.* **1991**, *3*, 51-61.

4. Hamilton, L.; Green, A.; Edge, S.; Badyal, J.; Feast, W.; Pacynko, W. *J. Appl. Polym. Sci*. **1994**, *52*, 413-419.

5. Cloete, W.J.; Adriaanse, C.; Swart, P.; Klumperman, B. *Polym. Chem*. **2011**, *2*, 1479-1481.

6. Jeong, J.; Byoun, Y.; Lee, Y. *React. Funct. Polym*. **2002**, *50*, 257-263.

7. Jia, H.; Zhu, G.; Vugrinovich, B.; Kataphinan, W.; Reneker, D.H.; Wang, P. *Biotechnol. Prog*. **2002**, *18*, 1027-1032.

8. Kim, T.G.; Park, T.G. *Biotechnol. Prog*. **2006**, *22*, 1108-1113.

9. Ding, H.; Shao, L.; Liu, R.; Xiao, Q.; Chen, J. *J. Colloid. Interface. Sci*. **2005**, *290*, 102-106.

10. Olofsson, L.; Rindzevicius, T.; Pfeiffer, I.; Käll, M.; Höök, F. S. *Langmuir* **2003**, *19*, 10414-10419.

11. Li, Z.; Chen, Y.; Li, X.; Kamins, T.; Nauka, K.; Williams, R.S. *Nano Letters* **2004**, *4*, 245-247.

12. Goldstein, I.; Hollerman, C.; Smith, E. *Biochemistry (N Y)*. **1965**, *4*, 876-883.

13. Scott J.K.; Loganathan, D.; Easley, R.B.; Gong, X.; Goldstein, I.J. *Proc. Nat. Acad. Sci. (U S A)*. **1992**, *89*, 5398-5402.

14. Hardman, K.D.; Agarwal, R.C.; Freiser, M.J.; *J. Mol. Biol*. **1982**,*157*, 69-86.

15. Carver, J.; Mackenzie, A.; Hardman, K. *Biopolymers* **1985**, *24*, 49-63.

16. Cronje, L.; Warren, R.; Klumperman, B. *J. Mat. Chem. B.* **2012**, *48*, 6608-6618.

17. Jeong, J.; Byoun, Y.; Ko, S.; Lee, T.Y. *J. Ind. Eng. Chem*. **2001**, 310-315

18. Bshena, O.; Heunis, T.D.J.; Dicks, L.M.T.; Klumperman, B. *Fut. Med. Chem.* **2011**, *3*, 1821-1847.

19. Kalb, A.J.; Levitzki, A. *Biochem. J*. **1968**, *109*, 669-672.

20. Kim, B.C.; Nair, S.; Kim, J. *Nanotechnology* **2005**, *16*, S382.

21. Lee, S.; Ahn, T.O. *J. Appl. Polym. Sci*. **1999**, *71*, 1187-1196.

22. Vermeesch, I.; Groeninckx, G. *J. Appl. Polym. Sci*. **1994**, *53*, 1365-1373.

23. Lampman, G.M.; Pavia, D.L.; Kriz, G.S.; Vyvyan, J.R. *Spectroscopy* **2010**, *4*, 15-77.

24. Moraes, L.G.P.; Rocha, R.S.F.; Menegazzo, L.M.; Araújo, E.B.D.; Yukimito, K.; Moraes, J.C.S. *J. App. Oral. Sci*. **2008**, *16*, 145-149.

25. Friedman, M. *J. Agric. Food. Chem*. **2004**,*52*, 385-406.

26. Hawkes, R. *Anal. Biochem*. **1982**, *123*, 143-146.

27. Keesey, J.; Putter, J.; Becker, R. *Sigma Aldrich* **2015**, 1-2.

28. Wang, Z.; Wan, L.; Liu, Z.; Huang, X.; Xu, Z. *J Molec. Catal. B*. **2009**, *56*, 189-195.

29. Yalçın, N.; Sevinç, V. *Carbon* **2000**, *38*, 1943-1945.

30. Širc, J.; Hobzová, R.; Kostina, N. *J. Nanomat*. **2012**, *2012*, 121.

31. Soer, W.J.; Ming, W.; Koning, C.E.; van Benthem, R.A.; Mol, J.; Terryn, H. *Progr. Org. Coat.* **2009**, *65*, 94-103.

32. Swaminathan, C.P.; Surolia, N.; Surolia, A. *J. Am. Chem. Soc*. **1998**, *120*, 5153-5159.

33. Sato, K.; Imoto, Y., Sugama, J.; *et al*. *Langmuir* **2005**, *21*, 797-799.

Chapter 5: Affinity studies between nanofibrous substrates and mycobacteria

5.1 Introduction

Styrene-maleic anhydride copolymer (SMA) was functionalized with a variety of low molecular weight primary *N*-alkylamines and *N*-arylamines via imidization to yield various styrene maleimide copolymers. One such derivative underwent further functionalization with various bromoalkane compounds of different chain lengths to yield quaternary ammonium alkyl conjugates. These compounds were electrospun into nanofibrous substrates by employing the single needle electrospinning technique to yield smooth, bead free fibers with diameters in the range of 218 – 468 nm as described in Chapter 3. In a different modification approach, SMA nanofibers were also surface-functionalized with Concanavalin A (Con A) via imidization to yield SMI-Con A and SMI-CLPA substrates as described in Chapter 4.

The modified compounds chosen for this study were selected based on their known[1] or possible chemical interaction[2] with the *Mycobacterium tuberculosis* (*Mtb*) cell wall. Concanavalin A, a mannose binding lectin,[3] has proved its affinity to bind with the mannose binding terminals of the BCG strain when the protein was covalently bound to SMA nanofibers. The *N*-alkylamines and *N*-arylamines that served as functionalization agents for the modification of SMA offered a variety of chemical groups for ionic interactions, lone-pair electron interactions, dipole-dipole interactions as well as hydrophobic interactions[4] with the *Mtb* cell wall. Polymer nanofibers were chosen as substrates due to their inherently large surface-to-volume ratio which render them ideal for the immobilization of high densities of bioactive molecules.[5] The functionalized nanofibrous substrates were synthesized to serve as potential capturing platforms for *Mtb* to improve the collection and concentration thereof as specimens for further diagnostic tests.[1] Affinity studies were conducted to establish whether these capturing platforms could be used for this objective.

This chapter reports the affinity studies between the various functionalized polymer nanofibers and *Mycobacterium bovis* bacillus Calmette-Guérin (BCG). BCG is a live-attenuated strain derived from *M. bovis*[6,7] that is genetically similar to *Mtb*[8-10] with the advantage of being non-pathogenic.[11] The general procedure entailed that the functionalized nanofibers were incubated with BCG at neutral pH, washed and analysed. Interaction between the functionalized nanofibers and BCG was evaluated using fluorescence microscopy (FM) to determine the substrates' ability to 'capture' and thus concentrate mycobacteria.

5.2 Affinity studies

The affinity studies between the functionalized nanofibers and mycobacteria were carried out using a kanamycin-resistant strain of BCG. Kanamycin is an aminoglycoside antibiotic that is used as a selective agent to prevent the growth of contaminating bacteria[12] that is present on the non-sterile polymer nanofibers.[1] Auto fluorescence was observed for the SMI-Con A and SMI-CLPA nanofibers incubated with BCG. Therefore, a fluorophore-tagged BCG was used, namely mCherry-BCG.[13] Refer to Figure 5.1 for the chemical structures of the functionalized nanofibers used in the affinity tests with BCG.

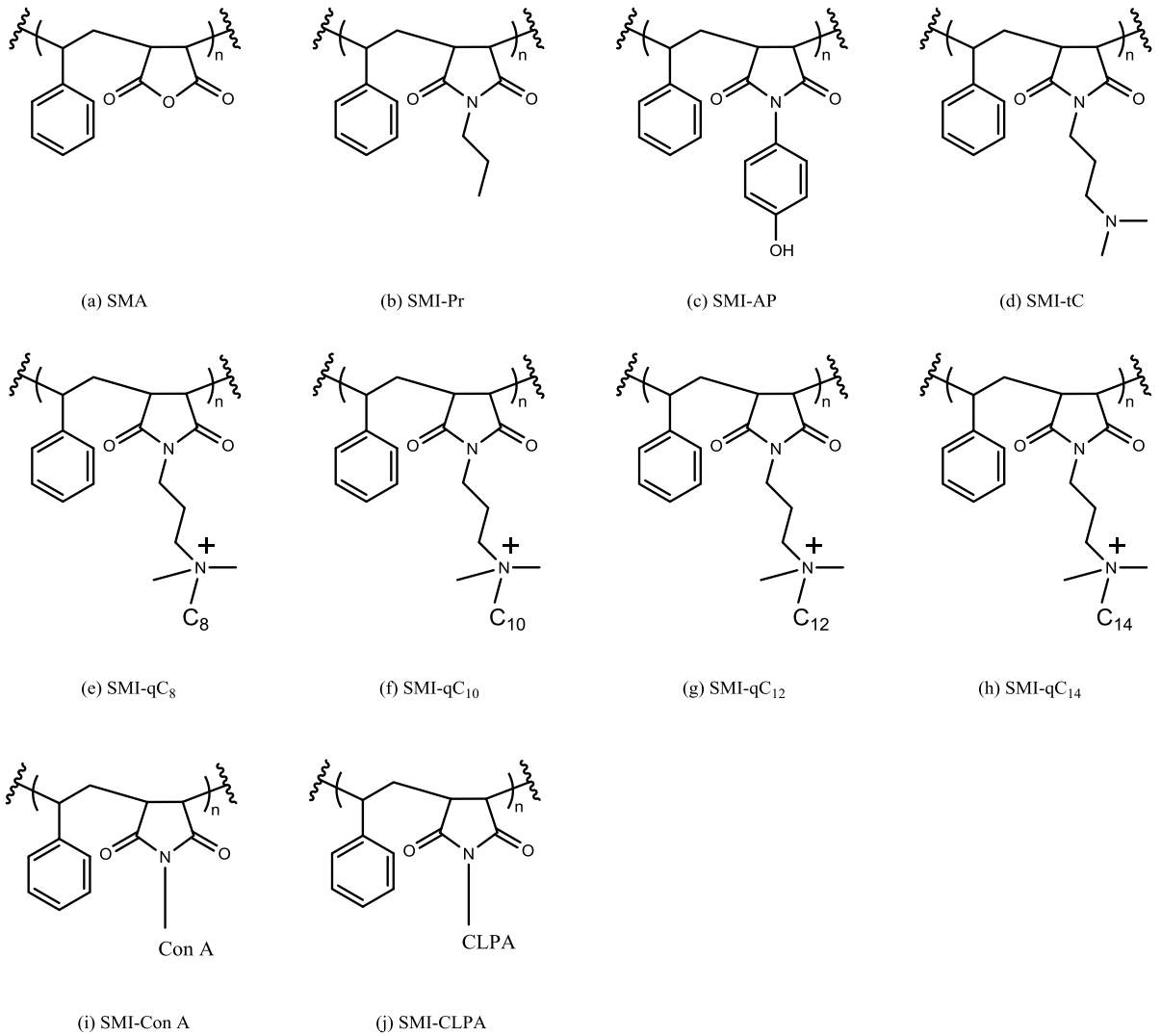

Figure 5.1 Chemical structures of the functionalized nanofibers used for the affinity tests with BCG (a-h) and mCherry-BCG (i, j).

The affinity studies entailed adding 10 mg of the functionalized polymer nanofibers to 10 mL of BCG culture in separate vials using tenfold serial concentrations (determined by measuring the optical density (OD_{600}) of the starting culture) and incubating the vials at 37 °C for 30 min on a laboratory shaker. The nanofibers were subsequently removed from the vials and washed twice with phosphate buffered solution (PBS) to remove any loosely adhered mycobacteria.[1]

The nanofibrous substrates were visualized by FM using two fluorescent nucleic acid-binding stains, namely SYTO-9 and propidium iodide. SYTO-9 penetrates all bacterial membranes and stains the cells green, while propidium iodide only penetrates cells with damaged membranes, staining them red.[14] All mycobacteria, regardless of their viability will thus be stained green, whereas only dead bacteria will be stained red. The SMI-Con A and SMI-CLPA nanofibers were incubated with mCherry-BCG and was visualized without propidium iodide or SYTO-9. mCherry is a red fluorescent protein that is expressed by the microbe which explains why the fluorophore-tagged BCG could be visualized on the nanofibers without the addition of stains.[13] Analysis of the FM images indicated that BCG interacted strongly with SMI-Con A and SMI-CLPA nanofibers as well as the quaternized SMI derivatives (SMI-qC_8, SMI-qC_{10}, SMI-qC_{12} and SMI-qC_{14}) as evidenced by large quantities of BCG

visible on the surfaces of these substrates and their ability to capture mycobacteria at low concentrations.

5.3 Analysis of capture efficiency of nanofibrous substrates

The interaction between BCG and the polymer nanofibers after incubation was visualized using FM. The FM images show green and red stained mycobacteria on the surface the nanofibers and can be split into four separate images to clearly illustrate the three channels of light as exemplified in Figure 5.2.

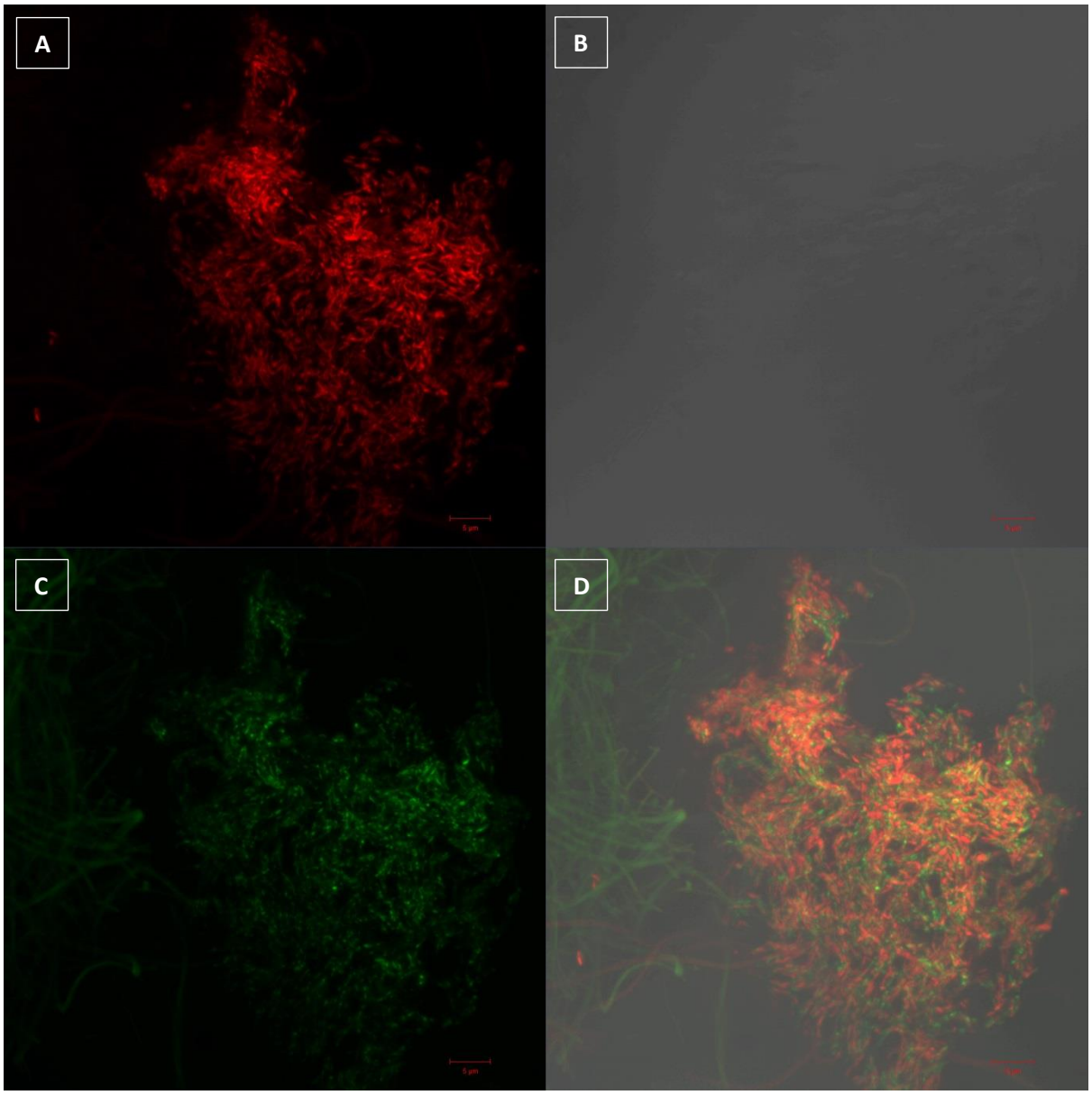

Figure 5.2 FM images of the washed SMI-qC$_{10}$ nanofibers after incubation in 10^{8} BCG/mL, (a) red channel, indicating only mycobacteria with damaged membranes, (b) light transmission, (c) green channel, indicating all mycobacteria and (d) combination of all light channels showing live and dead mycobacteria.

The representative FM images of the washed SMI-qC_{10} nanofibers after incubation with BCG at concentration 10^8 BCG/mL for one hour at 37 °C and pH 7 can be visualized using three different light channels to construct a final image (Figure 5.2 (d)) showing a combination of live and dead mycobacteria. All bacterial membranes are penetrated by SYTO-9, which stains all mycobacteria green (Figure 5.2 (c)), while propidium iodide only penetrates damaged membranes (dead bacteria), staining them red (Figure 5.2 (a)).[14] Washed nanofibers after incubation in PBS was used as negative control and showed no red or green fluorescence.

Biofilm formation is observed on nanofibers incubated with high concentrations of BCG, as observed in Figure 5.2. Microorganisms have a natural capacity to attach to surfaces, multiply, and embed themselves in a slimy exopolysaccharide matric, forming biofilms. Biofilm formation is a defence mechanism of pathogenic bacteria such as *Mycobacterium bovis* (*M. bovis*) against adverse environmental conditions.[15,16] Distinguishing between individual bacilli in biofilms prove to be difficult due to aggregation of the BCG caused by the hydrophobic character of the cell wall.[17]

The interaction between mCherry-BCG and the SMI-Con A and SMI-CLPA nanofibers was visualized using FM without the addition of stains. Analysis of the FM images showed that high numbers of BCG was captured onto the surfaces of these washed nanofibers as indicated by the red stained microbes. Refer to Figure 5.3 for the representative FM images of the washed SMI-CLPA nanofibers after incubation with mCherry-BCG at concentration 10^8 BCG/mL (Figure 5.3 (a)) and in PBS as negative control (Figure 5.3 (b)), both for one hour at 37 °C and pH 7.

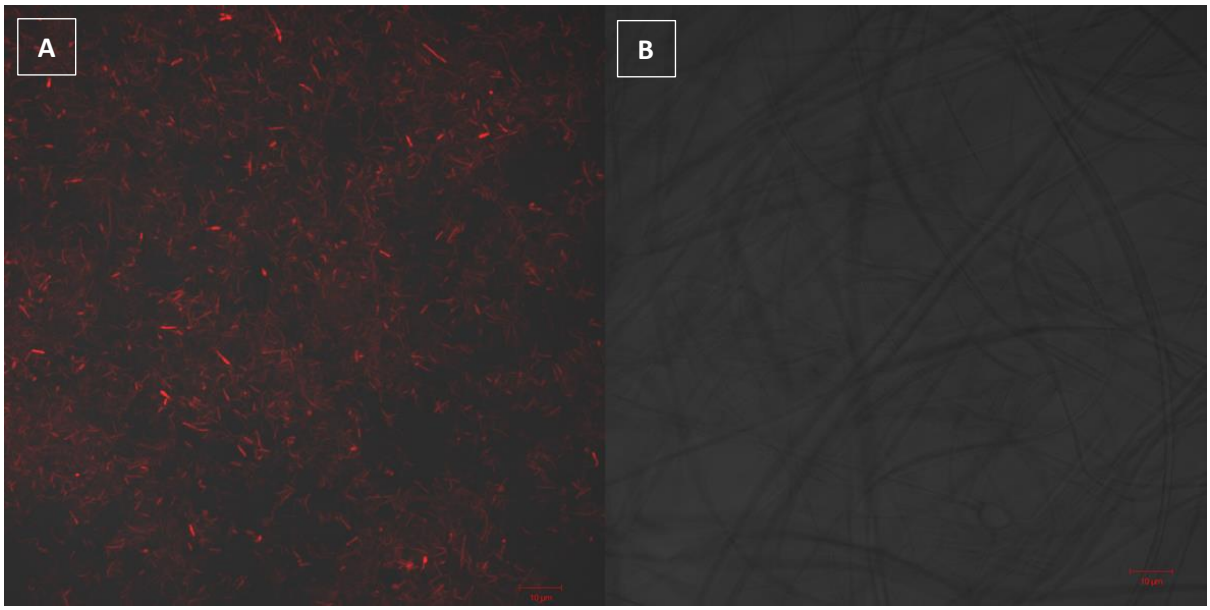

Figure 5.3 FM images of the washed SMI-CLPA nanofibers after incubation in (a) 10^8 BCG/mL and (b) PBS as negative control.

A comparative study between the various nanofibrous substrates was conducted at neutral pH by incubating specific weights of the relevant nanofibers with defined volumes of culture containing decreasing numbers of BCG bacilli, starting with 10^8 BCG/mL and ending with 10 BCG/mL, serially diluted 1:10, at 37 °C for one hour. The nanofibrous substrates were subsequently washed with PBS twice for 10 minutes at a time to remove any loosely adhered BCG and visualized using FM.

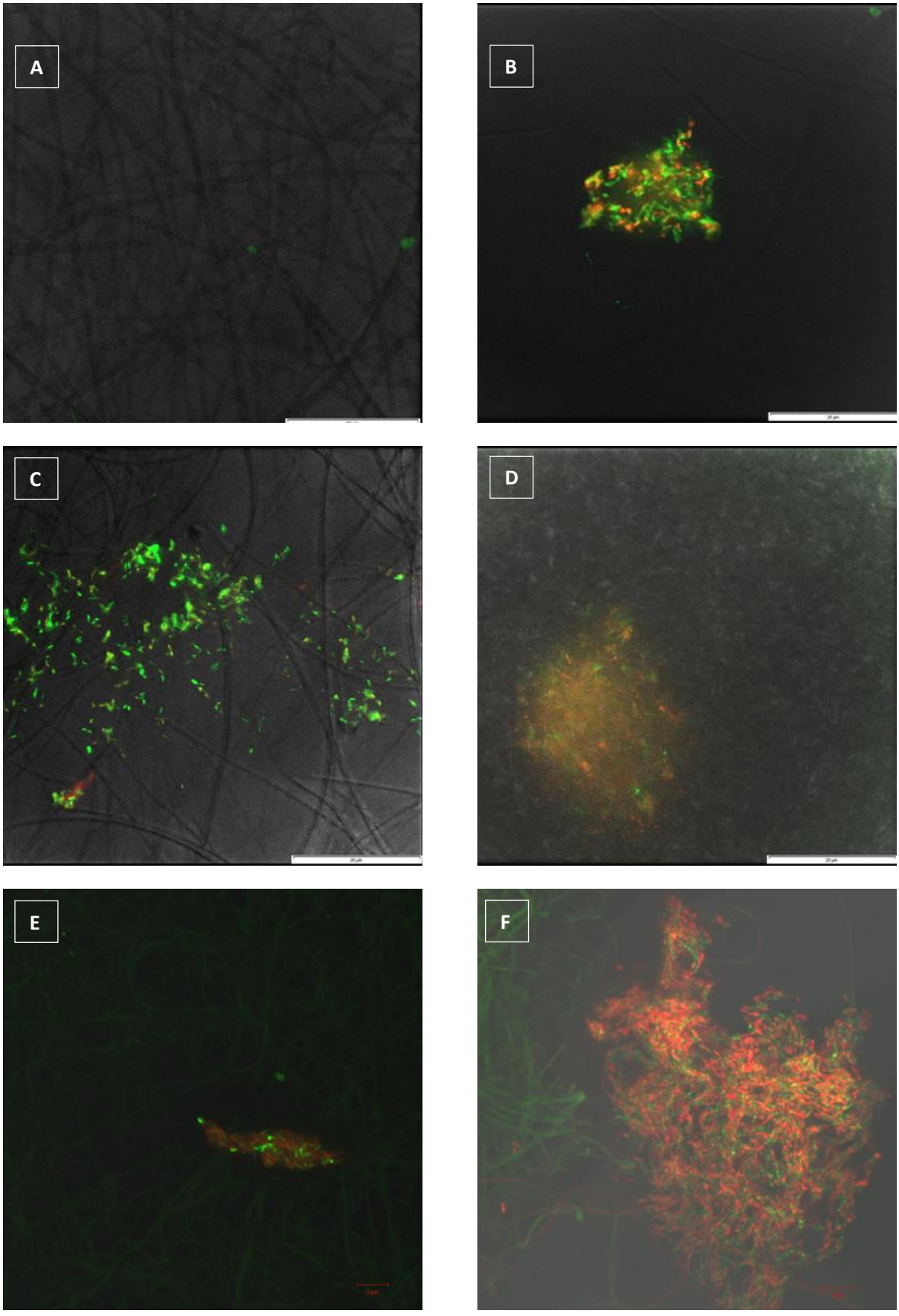

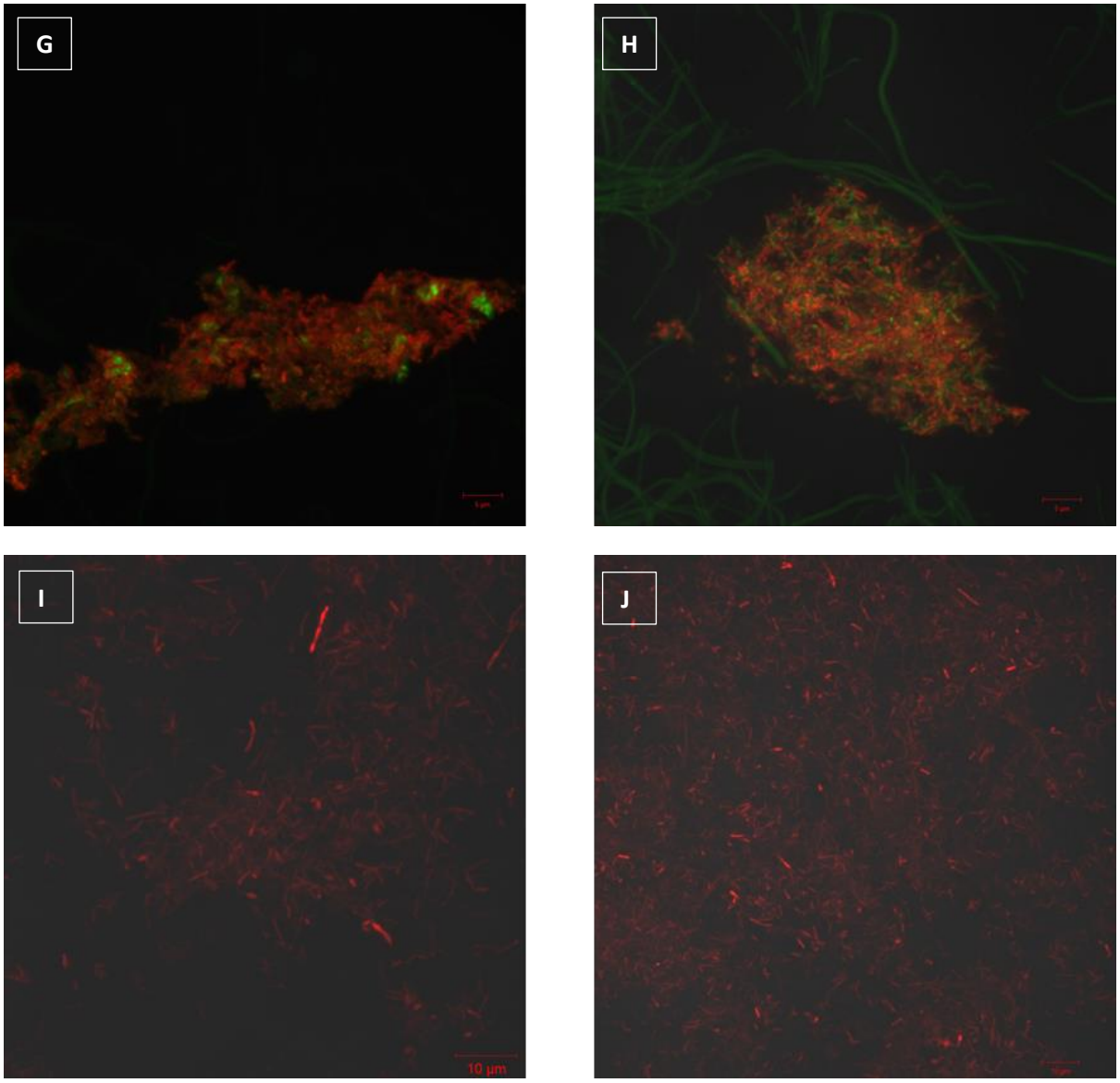

Figure 5.4 FM images of the washed nanofibers of (A) SMA, (B) SMI-Pr, (C) SMI-AP, (D) SMI-tC, (E) SMI-qC$_8$, (F) SMI-qC$_{10}$, (G) SMI-qC$_{12}$, (H) SMI-qC$_{14}$, (I) SMI-Con A and (J) SMI-CLPA after incubation with BCG (A-H) or mCherry-BCG (I,J) at 37 °C and pH 7 for one hour.

Refer to Figure 5.4 for the representative FM images of the washed nanofibers of (a) SMA, (b) SMI-Pr, (c) SMI-AP, (d) SMI-tC, (e) SMI-qC$_8$, (f) SMI-qC$_{10}$, (g) SMI-qC$_{12}$ and (h) SMI-qC$_{14}$ after incubation in 10^8 BCG/mL and (i) SMI-Con A and (j) SMI-CLPA nanofibers after incubation in 10^8 mCherry-BCG/mL at 37 °C and pH 7 for one hour.

Analysis of the FM images indicated that there was no BCG captured onto the surfaces of the washed SMA nanofibers and only a few BCG on the washed SMI-Pr nanofibers. Higher numbers of BCG were captured onto the surfaces of the washed SMI-AP, SMI-tC and SMI-qC$_8$ nanofibers, whereas the highest quantity of BCG were captured onto the surfaces of SMI-qC$_{10}$, SMI-qC$_{12}$, SMI-qC$_{14}$, SMI-Con A and SMI-CLPA, as indicated by the red and green stained microbes (Figure 5.4).

Children with tuberculosis (TB) usually have paucibacillary disease and poor bacteriological yields,[8] i.e. low concentrations of bacilli in the specimen. The emphasis thus falls on concentrating sputum or gastric aspirates, regardless of bacilli yields, to assist existing microscopy protocols for the

accurate and timely diagnosis of TB. The capture efficiency of the various nanofibrous substrates was evaluated by measuring the binding of BCG to the nanofibers at decreasing BCG concentrations using the obtained FM images. A comparative table was constructed to quantify the amount of bacilli attached to each nanofibrous sample at certain concentrations to define the lowest limit of detection. The FM images of all nanofibrous substrates incubated in serial BCG concentrations were analysed and the amount of bacilli captured onto the surfaces were counted using image analysis software (SEM Image Studio v7.1). Table 5.1 highlights the highest number of BCG counted in each division, thereby estimating which nanofibers exhibit the greatest affinity to capture BCG. It is evident that SMI-Con A and SMI-CLPA nanofibers display supreme strength of interaction with BCG regardless of concentration and could bind to the mycobacteria in concentrations as low as 10 BCG/mL (indicated in bold text). Three of the four SMI-qC$_x$ derivatives, namely SMI-qC$_8$, SMI-qC$_{10}$ and SMI-qC$_{12}$ also showed exceptional binding ability to BCG at the lowest concentration, with SMI-qC$_{14}$ failing to produce the same result.

Table 5.1 Amount of bacilli captured onto polymer nanofibrous substrates for concentrations 10 BCG/mL – 10^8 BCG/mL.

BCG/mL	SMA	SMI-Pr	SMI-AP	SMI-tC	SMI-qC$_8$	SMI-qC$_{10}$	SMI-qC$_{12}$	SMI-qC$_{14}$	SMI-Con A	SMI-CLPA
10^1	0	0	0	0	3	8	9	0	2	8
10^2	0	0	1	0	11	23	6	0	7	5
10^3	0	0	3	0	10	8	8	4	8	11
10^4	0	3	2	0	4	7	9	4	45	53
10^5	0	2	1	2	20	14	14	44	29	33
10^6	0	12	2	40	37	90	41	8	81	157
10^7	0	163	99	60	103	800	158	157	80	2880
10^8	0	174	257	386	126	1300	650	1100	3250	6848

A possible explanation for these results may be as follows: SMI-Con A and SMI-CLPA nanofibers were able to interact with BCG due to the saccharide binding properties of the protein.[18] These protein-carbohydrate interactions between BCG and Con A were made possible by Con A's ability to bind with oligosaccharides containing D-mannose and D-glucose,[19] of which mannose is displayed on the cell surface of BCG as mannose-capped lipoarabinomannan, also called ManLAM. ManLAM is a glycolipid that serves as the major cell wall component of BCG.[20] The saccharide binding specificity of Con A has been shown to be directed toward the monosaccharides glucose and mannose,[19] which could explain the high avidity of binding observed in the FM image of SMI-Con A and SMI-CLPA nanofibers in Figure 5.4 (i). Direct hydrogen bonds and Van der Waals interactions reportedly facilitate the anchoring of the protein to the sugars.[21] SMI-CLPA nanofibers displayed superior affinity in comparison to SMI-Con A nanofibers, probably due to the higher protein loading accomplished by glutaraldehyde (GA) treatment, which in turn increased the amount of binding sites on Con A available to interact with BCG.[22]

The nanofibers of the SMI-qC$_x$ derivatives consist of both charged and hydrophobic chemical moieties that are believed to have a high affinity for the phospholipid structures ubiquitous in the mycobacterial cell wall, as well as the mycolic acids present on the BCG cell surface.[23] The positive charge of the quaternary ammonium moieties of the SMI-qC polymers interacts with the negatively

charged phospholipid structures omnipresent in the cell membrane of BCG,[24] resulting in electrostatic interaction between the SMI-qC nanofibers and BCG. The cell envelope of BCG is also characterized by a highly complex hydrophobic array of unique glycolipids and mycolic acids[25] that could interact with the aliphatic hydrocarbon chains (C_8, C_{10}, C_{12} and C_{14}) via hydrophobic-hydrophobic interactions. A combination of ionic and hydrophobic interactions could possibly explain the binding capabilities of these functionalized SMI-qC_x derivatives to the cell surface of BCG. The variation in alkyl chain length of the SMI-qC_x derivatives determines the hydrophobic character of the polymer, where an increase in chain length leads to an increase in hydrophobicity. It is evident that SMI-qC_{10} captured BCG to a greater extent than its counterparts (Table 5.1), leading to a tentative conclusion that an aliphatic chain of C_{10} imparts the right amount of hydrophobicity in combination with ionic strength to bind BCG at concentrations as low as 10 BCG/mL. SMI-qC_{14} could be regarded as being too hydrophobic due to the longer alkyl chain, which in turn prevented sufficient wetting of the nanofibrous surface, inhibiting close contact between BCG and the nanofibrous substrate. This might be the reason why SMI-qC_{14} failed to produce the same results as SMI-qC_8, SMI-qC_{10} and SMI-qC_{12}.

Since the SMI-qC_x polymers' interaction originate from ionic interactions with the overall negatively charged BCG cell wall as well as hydrophobic interactions with the lipids contained in the cell envelope, the binding between the nanofibers and BCG can be regarded as non-specific. The interaction of Con A with ManLAM, however, can be regarded as specific binding interaction due to Con A's ability to bind with mannose, a saccharide present on the surface of the BCG cell wall. This is a very specific interaction, which makes SMI-Con A and SMI-CLPA nanofibers the choice of substrate to capture BCG.

The fairly poor interaction between the SMI-Pr nanofibers and BCG could possibly be explained by the lack of ionic species yielding no electrostatic interaction and the short propyl chain that doesn't impart enough hydrophobicity to make hydrophobic-hydrophobic interactions favourable between the nanofibers and the hydrophobic cell envelope of BCG. In contrast to its parent polymer SMA, however, the modification with propylamine did impart some amount of favourable interaction as indicated by the red and green stained microbes on the FM images of SMI-Pr at high BCG concentrations (refer to Figure 5.4 (b)) with 10^4 BCG/mL being the lowest limit of detection (refer to Table 5.1).

FM images of SMI-AP nanofibers demonstrated some binding interaction with BCG and the nanofibers were able to bind to BCG at concentrations as low as 10^2 BCG/mL. Hydrogen bonds between the aminophenol group of SMI-AP and the hydroxyl group in the β-position of mycolic acids could explain this binding phenomenon.[26]

SMI-tC nanofibers also exhibited poor binding to BCG with a lowest detection limit of 10^5 BCG/mL. The poor binding affinity to the mycobacterial cell surface could possibly be explained by the lack of hydrophobicity and ionic species. Hydrogen interactions between the electron lone pairs of the dimethylamino-group of SMI-tC were thought to increase binding capabilities. This was only the case for nanofibers incubated with high BCG concentrations. Furthermore, the good wettability of the nanofibers could possibly facilitate binding of BCG in aqueous media.

Based on these FM results it can be concluded that BCG can be captured onto SMI-qC_8, SMI-qC_{10}, SMI-qC_{12}, SMI-Con A and SMI-CLPA nanofibers with high avidity and at concentrations as low as 10

BCG/mL. The supreme capture efficiencies of these nanofibrous substrates developed in this study could be incorporated into specimen collection regimes for the timely diagnosis of TB.

5.4 Conclusion

BCG, a live-attenuated, non-pathogenic strain derived from *M. bovis*[6,7] that is genetically similar to *Mtb*[8-10], was successfully captured onto the surfaces of the functionalized nanofibers of SMI-qC_8, SMI-qC_{10}, SMI-qC_{12}, SMI-Con A and SMI-CLPA polymers as analysed by FM. The ability to concentrate BCG from solutions containing decreasing amounts of bacilli proved to be possible due to the interaction between the BCG cell surface and these functionalized nanofibrous surfaces. Supreme capture efficiencies were observed for the before-mentioned quaternary SMI polymer nanofibers at the lowest limit of detection as indicated by the red and green stained microbes, emphasizing the chemical interactions at play. These interactions are made possible by the electrostatic interaction between the negatively charged BCG cell surface and the positively charged quaternary ammonium moieties of the modified polymer, and the hydrophobic interactions with the mycolic acids for the SMI-qC_x derivatives, as well as carbohydrate-protein interactions between Con A and ManLAM of the SMI-Con A and SMI-CLPA nanofibers, respectively.

The work discussed in this chapter therefore confirms that SMA, modified with a C_8, C_{10} and C_{12} aliphatic quaternary ammonium moieties, as well as SMA modified with Con A, successfully captured BCG at the lowest possible concentration of 10 BCG/mL. The nanofibrous substrates that have been investigated in this study could thus provide an alternative method to concentrate *Mtb* from sputum samples which can easily be integrated into existing laboratory microscopy protocols.

5.5 Experimental

5.5.1 Fluorescence microscopy (FM)

Images of the functionalized nanofibers incubated in BCG were obtained using an Olympus IX81 inverted fluorescent microscope coupled to a Xenon-Arc burner (Olympus Biosystems GMBH) as light source. The nanofibers (excluding SMI-Con A nanofibers) were incubated with SYTO-9 nucleic acid and propidium iodide for 10 minutes in Eppendorf tubes before being transferred to microscope slides. The samples were excited using the 492 nm and 572 nm excitation filters for green and red staining, respectively. Emission was collected using a UBG triple-bandpass emission filter cube (Chroma).

5.5.2 Culture

(a) BCG

One mL BCG (containing pJV 75 Amber) freezer stock was inoculated in 10 mL Middlebrook 7H9 medium containing 0.2% glycerol, 0.05% Tween-80, 10% ADC and 25 µg/mL kanamycin and grown to an optical density of 0.78, when measured at 600 nm in a spectrophotometer (OD_{600}). The cells were pelleted by centrifugation at 3000 x g for 10 minutes at 4 °C and resuspended in 10 mL Middlebrook 7H9 medium containing 0.2% glycerol, 10% ADC and 0.05% Tween-80. The centrifugation and resuspension steps were repeated. The cells were inoculated to approximate OD_{600} of 0.05 in 7H9 medium containing 0.2% glycerol, 10% ADC and 25 µg/mL kanamycin (no Tween) (50-100 mL cultures) and grown to approximate OD_{600} of 0.81.

(b) mCherry-BCG

mCherry-expressing BCG (mCherry-BCG) was created by transforming BCG Pasteur with pMSG432 (episomal plasmid encoding mCherry and conferring hygromycin resistance). BCG strains were grown at 37 °C in Middlebrook 7H9 growth medium supplemented with 10% albumin/dextrose/saline, 0.5 % glycerol and 0.05% Tween-80 in the presence of 50 µg/mL hygromycin to approximate OD_{600} of 0.80.

5.5.3 Affinity studies with BCG or mCherry-BCG

BCG culture dispersion was diluted serially 1:10 in PBS and 7H9 growth medium (1:1 solution) from approximately 10^8 BCG/mL to 10 BCG/mL. Aliquots of 5 mL of the final dispersions were pipetted into conical tubes in duplicate. A 10 mg piece of nanofibrous mat was added to each of the tubes and incubated at 37 °C for one hour whilst shaking on a laboratory shaker. The nanofibrous mats used as negative control were incubated in PBS. The nanofibrous mats were removed and washed twice with PBS in clean tubes for 10 minutes each and returned to clean Eppendorf tubes. FM analysis followed to evaluate the BCG-polymer interaction.

5.6 References

1. Cronje, L.; Warren, R.; Klumperman, B. *J. Mat. Chem. B.* **2012**, *48*, 6608-6618.

2. Bshena, O.; Heunis, T.D.J.; Dicks, L.M.T.; Klumperman, B. *Fut. Med. Chem.* **2011**, *3*, 1821-1847.

3. Scott, J.K.; Loganathan, D.; Easley, R.B.; Gong, X.; Goldstein, I.J. *Proc. Nat. Acad. Sci. (U S A)* **1992**, *89*, 5398-5402.

4. Williams, L.D. *Instit. Bioeng. Biosci*. **2015**, 1-7.

5. Kim, T.G.; Park, T.G. *Biotechnol. Prog*. **2006**, *22*, 1108-1113.

6. Menzies, D.; Pai, M.; Comstock, G. *Ann. Intern. Med*. **2007**, *146*, 340-W88.

7. Corrigan, D.; Paton, J. *Breathe* **2007**, *3*, 351-363.

8. Marais, B.J.; Pai, M. *Arch. Dis. Child*. **2007**, *92*, 446-452.

9. Kolattukudy, P.; Fernandes, N.D.; Azad, A.; Fitzmaurice, A.M.; Sirakova, T.D. *Mol. Microbiol*. **1997**, *24*, 263-270.

10. Maeda, N.; Nigou, J.; Herrmann, J.L.; *et al*. *J. Biol. Chem*. **2003**, *278*, 5513-5516.

11. Sasano, K.T.; Medlar, E.M. *Tubercle* **1931**, *12*, 214-219.

12. Nascimento, I.P.; Dias, W.O.; Mazzantini, R.P.; *et al*. *Infect. Immun*. **2000**, *68*, 4877-4883.

13. Shaner, N.C.; Campbell, R.E.; Steinbach, P.A.; Giepmans, B.N.; Palmer, A.E.; Tsien, R.Y. *Nat. Biotechnol*. **2004**, *22*, 1567-1572.

14. Boulos, L.; Prévost, M.; Barbeau, B.; Coallier, J.; Desjardins, R. *J. Microbiol. Methods* **1999**, *37*, 77-86.

15. Costerton, J.W.; Stewart, P.S.; Greenberg, E.P. *Science* **1999**, *284*, 1318-1322.

16. Blankenship, J.R.; Mitchell, A.P. *Curr. Opin. Microbiol*. **2006**, *9*, 588-594.

17. Jarlier, V.; Nikaido, H. *FEMS Microbiol. Letters* **1994**, *123*, 11-18.

18. Brewer, C.F.; Brown, R.D. *Biochemistry (N Y)* **1979**, *18*, 2555-2562.

19. Goldstein, I.; Hollerman, C.; Smith, E. *Biochemistry (N Y)* **1965**, *4*, 876-883.

20. Nigou, J.; Gilleron, M.; Puzo, G. *Biochimie* **2003**, *85*, 153-166.

21. Naismith, J.H.; Field, R.A. *J. Biol. Chem*. **1996**, *271*, 972-976.

22. Kim, B.C.; Nair, S.; Kim, J.; *et al*. *Nanotechnology* **2005**, *16*, S382.

23. Wilson, S.; Lane, A.; Rosedale, R.; Stanley, C. *Int. J. Tuberc. Lung Dis*. **2010**, *14*, 1164-1168.

24. Homhuan, A.; Harashima, H.; Yano, I. *ScienceAsia* **2008**, *34*, 179-185.

25. Glickman, M.S.; Cox, J.S.; Jacobs, W.R. *Mol. Cell*. **2000**, *5*, 717-727.

26. Asselineau, J.; Lederer, E. *Nature* **1950**, *166*, 782-783.

Chapter 6: Conclusions and recommendations

6.1 Conclusions

The synthesis, characterization and electrospinning of SMA and SMI derivatives were presented in this thesis with the purpose of being used as capturing platforms for *Mycobacterium tuberculosis* (*Mtb*). The nanofibrous substrates were subjected to affinity studies with *Mycobacterium bovis* bacillus Calmette-Guérin (BCG), a non-pathogenic, attenuated strain and mimic of *Mtb*, to evaluate the interaction and capturing abilities of these substrates. The main findings and recommendations are discussed in this chapter.

6.1.1. Polymer modification

Poly(styrene-*alt*-maleic anhydride) (SMA) was synthesized using conventional free radical copolymerization with a weight average molecular weight of 15 901 g/mol, polydispersity of 2.15 and 50% maleic anhydride content. SMA was bulk-modified with a variety of low molecular weight compounds to yield maleimide derivatives (SMI). These compounds were electrospun into nanofibrous mats. Prefabricated SMA nanofibers were surface functionalized with Concanavalin A (Con A), a lectin binding protein, to yield SMI-Con A and SMI-CLPA nanofibers.

SMA was functionalized with various low molecular weight compounds containing amine and hydroxyl groups. These active agents were covalently linked to SMA via ring-opening of the maleic anhydride residue. The modification agents chosen for this study was propylamine, 4-aminophenol and 3-(*N,N*-dimethylamino)-1-propylamine. Ring closure was successfully achieved with the application of heat and the corresponding loss of water to yield poly(styrene-*N*-propylmaleimide) (SMI-Pr), poly(styrene-*N*-[4-hydroxyphenyl] maleimide) (SMI-AP) and poly(styrene-[*N*-3-(*N',N'*-dimethylamino)propyl maleimide]) (SMI-tC). The latter was further functionalized with 1-bromooctane, 1-bromodecane, 1-bromododecane and 1-bromotetradecane to yield SMI quaternary ammonium alkyl conjugates poly(styrene-[*N*-3-(*N'*-octyl-*N',N'*-dimethylammonium)propyl maleimide]) (SMI-qC_8), poly(styrene-[*N*-3-(*N'*-decyl-*N',N'*-dimethylammonium)propyl maleimide]) (SMI-qC_{10}), poly(styrene-[*N*-3-(*N'*-dodecyl-*N',N'*-dimethylammonium)propyl maleimide]) (SMI-qC_{12}) and poly(styrene-[*N*-3-(*N'*-tetradecyl-*N',N'*-dimethylammonium)propyl maleimide]) (SMI-qC_{14}), respectively. All functionalized polymers were electrospun into nanofibers that were subjected to an additional heat treatment step at 130 °C under vacuum to facilitate cross-linking of the fibers, rendering them water insoluble and suitable for affinity studies in aqueous media.

The synthesized polymers were characterized using ^{1}H-NMR and ^{13}C-NMR spectroscopy, as well as attenuated total reflectance Fourier transform infrared spectroscopy (ATR-FTIR). The latter confirmed that all synthesized polymers had conversion percentages above 74%. Characterization of the electrospun nanofibers by means of scanning electron microscopy (SEM) was used to evaluate fiber diameters and morphology and indicated that nanofibers were produced with fiber diameters in the range of 218 – 468 nm.

SMA nanofibers were also used as substrate to immobilize Con A via covalent coupling. Surface functionalization with Con A was accomplished via an imidization reaction between the very reactive

and accessible α-amine group present on the N-terminus (of the protein) or the ϵ-amino group of the lysine residues of the protein that react spontaneously with the anhydride groups of SMA under neutral conditions yielding SMI-Con A functionalized nanofibrous mats. In a different approach, the covalent attachment of a monolayer of Con A to prefabricated SMA nanofibers was followed by glutaraldehyde treatment that cross-linked additional protein molecules and aggregates from the solution onto the covalently attached seed protein molecules to yield SMI-CLPA nanofibers. The SMI-Con A and SMI-CLPA substrates had significantly larger fiber diameters after functionalization as observed using SEM, but the morphology remained the same. ATR-FTIR confirmed that conversions above 73 % were obtained.

6.1.2 Affinity studies

Affinity studies were conducted between the various nanofibrous substrates and BCG to ascertain the strength of interaction and capturing abilities of the substrates. BCG was used as a non-pathogenic *Mtb* mimic and was successfully and with great avidity captured onto SMI-CLPA, SMI-Con A, SMI-qC_8, SMI-qC_{10} and SMI-qC_{12} nanofibers, even at the lowest possible concentration of 10 BCG/mL. SMI-qC_{14} proved less effective in comparison to its shorter alkyl chain equivalents.

The successful capture of BCG onto the surfaces of the various polymer nanofibers was confirmed by FM. The FM images revealed that high numbers of BCG were captured onto aforementioned substrates as indicated by the red and green stained microbes. A combination of ionic and hydrophobic-hydrophobic interactions could account for the BCG-affinity observed for the SMI-qC_x polymer nanofibers, whereas Con A nanofibers were able to interact with BCG due to the saccharide binding properties of the protein.

6.2 Recommendations for future research

The results obtained from this study presented various nanofibrous substrates that had an affinity for the cell wall of BCG to act as concentrating substrates in aqueous media. However, none of the substrates were subjected to *Mycobacterium tuberculosis* (*Mtb*). Future research could therefore include affinity tests between SMI-qC_8, SMI-qC_{10}, SMI-qC_{12}, SMI-Con A and SMI-CLPA nanofibers and *Mtb* to ascertain whether the interactions would be similar. Using existing smear microscopy techniques, it would also be advisable to determine whether the ZN-staining method could be used directly on the incubated nanofibers. The aforementioned nanofibrous substrates proved able to capture BCG at concentrations as low as 10 BCG/mL, and should the same apply to *Mtb*, and should the ZN-staining method be able to detect these microbes at such low concentrations, the diagnosis of paediatric TB – taking into account that the disease is paucibacillary – could be simplified dramatically.

Acknowledgements

Firstly I would like to thank my Heavenly Father for leading me every step of the way. "If any of you lack wisdom, let him ask of God, who gives to all liberally and without reproach, and it will be given to him." (James 1:5)

To Dr. Lizl Cronje: thank you for your undivided attention and encouragement. I couldn't ask for a better supervisor.

To Dr. Tiaan Heunis for culturing BCG numerous times and for your friendly assistance. You were always willing to help myself and Lisa and I appreciate it greatly. Thank you!

To Lize Engelbrecht, Rozanne Adams and Dumisile Lumkwana, thank you for your efforts in providing me with the best FM images. Your patience and expertise in this regard is highly praised.

I would like to thank Stellenbosch University and the National Research Foundation for the financial support.

Madeleine Frazenberg and Dr. Angelique Laurie, thank you for teaching me how to become an expert SEM analyst. My images look fantastic.

Thank you to Professor Albert van Reenen for the use of your laboratory and input during group meetings.

To Elsa Malherbe, for providing my NMR spectra without delay. Thank you.

Waldo Adams, thank you for your input and effort in the Biochemistry department.

Lisa Fortuin, without you I would've been very lonely in the office, laboratory and at Tygerberg. You never failed to brighten up my day. I couldn't thank you enough.

A big thank you to Erinda Cooper, Aneli Fourie, Deon Koen, Calvin Maart and Jim Motshweni for making sure everything runs smoothly in the Polymer Science building.

Aan Daniël en Marlé, ek is bevoorreg om julle my beste vriende te kan noem. Dankie vir bemoediging, Neelsie-koffies en baie liefde.

Laastens wil ek vir my ouers, Paul en Anne-Marie, duisend dankies sê vir al julle ondersteuning, omgee en vertroue in my. Ek is baie lief vir julle en sou dit nie sonder julle kon doen nie.